UNIVERSITÀ DI PARMA

UNIVERSITÀ DEGLI STUDI DI PARMA

DOTTORATO DI RICERCA IN INGEGNERIA INDUSTRIALE

CICLO XXXIII

Development and application of innovative methods for smart control of district heating networks

Coordinatore:
Chiar.mo Prof. Gianni Royer Carfagni

Tutore:
Chiar.mo Prof. Mirko Morini

Dottorando:
Costanza Saletti

Anni Accademici 2017/2018 – 2019/2020

"We can only see a short distance ahead,
but we can see plenty there that needs to be done."

Alan Turing, 1950

Acknowledgements

I am extremely grateful to all the people that have walked with me during my PhD journey and without whom this work would not have been possible. I have said this before, but it is worth saying it once more: *happiness and*, I add this time, *accomplishment are only real when shared*.

I would like to deeply thank my supervisor, Prof. Mirko Morini, for his determinant support, for the constant guidance over these three years and for giving me countless opportunities of professional growth, starting from my very first international conference. I also deeply thank Prof. Agostino Gambarotta for the interesting discussions, questions and insights on many topics, related to our research or not.

I wish to thank Prof. Konstantinos Kyprianidis for allowing me to spend four challenging and inspiring months at Mälardalen University and for the support he provided. Thanks also to Dr. Nathan Zimmerman for the fruitful collaboration, and to all the researchers and students with whom I shared my Swedish months.

I would like to express my gratitude to Prof. Umberto Desideri who, when I was in front of a sliding door, gave me the precious advice that brought me where I am today; and to Dr. Mike Steilen, who gave me the first glimpse of what it takes to do research and taught me tools and methods that have been essential throughout all my path.

Thanks to the old friends from Pisa and the new friends from Parma, in particular to Andrea, Antonio, Matteo, Nora, Alex and Paola, and to all my swim team, for making great my time here.

Special thanks to Leonardo and Grazia, for welcoming and supporting me as if I were a daughter to them.

Most of all, thanks to my Family: to Dad, Mum, my sister Virginia and my brother Riccardo. I have no words to describe how important your strength, inspiration, love and encouragement were throughout these years. You made me who I am today.

And, from the deepest of my heart, thanks to Nicola for the unlimited support and patience in all my choices, even when they kept us distant, for making me believe in myself when I did not, for remembering me to turn on the light in dark times. You have shown and show me everyday who I want to be.

Abstract

The mitigation of the effects of human activities on the climate and environment has become essential to guarantee environmental sustainability and safety. As regards the energy sector, reduction in greenhouse gas emissions and energy efficiency improvement are fundamental targets of the clean energy transition to be pursued over the next decades. Since it accounts for half of final energy use in the European Union, the heating and cooling sector offers significant opportunities for decarbonization. In particular, district heating networks are regarded as highly promising due to their ability to distribute thermal energy in urban areas more efficiently compared to individual heat generation devices, to the possibility to integrate renewable energy sources, and to their flexibility potential. However, the complexity of these systems is increasing and their traditional management approaches, based on the experience of the operators, are not able to fully unlock their benefits. On the other hand, optimal controllers, which are made possible by new digital technologies, may allow this goal to be achieved. Model Predictive Control (MPC) is a smart control strategy which takes advantage of the prediction of the system behavior over a future horizon to optimize its operation. Therefore, it is an adequate solution to cope with the high variability of the external conditions and to perform system optimization.

The scope of this thesis is to investigate and develop a complete set of original methods for the application of MPC to district heating networks with different sizes and levels of complexity. Since MPC requires a dynamic model of the system and a computationally efficient optimization algorithm, these two fundamental tools are developed for small-scale and large-scale networks. In particular, the models are control-oriented and physics based and, thus, maintain the representation of the main governing phenomena and physical parameters, such as the heat capacity of the end-users connected to the network.

The developed tools are embedded within MPC solutions and their performance is verified in Model-in-the-Loop simulation environments, which enable a reliable comparison of different control strategies without affecting the real system.

As for small-scale district heating, the novel optimization algorithm is based on Dynamic Programming and is particularly suitable for a multi-agent hierarchical control architecture. This is tested on a case study located in northern Italy and achieves both minimization of the heat supplied to the end-users and reduction in the production unit operating cost, with reference to a traditional control strategy. In addition, the potential of the system controlled by the MPC in providing

flexibility service to the power grid in presence of uncertainty is investigated and verified.

Concerning large-scale district heating, the developed optimization algorithm aims to shift the peaks of energy supplied to the various regions of the network by storing heat in their thermal capacity and, at the same time, to reduce the distribution temperature. The algorithm is embedded in an MPC and its application to a city district heating in central Sweden results in up to 16 % peak shaving and up to 20 % reduction in heat losses, with reference to historical data.

Overall, the proposed solutions for smart control bring noteworthy advantages to district heating networks in terms of energy and cost saving. Their versatility and independence from the specific problem can aid the extension of MPC to multi-source networks, toward its implementation in real-life cases. This constitutes a promising step in the direction of smart, optimal and efficient energy systems.

Contents

List of Figures

List of Tables

Nomenclature

Acronyms

Symbol	Description
1D	One-Dimensional
Al	Algebraic
CHP	Combined Heat and Power
DHC	District Heating and Cooling
DHN	District Heating Network
DP	Dynamic Programming
Dy	Dynamic
L	Lumped
LP	Linear Programming
MiL	Model-in-the-Loop
MIMO	Multi-Input-Multi-Output
MPC	Model Predictive Control
NLP	Nonlinear Programming
ORC	Organic Rankine Cycle
PID	Proportional-Integral-Derivative
PO	Plant Operator
RES	Renewable Energy Sources
SoC	State of Charge
TES	Thermal Energy Storage
TSO	Transmission System Operator
UVAM	Mixed Virtual Aggregated Units

Constants

Symbol	Description	Unit
g	Gravity acceleration	$9.81\,m\,s^{-1}$

Greek Symbols

Symbol	Description	Unit
α	First building performance coefficient	s^{-1}

Symbol	Description	Unit
β	Second building performance coefficient	$°C\,kJ^{-1}$
δ	Fourth building performance coefficient	s^{-1}
$\Delta\dot{Q}$	Difference between predicted and actual thermal power	kW
ΔT	Temperature difference	°C
Δt	Time-step	s
Δt_d	Time delay factor	s
Δu	Input grid step	
Δx	State grid step	
η	Efficiency	-
γ	Third building performance coefficient	s^{-1}
Λ	Ratio of actual to nominal heat	-
λ	Flow coefficent	-
μ	Feasible input	
ω	Weight	
ϕ	Valve opening factor	-
π	Control policy	
π_1	Dimensionless head coefficient	-
π_2	Dimensionless flow coefficient	-
ρ	Density	$kg\,m^{-3}$
τ	Characteristic time	s

Latin Symbols

Symbol	Description	Unit
$\dot{m}$	Mass flow rate	$kg\,s^{-1}$
$\dot{Q}$	Thermal power	kW
$\dot{V}$	Volumetric flow rate	$m^3\,s^{-1}$
A	Area	m^2
a	Envelope heat loss coefficient	s^{-1}
b	Supplied power coefficient	$°C\,kJ^{-1}$
C	Aggregated heat capacity coefficient	$kJ\,°C^{-1}$
C	Specific cost	€ kWh^{-1} or € kg^{-1}
c	Specific heat capacity	$kJ\,kg^{-1}\,K^{-1}$
D	Diameter	m

Symbol	Description	Unit
d	System disturbance	
e	Error between measured output and set-point	
f	Pipe friction factor	-
H	Pressure head	m
H_{TES}	TES height	m
In	Incidence matrix	
J	Objective function	
k	Specific heat capacity ratio	-
k_{D}	Derivative gain	
k_{I}	Integral gain	
k_{P}	Proportional gain	
k_{r}	Resistance coefficent	-
K_{v}	Valve nominal flow coefficient	m^2
L	Length	m
LHV	Lower Heating Value	$\mathrm{kJ\,kg^{-1}}$
M	Mass	kg
N	Number of time-steps	
n	Pump rotational speed	$\mathrm{s^{-1}}$
N_{m}	Number of measurements	-
N_{r}	Number of regions	-
N_{s}	Number of pipeline segments	-
P	Power	kW
p	Pressure	Pa
Q	Heat	kJ
$RMSE$	Root Mean Squared Error	
SW	Boiler on-off signal	-
T	Temperature	°C
t	Time	s
U	Aggregated heat transfer coefficient	$\mathrm{kW\,°C^{-1}}$
u	System input	
U_{TES}	TES heat transfer coefficient	$\mathrm{kW\,m^{-2}\,°C^{-1}}$
UA	Overall heat transfer coefficient	$\mathrm{kW\,°C^{-1}}$
V	Volume	m^3
w	Fluid velocity	$\mathrm{m\,s^{-1}}$
x	System state	

Symbol	Description	Unit
X_{TES}	Thermocline	m
y	System output	
z	Height	m
ER	Energy Reduction	%
PS	Peak Shaving	%
RVR	Reduction in Variation Range	%
SoC	State of Charge	-

Superscripts

Symbol	Description
$*$	Optimal

Subscripts

Symbol	Description
0	Initial
a	Air
actual	Actual
air	Forced ventilation
avg	Average
b	Boiler
base	Baseline
bg	Bought from the grid
bld	Building
C	Control horizon
conc	Concentrated
dem	Demand
dist	Distributed
el	Electrical
ext	External/outdoor
f	Final
f	Fuel
geo	Geodetic
h	High

Symbol	Description	Unit
HEX	Heat exchanger	
hist	Historical	
hs	Heating system	
i	Region index	
in	Inlet	
in(1)	First pipeline segment	
j	Arc index	
k	Time-step index	
l	Low	
loss	Loss	
m	Mechanical	
max	Maximum	
min	Minimum	
mix	Mixing	
new	New	
nom	Nominal	
occ	Occupants	
out	Outlet	
P	Prediction horizon	
previous	Previous input	
prod	Production unit	
pump	Pump	
R	Return	
rad	Solar radiation	
rec	Recovery	
ref	Reference	
S	Supply	
sg	Sold to the grid	
soil	Soil	
SP	Set-point	
stored	Stored	
th	Thermodynamic	
tot	Total	
valve	Valve	
w	Water	

1 Introduction

Over the last few decades, numerous studies have produced scientific evidence of the influence of human activities on the climate system [1]. Indeed, global warming (i.e. increase in global average temperature) and the mutations it induces on the global ecosystem [2], have been linked to the continuous increase in anthropogenic greenhouse gas emissions such as CO_2, related in particular to the exploitation of fossil fuels.

In order to mitigate these effects, the United Nations member states have undertaken many political actions starting from the "Kyoto Protocol" in 1997, which was the first international treaty to legally commit governments to reduce emissions with agreed individual targets. Another turning point in the sustainable transition was the Paris Agreement signed during the United Nations Framework Convention on Climate Change (COP21) held in 2015 [3]. The document certifies the agreement on limiting the rise in temperature of the planet to no more than 2 °C before 2050, with reference to pre-industrial levels, in order to prevent environmental damages.

In this regard, environmental sustainability in the energy sector is recognized as one of the key priorities for the present and future. It can be achieved through energy technology development and innovation [4], with a more rational use of energy and the uptake of Renewable Energy Sources (RES) in spite of fossil fuels in its production.

The European Union is leading this clean energy transition. Since 2007, the European Commission has set fundamental targets for reducing carbon dioxide, increasing the percentage of energy production by RES, and reducing primary energy consumption (i.e. energy efficiency) by 2020 [5], with 1990 as reference year. The strategy for the transition toward a low-carbon and sustainable energy scenario in Europe has been updated over the years (Table 1.1) with new ambitious objectives up to 2030 [6], as well as with the European Green Deal, a plan to realize an economy with net-zero greenhouse gas emissions by 2050 [7].

Table 1.1. Targets established by the European Commission.

Target	2020	2030	2050
Reduction in carbon dioxide emission	20 %	40 %	90 %
Share of energy from RES	20 %	32 %	80 % to 95 %
Increase in energy efficiency	20 %	32.5 %	50 %

Nevertheless, the road to achieve climate neutrality is still long. Indeed, despite a 5 % decrease in 2020 compared to the previous year due to the COVID-19 pandemic, the global primary energy demand is expected to continue its growth [8] in future years. Furthermore, the initial target of 40 % emission reduction before 2030 has been recently increased to 55 % [9]. Hence, substantial improvements are required, especially in the sectors which have been less decarbonized so far.

According to the Heat Roadmap Europe [10], the heating and cooling sector accounts for around 50 % of total energy demand in the European Union, with more than 60 % of it being used for space heating and hot water in buildings (Fig. 1.1a). However, at least 66 % of the total thermal energy is produced by fossil fuels such as natural gas and oil, while only 13 % explicitly derives from RES (Fig. 1.1b). The electricity and district heating share instead may or may not be from RES, depending on the local conditions. For these reasons, heating and cooling is the area with largest potential for decarbonization and energy efficiency improvement.

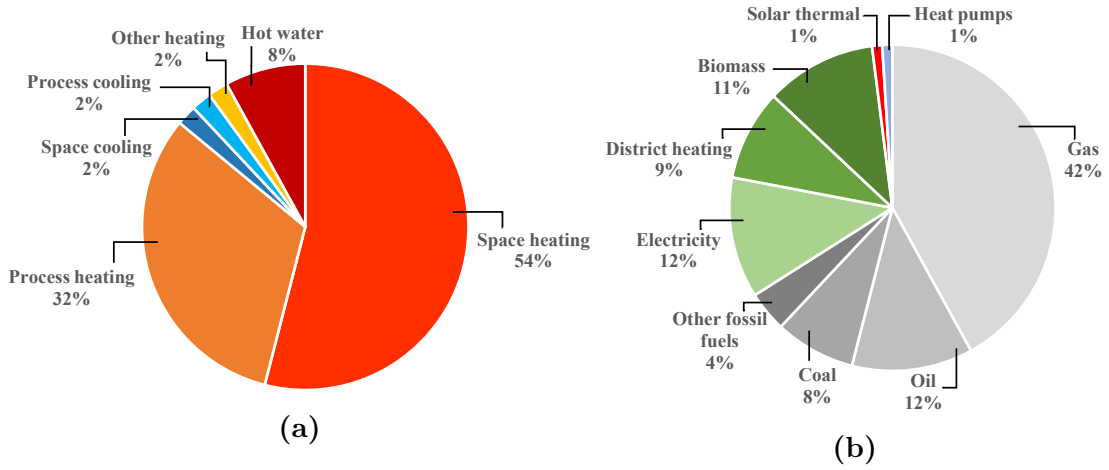

Fig. 1.1. Heating and cooling final energy in 2015 (a) by end-use and (b) by energy carrier. Data are adapted from [10].

In addition, the Renovation Wave Strategy, published by the European Commission in the last few days at the time of writing [11], strongly supports refurbishment and efficiency measures for built environments to be tackled with district and community-based approaches. In this way, synergies between the various elements of an energy system may be exploited and optimized, potentially leading to net-zero or positive energy districts.

In this context, great opportunities are offered by District Heating Networks (DHNs), which could integrate large amounts of RES and excess heat from indus-

trial and commercial activities, meeting most of building heat demand in Europe.

1.1 District heating networks

District heating is a system designated for the transportation and distribution of thermal energy, typically produced in centralized locations, to meet heating requirements (e.g. space heating and domestic hot water) of residential, commercial and industrial dwellings by means of a network of insulated pipelines positioned underground. This mainly comprises two sets of pipes, namely supply and return. The supply pipe collects hot water produced by the heat generation sites and transports it to the customer substations. Here, heat is transferred to the own heat distribution system of the connected building by means of a heat exchanger. Cold water is transported from the substation back to the production sites through the return pipe. The pipelines from production to substations constitute the primary side, while those within the end-users constitute the secondary side. A graphic representation of the DHN principle is given in Fig. 1.2. The same concept can be repeated for district cooling which, however, is less widespread in Europe.

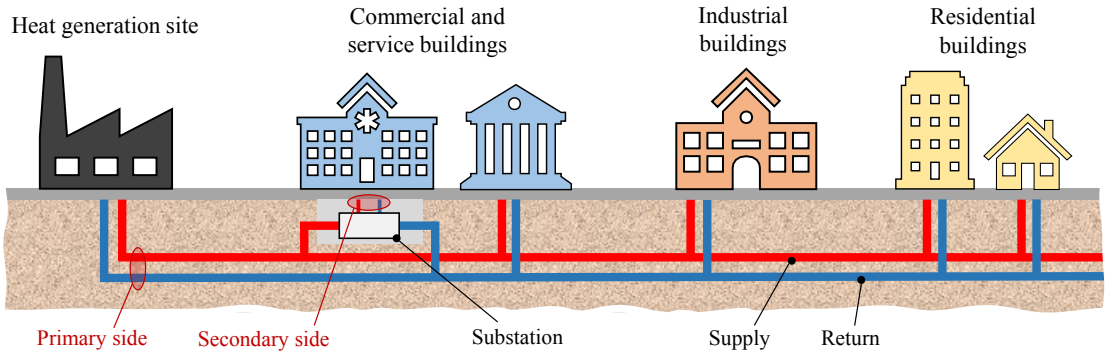

Fig. 1.2. Qualitative representation of a district heating network (the substation is shown only for one building for graphical reasons).

Historically, the concept of DHN was developed at the end of the 19$^{\text{th}}$ century and improved over the decades. Four generations of the technology have been identified by Lund et al. [12, 13] together with the period in which they have been the best available technology:

- 1$^{\text{st}}$ generation (1880–1930): the heat carrier is steam and the main source is coal; distribution is done through steel pipes insulated in situ.

- 2nd generation (1930–1980): the heat carrier becomes pressurized water with temperature higher than 100 °C; Combined Heat and Power (CHP) generation plants based on coal and oil begin to become widespread.

- 3rd generation (1980–2020): the heat carrier is pressurized water with temperature lower than 100 °C; additional sources include biomass CHP, large-scale solar and industrial surplus heat; distribution is done through preinsulated steel pipes.

- 4th generation (2020–onward): the heat carrier is pressurized water with temperature lower than 70 °C; integration of low-temperature sources such as geothermal, waste heat from data centers and heat pump is possible.

Despite the lack of a uniformly accepted definition, a 5th generation has recently been proposed with water temperature around 20 °C and hybrid substations in which the temperature level is increased by water source heat pumps [14].

The share of heat supply by DHNs in European countries is highly non homogeneous, going from 50 % in Sweden and Finland, to around 25 % in Austria and Poland, down to less than 5 % in Italy and Spain. However, future decarbonization scenarios up to 2050 assign a predominant role to district heating, indicating its ability to provide 50 % of heating demand and 30 % energy saving [10].

Indeed, DHNs provide several benefits and opportunities in urban areas compared to individual heating devices [15]:

- Least-cost and most efficient solutions to supply thermal power in cities and towns and, therefore, to reduce emissions and primary energy use [10]. These are achieved through the economy-of-size (i.e. technologies with lower cost for higher product volume).

- Integration of solutions for decarbonization, such as RES, large heat pumps, waste heat recovery and CHP.

- Flexibility and possibility to interact with other energy networks (e.g. electric and natural gas grids) to achieve flexible smart energy systems [16] via sector integration.

- Reduced local environmental impact due to lower emission of pollutants (NO_x and particulate matter), as local combustion of fuels is substituted by more efficient combustion in centralized generation sites.

However, the sector presents also several challenges that still need to be addressed. Firstly, the distribution of hot water over pipelines is inherently characterized by heat losses caused by the temperature difference with the external environment. The evolution over the generations of DHN mentioned above is going in the direction of lowering the distribution temperature to reduce heat losses, increase system efficiency and better integrate alternative sources [17].

Secondly, the growing penetration of discontinuous sources, highly variable thermal demand throughout the year and time delays between heat production and actual supply due to pipeline lengths [18] are some of the factors contributing to the growing system complexity. Hence, the flexibility and various benefits of DHNs can be fully unlocked only by exploiting innovative optimization and control strategies which are able to remove the barriers of location and time in heat distribution [19].

As a matter of fact, existing traditional DHNs are operated with raw control strategies and outdated control systems, generally adjusted manually based on technical experience of the system operators or on rules defined *apriori* [15]. These methods encompass very limited optimization features.

This bottleneck can be addressed through **digitalization**, which can be defined as the wide implementation of digital technologies to provide optimal network management and control based on real-time data [20]. The Digital Roadmap for District Heating and Cooling [21] indicates the necessity to develop and implement **smart control** to lead to more efficient networks, in particular by:

- maximizing the operation of sustainable sources while optimizing heat distribution;
- cutting the peaks of thermal demand (i.e. peak shaving), which usually happen for a very limited number of hours over the year and, being typically covered by natural gas back-up boilers, represent a significant cost;
- exploiting passive storage means (e.g. building heat capacity) for demand side management and flexibility.

It is finally worth stating that DHNs can span across very different size ranges: **small-scale DHNs** comprise a relatively small-number of connected buildings, as is the case of a university campus, an education complex, a hospital or a small neighborhood, while **large-scale DHNs** comprise hundreds to thousands of end-users and are spread over large cities. Both types are widespread. For instance, in Italy around 30 % of 314 existing DHNs have an extension lower than 2 km [22].

The techniques for modeling, optimizing and controlling these systems vary significantly depending on their size and complexity. Hence, innovative methods that can be scaled and applied to different system sizes are paramount to achieve the new generation of intelligent heating networks.

1.2 Scope of the thesis

Based on the considerations outlined in the previous section, the present thesis aims to develop innovative methods for smart control of district heating networks, and to apply them to case studies with different objectives and different levels of complexity. Solutions for both small-scale and large-scale DHNs are investigated.

The work tackles all the limitations mentioned above by addressing, in particular, the following tasks: (i) the minimization of energy consumption and operating cost in heat distribution, (ii) investigation of end-users' heat capacity as thermal storage for shifting thermal load peaks, and (iii) supply temperature reduction.

The proposed solutions rely on Model Predictive Control (MPC), which aims to perform optimal control based on predictions produced by a mathematical model of the system. Thus, dynamic modeling strategies and optimization algorithms for DHNs are essential tools for this investigation.

Furthermore, since real system operation is highly dependent on a large number of exogenous inputs and boundary conditions and repeatable field tests are not feasible, Model-in-the-Loop (MiL) simulation platforms are adopted to carry out control verification.

The thesis focuses on DHNs. Nevertheless, the extension of the developed methods to district cooling is straightforward.

1.3 Outline of the thesis

The present thesis is divided into four main parts.

Section 2 reviews the current status of literature research on the subject of the thesis, in order to support the motivation of the study. The most common modeling and control strategies of district heating networks are described and critically compared. The section also includes an overview of European research and innovation projects on smart District Heating and Cooling (DHC) funded within the Horizon 2020 Framework Programme.

In Section 3 the basic theoretical background on mathematical models, optimization algorithms and control strategies is outlined. It provides the tools and references for the novel methods developed in the work and for their application

in control architectures. Special regard is given to the techniques exploited in the work, such as Dynamic Programming and Model Predictive Control.

Section 4 contains the innovative methods developed with the final goal of controlling district heating networks in an intelligent way:

- A dynamic model and an optimization algorithm based on Dynamic Programming suitable for multi-agent hierarchical control applications to **small-scale DHNs**.
- A scale-free dynamic model and a two-stage optimization algorithm suitable for control applications to **large-scale DHNs**. It optimizes the network state and operating parameters based on a first Linear Programming step and a second Nonlinear Programming step.

In Section 5, the aforementioned methods are evaluated in **MPC control applications** for both a small-scale network (i.e. school complex in northern Italy) and a large-scale network (i.e. peripheral areas of a city in central Sweden). In the former case, the additional potential of the system in providing flexibility service to the power grid under uncertainty is demonstrated.

Finally, the conclusions of the work are delineated and the outlook on future improvements is discussed.

The sections containing the proposed elements for small-scale and large-scale systems can be accessed through the outline in Table 1.2.

Table 1.2. Outline of methods and applications in the present thesis.

Tool	Small-scale DHN	Large-scale DHN
Model	Section 4.1	Section 4.3
Algorithm	Section 4.2	Section 4.4
MPC application	Sections 5.1 and 5.2	Section 5.3
Model-in-the-Loop platform	Appendix A	Details in [23]

2 State-of-the-art research overview

This section describes the current state of scientific research on district heating and on the fundamental tools for their analysis and optimization: modeling and control strategies. It aims to draw a complete framework of the latest developments and mature technologies in order to highlight research gaps and support the motivation for this work.

The literature review is divided into three parts:

- district heating mathematical models;
- district heating control;
- international research and innovation projects on smart DHCs in the Horizon 2020 Framework Programme.

2.1 District heating modeling

The operation and control of DHNs can be subject to significant variations depending on the geographical area, system topology and scale, and availability of data and information (e.g. energy demand, building type and weather data). In particular, the thermal demand of the consumer is highly influenced by the environment conditions.

In most cases, the experimental investigation of these aspects in proper test rigs is not feasible due to the large system size and characteristic times, and imposes technical risks due to strict comfort requirements for customers.

Under those circumstances, mathematical models of the system are fundamental tools for providing insights on system design, management and control-oriented applications. Each of these activities, as well as the scale of the system, require different levels of resolution in time and space, depending on the computational constraints [24]. Indeed, each energy system model has to fit its specific purpose [25].

The development of dynamic mathematical models of the production, distribution and consumption sides of DHNs is a highly tackled topic in the literature [26, 27]. In particular, distribution and consumption represent the dominant dynamics in DHNs. Hence, the main modeling approaches with a focus on distribution network and heat load are illustrated in Fig. 2.1 and reviewed below.

Models of the distribution network Various models with different levels of detail are employed to represent the global distribution system. Some works inves-

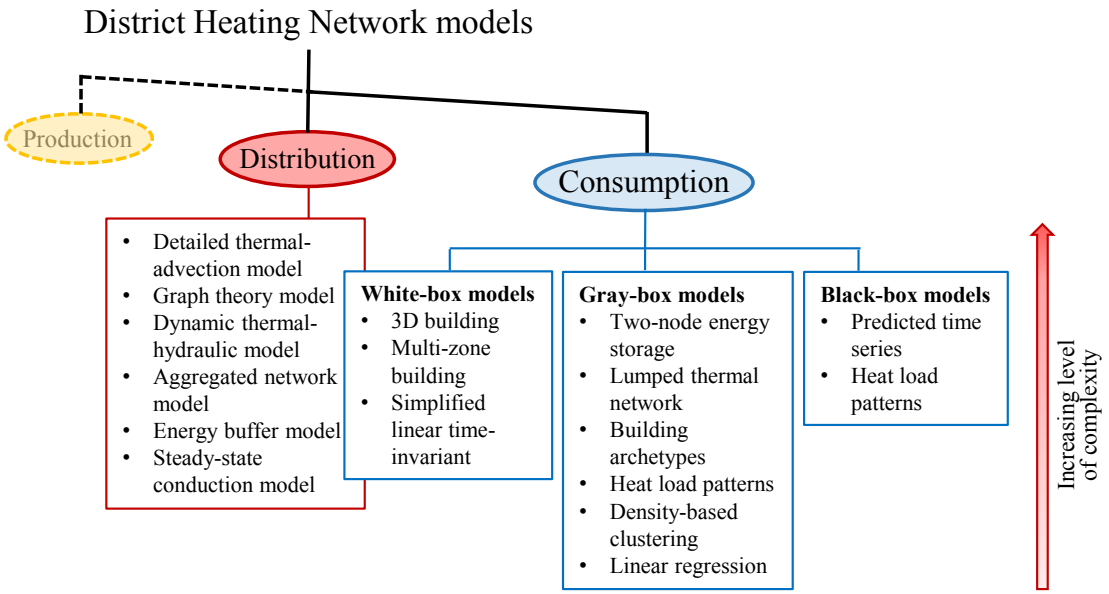

Fig. 2.1. Summary of the main modeling approaches of district heating networks: focus on the consumption and distribution.

tigate the transient physical phenomena occurring within the pipelines of DHNs by coupling the detailed hydraulic equations with the thermal advection-diffusion equations, and solving them with an analytic form [28]. While this approach introduces significant complexity to the overall system model, heat transmission over DHN pipelines can also be represented by dynamic thermal-hydraulic models which neglect diffusion but include the time delays [29, 30]. Several studies adopt the graph theory to represent the topology of large-scale DHNs in a more compact way [31–33]. According to this method, each pipe is a branch and each connection is a node. Nevertheless, the network can be further simplified by applying two different aggregation methods (i.e. German and Danish) as described in [34], or by adopting dynamic models for topology analysis [35] and steady-state models for system planning [36].

Since hydraulic dynamics are significantly faster than thermal dynamics, it is common practice to neglect the former while including pressure losses.

Recently, several works have proposed software packages and libraries for detailed simulation of DHNs by means of different programming tools [37–39]. These platforms can be used as virtual test beds for network performance assessment and feasibility analysis [40]. Nevertheless, they are not efficient as models embedded in real-time optimization and control [41], for which model simplicity and computational speed are paramount. In this direction, an interesting network aggregation

approach for continuous optimization of DHNs up to 200 consumers is proposed by Schweiger et al. [39].

Generally, these models incorporate the consumers' thermal demand by means of other external methods.

Models of the consumption Concerning the estimation of district heating thermal demand, the most common classification is reviewed by Ma et al. [42]:

- Physical models, or white-box models, rely on physical principles, conservation laws (e.g. energy conservation equation) and detailed building characteristics, but typically require a significant computational effort, leading to impracticable calculation times in optimization and control applications.
- Statistical models, or black-box models, are based on experimental data and are trained with large datasets, but they do not include a physical representation of the phenomena underlying the system.
- Hybrid models, or gray-box models, are based on a manageable physical representation of the system that relies on empirical relationships identified from available data, thus combining physical and data-driven knowledge.

The advantages and limitations of each approach are reported in Table 2.1. In the light of this, connected buildings can be modeled with several techniques depending on the level of detail required by the simulation aim.

As regards **white-box** techniques, 3D models can be adopted for a detailed representation of the architecture and materials [43] as well as multi-zone models with detailed heat transfer phenomena [44, 45]. In other cases, model order reduction through linearization and simplification allows the model of the building envelope to be scaled into an equivalent model [46].

As for **gray-box** models, the most common technique is to represent the building as a thermal-capacitance network or lumped thermal model [47] and to derive the values of the parameters via calibration procedures, which aim to match the output of a building model with measured data [48]. Although these models are reliable and computationally fast when compared to detailed building simulation tools, they focus on individual buildings without connection to the DHN. The challenges in obtaining a fast representation of DHN customers due to the large number of interacting variables and complex architectures is highlighted. Simpler approaches involve the development of building archetypes characterized by representative parameters and construction details [49], heat consumption patters of

building clusters deriving from a combination of statistical and analytical methods [50], density-based clustering [51], and linear regression models [52]. This may enable the investigation of demand side management strategies to explore the system flexibility at building level.

Concerning **black-box** models, a large number of studies developing DHN heat load patterns or its prediction as time-series has been recently proposed [53–57]. These models are trained through machine learning (e.g. neural networks), deep learning and regression techniques.

Table 2.1. Main modeling approaches for the prediction of thermal load in district heating networks, with advantages and disadvantages.

Approach	Advantages	Limitations
White-box	Detailed dynamic simulation in every condition	Costly, time-consuming, high computational time, much information required
Black-box	Low computational time, good accuracy	Large datasets required, not suitable for conditions other than training set
Gray-box	Good accuracy, feasible computational time, physical meaning of parameters	Data and expert knowledge required

Models of the heat capacity for flexibility According to Vandermeulen et al. [58], in energy systems flexibility is *the ability to speed up or delay the injection or extraction of energy into or from a system* in order to improve performance and sustainability. Hence, it requires the system to have a thermal capacity which acts as a buffer between energy production and actual delivery.

There are three main storage solutions in DHNs:

- Dedicated thermal storage tanks [59], classified according to the occurring physical phenomenon (sensible, latent or chemical storage), the duration (short-term or long-term) and the layout (distributed or centralized storage). If such a device is not arranged in existing systems yet, its installation may require significant investment costs.

- Thermal capacity of the water within the distribution pipelines [60–62], exploited by raising the supply temperature and preheating the network to lower the typical demand peaks. This is mainly suitable in large-scale DHNs due to the large number of pipelines. However, it may have a lower potential and limited controllability compared to the other methods, and it is accompanied by higher heat losses [63].

- Thermal capacity of the connected buildings [54, 64, 65], exploited to achieve peak shaving and valley filling, which consist of shaping the demand in such a way that it is kept as constant as possible [66]. It does not required modifications of the system architecture.

As mentioned in Section 1.1, the latter should be investigated further, for instance by introducing limited temperature fluctuations in order to achieve flexibility through demand side management strategies [67]. The heat storage potential of buildings has been tackled with an experimental study by Kensby et al. [68], showing that storing an energy amount of 0.1 kWh per square meter of heated floor area causes variations in indoor temperature lower that 0.5 °C in heavy buildings. Subsequent simulation [69] and optimization studies are also reported [70].

These heat capacity models, however, require an extensive knowledge of the building construction details [71] and properties, which may be not available. Oftentimes, a significant set of assumptions has to be made with high chances of reducing the prediction robustness [72].

Remarks on system scale In real-time control based on MPC, the most time-consuming part is generally the development of a suitable building model for control and operation, as a standard procedure does not exist [73]. When dealing with modeling heat distribution in buildings, the model approaches reviewed above are used according to the characteristic scale on which the problem is investigated [74]:

- On a micro-scale (e.g. when rooms or zones are of concern) much information about the system (e.g. wall characteristics, glazed surface size and orientation) and about the disturbances (e.g. external temperatures, occupants' behavior, other internal heat gain sources) can be accurately collected. Thus, dynamic detailed models that include envelope characteristics, internal gains and irradiance can be used [75].

- On a meso-scale, as is the case of **small-scale DHNs**, each building should be considered as a whole, therefore heat exchange and capacity properties

should be lumped together. Moreover, occupancy and the state of the glazed surfaces are difficult to estimate with an adequate accuracy for a whole building. Nevertheless, all consumers can still be modeled individually.

- On a macro-scale, as is the case of **large-scale DHNs**, less information is available for the characterization of the system. Therefore, building heat demands are estimated through statistical analysis based on historical data and aggregated by means of statistical elaborations. In many networks, however, datasets with enough detail to characterize all substations are missing.

A control-oriented model that is not case-dependent and can be scaled to DHNs with different sizes and architectures could significantly foster the applicability of smart controllers in practice. In this regard, gray-box models seem to be advantageous as they are able to combine knowledge of the physical system and coarse datasets.

2.2 District heating control

Real-time control in DHNs is handled by operative personnel in a control room. It is based on operational planning, but the parameters are adjusted in case of anomalies or forecasting errors [76].

Traditional control in DHNs has the main priority of meeting the thermal demand of the end-users, which varies with the external conditions. In practice, four main control systems are present [15]. On the local consumer side, there are (i) heat demand control of the space heaters via thermostatic valves or even manually in outdated systems, and (ii) mass flow rates control of the secondary side of the substation. In parallel, on the primary side, (iii) the differential pressure control by means of pump stations assures sufficient mass flow rate, while (iv) the supply temperature control aims to ensure that the supply temperature, which is regulated through the amount of heat transferred from the heat source to the distribution water, reaches a given set-point. This is traditionally given by heating curves, which are linear functions of the outdoor temperature determined *apriori*.

In general, the system operator is able to manage the system operation by regulating the pumps and the supply temperature independently. A widely used operation mode is named quality regulation mode, in which mass flow rates remain constant while the water temperature changes with the demand [77]. Another mode, instead, regulates only the mass flow rates while maintaining a fixed supply temperature.

Clearly, traditional control systems in DHNs are rather basic and non optimal, as each of them has an individual target. Moreover, being based on time-scheduling and on the experience of operators and technicians [78], they are not able to deal with RES fluctuations or to rapidly react to the high weather variability caused by climate change.

As stated in Section 1.1, advanced control systems can provide customized solutions according to the actual conditions. Hence, they unlock the benefits of low-temperature networks [79], optimization and flexibility measures, without having to change the system hardware configuration.

In the literature, a widespread method, regarded as operational optimization in [58], generally includes a model of the system and calculates the optimal control actions offline, i.e. a few hours or a few days ahead [41, 80, 81], or performs optimal scheduling by aggregating the thermal inertia of different buildings [82].

Alternatively, remarkable improvements in terms of robustness [83] can be achieved when the optimal control action is calculated online, i.e. the calculation is updated at each given time increment to compensate modeling and prediction errors, which are inherent in the previous case. This promising real-time strategy is **Model Predictive Control**. Its investigation and application to small-scale and large-scale DHNs are the focus of the present thesis. Details on its concept and theoretical framework are provided in Section 3.3.2.

Model Predictive Control for buildings In the last decade, the number of studies on MPC for energy systems has become considerable, especially as far as individual building systems are concerned.

In a review paper from 2009 [84] regarding advanced control for building environments, MPC is not cited, yet predictive control is regarded as interesting at coordinator level. First experiences of MPC for heating, ventilation and air conditioning systems of buildings date back to 2011 [85, 86]. In subsequent reviews [87–89], MPC becomes the most widely used optimal control method in literature studies on comfort management and flexibility of smart, sustainable buildings.

Some remarkable results regard successful implementation of MPC in real field tests on residential [90] and commercial buildings [91], as well as simulation cases, where a detailed model emulates the behavior of the system [92]. Research has mainly focused on the assessment of suitable physics-based or data-driven models, as they represent an essential part of the controller [93].

Nevertheless, the mentioned efforts are exclusively devoted to buildings with individual heating systems. The connection to a DHN implies greater system

complexity, longer dynamics (and delays to be predicted and anticipated) and a higher computational burden that should not be underestimated.

Model Predictive Control for district heating The most part of research on DHNs focuses on design and operation [94], long-term production planning [95], but not on real-time control. The extension of MPC to DHNs presents some challenges and studies in the literature, as well as real world case studies, are not frequent. Thus, this is a relatively new field.

According to Lyons et al. [96], the development of models that are complex enough to capture the behavior of large sets of buildings without introducing excessive computational effort is still a challenge. The authors develop an MPC strategy for a block of flats with communal heating (i.e. **small-scale DHN**) in two architectures to achieve lower cost: (i) a centralized MPC that solves the optimization problem for the entire system, with impracticable computational demand for larger networks, and (ii) a decentralized MPC in which different subsystems are optimized separately according to local objectives. Here, the MPC calculates optimal set-points for the low-level feedback controllers of the actuators [97].

Another paper shows the benefits of the technique for a multi-energy system with three buildings with an economic objective [98]. In other cases, instead, MPC can be used to improve set-point tracking of low-level control strategies, in order to reduce their oscillations [99]. Similarly, Hou et al. [100] perform the simulation test of two different MPC controllers in a building substation, in order to keep indoor air temperature at reference values.

Aoun et al. [101] shift space heating consumption of an archetype building with an MPC without feedback on internal air temperature. This may lead to less accurate state estimation and, consequently, control performance, yet it may be applicable in districts where extensive indoor monitoring would be intrusive.

As for **large-scale DHNs**, it is challenging to consider each consumer as a separate individual element when the number of buildings increases significantly. Verrilli et al. [102] design an MPC for optimal scheduling of energy production from multiple sources while the demand is predicted through data mining methods. Similarly, Zimmerman et al. [23] build a demand prediction model identified with historical data and provide it to a feed-forward MPC. Lennermo et al. [103] study the control of solar heat collectors as decentralized sources for district heating without, however, including the demand side. In the work by Vanhoudt et al. [104], the building load is represented through thermal-electrical analogy while the grid components are fitted to supplier data.

On a final note, the methods proposed are oftentimes case-dependent and the possibility to extend the analysis to real scenarios is not straightforward. In addition, MPC implementation requires continuous monitoring of the system state, as detailed in Section 3.3.2. However, monitoring instruments, sensors and smart meters are not installed in a widespread manner. The availability of extensive data or the online knowledge of the network variables, even in countries with a high degree of diffusion of DHNs, cannot be taken for granted.

2.3 European Research and Innovation projects

Since scientific papers and reviews seldom take into consideration research and innovation projects funded by national and international institutions [13, 105], it is essential to investigate also these actions, in order to complete the state-of-the-art literature framework outlined in the previous sections. Indeed, including such activities can be helpful for researchers and practitioners in the energy sector for several reasons:

- to provide an overview of the innovative results obtained by the cooperation of academic and industrial partners from different countries;
- to explore the potential of public engagement (i.e. participation of the public in energy-related research [106]), usually not included in technical papers, in the identification of technical solutions that are more attractive for customers;
- to keep track of the most recent practical applications, since international projects often propose the demonstration of technologies in operative environments up to market uptake;
- to identify the research gaps partially addressed or not yet considered;
- to understand the direction of the global interest and to locate future funding opportunities.

With these aims, this section summarizes the results from an overview of the research and innovation projects on smart heating and cooling networks funded by the European Union over the last few years. Extended details on the study can be found in [107]. A brief description of the methods and main outcomes is reported below.

The paper collects and analyzes the European projects relevant to the *Secure, Clean and Efficient Energy* challenge within the 8th Framework Programme for Research and Technological Development, known as Horizon 2020, which is going to be concluded at the end of 2020. The program is aligned with the European Union key priority for 2020 and the following years: an intelligent, sustainable and inclusive growth and the realization of a knowledge- and innovation-driven society. Coherently with the present thesis, the focus of the review concerns smart district heating networks as smart energy systems and, therefore, comprises their smart management, optimization and control strategies.

Similarly to three recent papers reviewing research projects on smart buildings [108], smart cities [109] and energy poverty [110], the method adopted consists of a detailed examination of the CORDIS (Community Research and Development Information Service) portal [111], which is the primary source for every project funded by the European Union over the last twenty years. The search has been conducted with the following keywords and their combinations: *District Energy*; *District Heating and Cooling*; *Smart Energy System*; *Optimization*; *Intelligent Control and Management*; *Predictive Control*; *Digitalization*. The selected 58 projects, further explored by analyzing websites, publications and cross-references, are collected in a database, each with a project profile sheet that gathers key information such as project dates, partnership, main goals and demonstration sites. In addition, the investigation underlines for each work action specific features relevant to the development of smart tools and approaches for heating and cooling networks as well as to their integration within the global energy system. They are mainly related to:

1. the energy vector analyzed in the project;
2. the main application (i.e. district level or building level);
3. the project output (i.e. software, library of models, optimization tool and business model);
4. the purpose of the work (i.e. planning, sizing, retrofitting, real-time control, management, diagnosis, MPC);
5. additional methods, e.g. machine learning, peak shaving, renewable energy integration.

The characteristics of each project as well as the highlighted features are detailed by comprehensive tables in [107], while the main quantitative results of the analysis are reported in the following paragraphs.

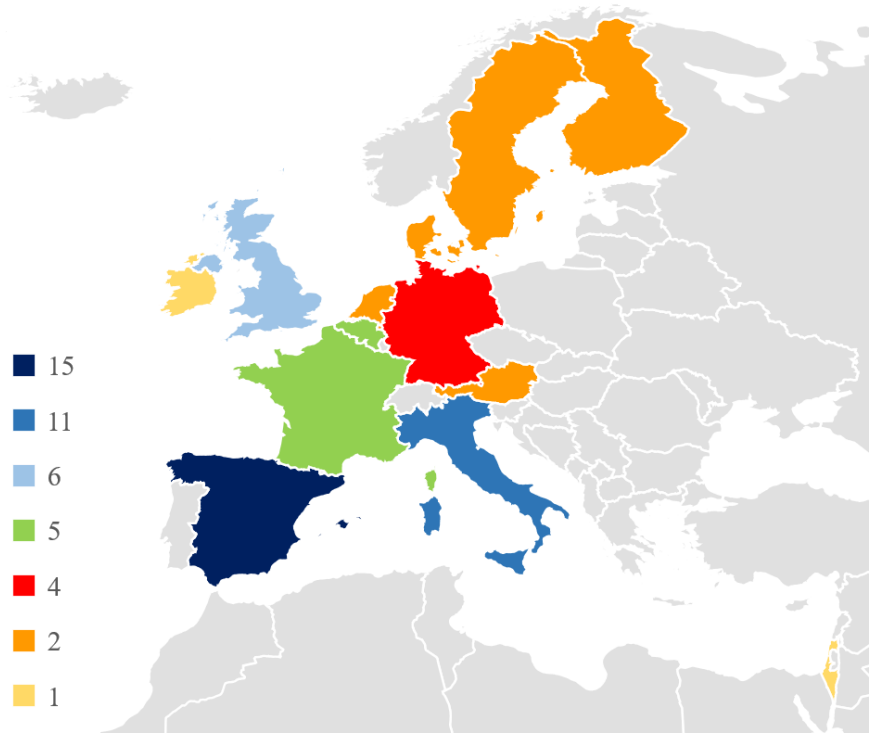

(a)

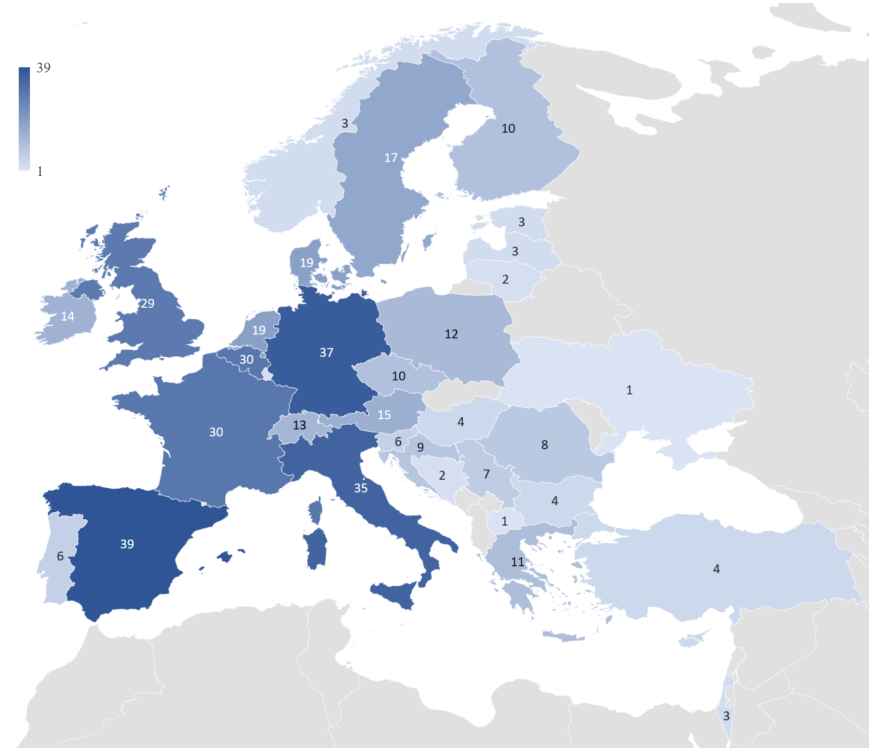

(b)

Fig. 2.2. Number of projects (a) per coordinator country and (b) per participating country.

Fig. 2.2a and Fig. 2.2b illustrate the geographical distribution of the project coordinators and project partners, respectively, showing that most innovative works are located in western and northern Europe, where thermal networks are more widespread. Nevertheless, almost all countries participate to at least one project, demonstrating the increasing attention paid to smart district heating and cooling all over Europe and the importance of collaborative actions.

The analysis of the specific features tackled by the projects is reported in Fig. 2.3. Due to the focus of the study, the most exploited energy vector is heating combined with cooling technologies. However, it is possible to recognize a trend toward sector integration, as six actions propose a global urban energy system by exploiting the synergies between heating, cooling, electricity and natural gas at the same time. The same can be observed regarding the main application, since 20 projects integrate the building level with the district level, providing methods that can be implemented to an energy system in its entirety, from energy conversion to end-user supply. The trend toward the digitalization of the sector is shown by the main outcomes, as more than half of the projects plan to develop a library of models, software platform, or web application for several purposes, e.g. automatically managing and monitoring the system. Fewer works focus on smart real-time control strategies, such as MPC, which, therefore, deserves to be further explored in its applicability to district heating.

This overview of European projects also leads to the identification of four key drivers that will be paramount in future research and innovation on smart district heating:

1. Digitalization. The energy sector can benefit from new ICT tools and data-driven techniques (e.g. data mining, machine learning) in order to achieve smarter systems. For instance, innovative real-time control strategies, which require online data processing and computationally efficient algorithms, are enabled by the synergic match (e.g. MPC) between physics-based system modeling and the latest developments in programmable controllers, innovative software and hardware architectures.

2. Sector integration. The conversion of energy into the form that is most cost-effective or energy-efficient for the global system (depending on the actual boundary conditions) will lead to optimal exploitation of RES and energy saving. For this purpose, the integration of different energy domains (i.e. heating and cooling, electricity, natural gas) and new management strategies to optimally exploit their synergies will be key developments for future energy

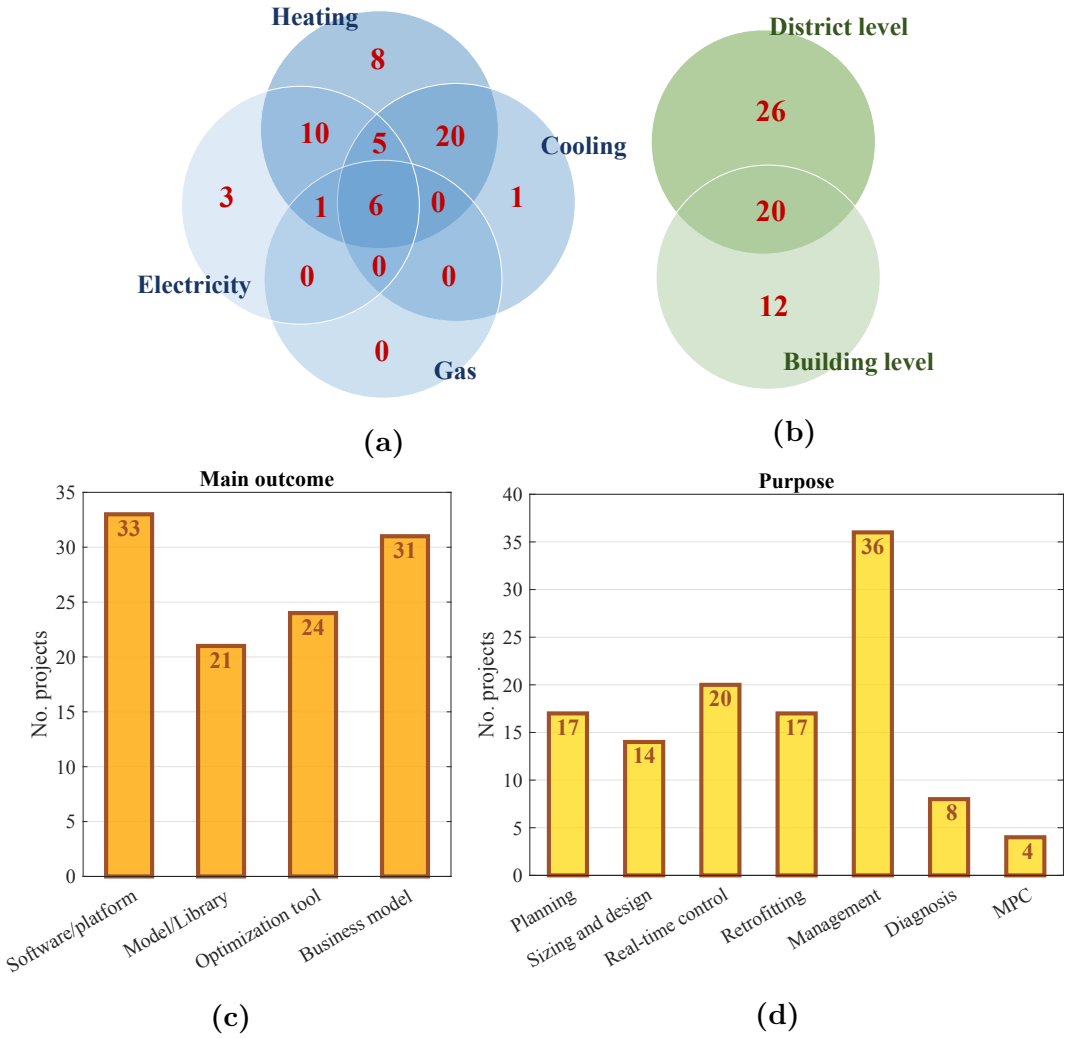

Fig. 2.3. Number of projects per (a) energy vector, (b) main application, (c) outcome and (d) purpose.

systems.

3. Decarbonization. Since a 100 % renewable energy system requires storage technologies to be strongly implemented, it will be necessary to investigate also unconventional types of storage, such as building thermal capacity in large-scale districts.

4. Resilience. It is of utmost relevance due to the COVID-19 containment measures that have greatly affected the global energy system [112], which will have to be able to adapt to other unpredictable global events that are likely to occur in the future.

Although the funding opportunities within Horizon 2020 are going to end in

2020, these research topics are expected to be at the forefront of innovation also over the next decade, in which the next programme approved by the European Commission, named Horizon Europe, will take place [113].

2.4 Novelties of the thesis

From the overview drawn in the previous sections, it can be concluded that suitable reduced-order model and computationally efficient optimization algorithms are of key importance to promote and realize the full potential of smart controllers in heat distribution. Furthermore, scalability is an essential feature that would enable a modular expansion of MPC to different system layouts and sizes, ensuring its long-term success [97].

Based on these research gaps, the present thesis aims to develop innovative methods for MPC application at small-scale and large-scale levels. In particular, it aims to introduce the following novelties:

- a *deterministic model* of building and district heating branch that does not require specific knowledge of the system and is readily extendable to multiple end-users in **small-scale DHNs**;
- a novel and computationally fast *optimization algorithm* for online control of **small-scale DHNs**;
- a *multi-agent hierarchical MPC architecture* (exploiting the mentioned elements) demonstrated in a **small-scale DHN** by means of an in-house modular simulation platform;
- a *reduced-order scalable model* of the aggregated consumers in **large-scale DHNs**, which includes their heat capacity for demand side management and online control;
- a novel *optimization algorithm* which optimally manages heat delivery to aggregated consumers and network operation of **large-scale DHNs**.

All characteristics elements of MPC control are therefore investigated in a general way (Section 4) and applied to specific case studies with different complexity (Section 5). This may represents a considerable step toward widespread implementation of smart control in DHNs.

3 Theoretical background

After outlining the research gaps and the need for smart controllers for DHNs, it is important to provide the theoretical fundamentals and frame the development of novel methods. This section reports the basic theoretical tools which lay the foundations for the new methods proposed in this thesis. Since the main parts of an MPC are models and optimization algorithms, a first description and classification of mathematical models according to their characteristics is followed by an outline of optimization techniques, useful for solving energy-related optimization problems. Lastly, general information on traditional control strategies is given together with a specific focus on the advanced methods of MPC.

3.1 Modeling

According to the operational definition by Witelski and Bowen, a mathematical model is a "*useful, practical description of a real-world problem, capable of providing systematic mathematical predictions of selected properties*" [114]. Hence, models have two basic features that make them useful in scientific research: they are *descriptive*, as they allow the user to simulate and gain knowledge on a real system for which experimentation cannot be performed (e.g. it is expensive and dangerous, or the system still have to be conceived); and they are *predictive*, as they are able to anticipate the behavior of the considered process or system and, thus, to provide quantitative and qualitative insights for its technical improvement and optimization.

Mathematical modeling is the procedure that brings to translating the real world problem into a mathematical problem, to finding the solution with various mathematical tools and to interpreting the results, which provide an approximated solution of the real problem. The degree of this approximation is correlated with the level of detail required by the objective of the study. This is generally brought by a compromise between the accuracy of the representation and the computational effort needed to solve the problem.

The process of developing a mathematical model of a physical system such as an energy system can be split into the following phases:

1. Problem identification and definition: the objective, relevant phenomena, constraints, required quality and maximum computational cost are defined.

2. Problem simplification: different aspect are included or neglected through assumptions in order to approximate the problem in an effective way.

3. Problem translation into a mathematical form as a system of equations and/or inequalities, generally deriving from physical principles (e.g. conservation laws) and constraints.

4. Model analysis, e.g. solution with analytical or numerical methods and sensitivity analysis on the model parameters.

5. Interpretation of the results and comparison with the system expected behavior, in order to evaluate the model coherency with the real world.

6. Model validation, generally done through a comparison with experimental or simulation data. This step is required to establish the validity of the model predictions regarding the real system.

7. Model application to achieve the objective of the study.

3.1.1 State-space representation

Dynamic systems can typically be represented by state-space models [115], which consist of an input/state/output formulation schematized in Fig. 3.1.

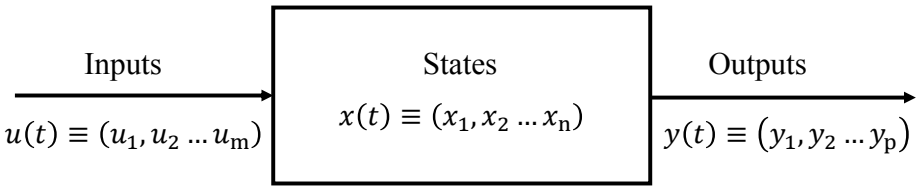

Fig. 3.1. Generic state-space model.

This type of models is characterized by:

- State variables x, which correspond to the minimum set of variables required to describe the system configuration and its behavior over time.
- Input variables u, also known as exogenous variables, which are the external phenomena that influence the system. The inputs can be manipulated, if they can be changed with an actuator to control the system, and non-manipulated, also named disturbances, if they cannot be changed.
- Output variables y, which are the observable effects of the system.

The relationships between these variables are expressed by the state-space representation, which comprise a state function f (representing the evolution of the states when the inputs are applied) and an output function g:

$$\begin{cases} \frac{dx(t)}{dt} = f\left(x(t), u(t), t\right) \\ y(t) = g\left(x(t), u(t), t\right) \end{cases} \tag{3.1}$$

This form is well suited for the representation of energy systems, for which the conservation laws of e.g. mass, energy and momentum can be written. The balance of a generic physical quantity M in a control volume is:

$$\frac{dM(t)}{dt} = \sum_{\mathrm{i}} m_{\mathrm{i}}(t) + m_{\mathrm{s}}(t) \tag{3.2}$$

where $m_{\mathrm{i}}(t)$ are the flow rates of the quantity entering or leaving the control volume (with sign + and –, respectively), while $m_{\mathrm{s}}(t)$ is the source or sink (with sign + and –, respectively) of the quantity within the control volume. In this case, M is the state of the system and Eq. (3.2) is the state function.

3.1.2 Model classification

Mathematical models can be classified according to different criteria. As far as their aim is concerned, there can be detailed models for accurate simulation of a process or system, as well as simplified models for system optimization or control-oriented applications.

An interesting classification regards the various model features and is summarized in Table 3.1.

Table 3.1. Classification of mathematical models according to various features.

Feature	Classification	
Relationship between variables	Linear	Nonlinear
State over time	Static/algebraic	Dynamic
Time discretization	Discrete	Continuous
Space discretization	Lumped	Distributed
Variable randomness	Deterministic	Stochastic
Model type	Black-box	White-box

Relationship between variables A model is linear if all relationships between

generic variables ϕ_1 and ϕ_2 are linear operators $\mathcal{L}$ and, therefore, satisfy the following property:

$$\mathcal{L}\,(\phi_1 + \phi_2) = \mathcal{L}\,\phi_1 + \mathcal{L}\,\phi_2 \tag{3.3}$$

If this property is not satisfied, the model is nonlinear. The state-space form Eq. (3.1) of a linear model can be expressed in matrix form, as follows:

$$\begin{cases} \frac{dx(t)}{dt} = A(t)\,x(t) + B(t)\,u(t) \\ y(t) = C(t)\,x(t) + D(t)\,u(t) \end{cases} \tag{3.4}$$

The model is time-invariant if the matrices A, B, C and D are constant parameters over time, while it is time-variant otherwise.

State over time A model is dynamic if the system states are subject to time-dependent changes and can be represented by differential equations, such as Eq. (3.1). Dynamic models maintain the memory of the state past evolution, which influences its future evolution. On the other hand, a model is static if the states remain constant, the system equilibrium is calculated and, hence, it is described only by algebraic equations (there is no state function):

$$y(t) = g\,(u(t), t) \tag{3.5}$$

Time discretization A model is continuous if it is characterized by time-continuous variables and functions, while it is discrete if its variables and functions are determined for given time-steps. Finding the exact analytic solution of continuous problems can be challenging and feasible only for simple sets of problems. Hence, oftentimes these problems are tackled with approximated numerical methods, which require the discretization of the time coordinate. The continuous and discrete models are basically equivalent for smaller amplitudes of the time-step Δt. This approximation can be done mainly with two one-step methods [116]:

- Forward Euler method, which is an explicit method based on the forward difference derivative. The approximation quality depends on Δt and it might lead to instability. However, since it requires only the knowledge of the variables at the current time step, it is easy to solve and computationally fast. The discrete state function becomes:

$$x(t+1) = x(t) + f\,(x(t), u(t), t)\;\Delta t \tag{3.6}$$

- Backward Euler method, which is an implicit method based on the backward difference derivative and is unconditionally stable. However, since it needs the evaluation of the variables at the following time step, numerical iterative methods (with greater computational effort) are required for its solution. The discrete state function becomes:

$$x(t+1) = x(t) + f\left(x(t+1), u(t), t\right)\ \Delta t \tag{3.7}$$

Space discretization A model is lumped if its variables are considered uniform in space and, therefore, spacial variations are not taken into account, and it is characterized by ordinary differential equations. In this case, time t is the only independent variable. On the other hand, a model is distributed if its parameters are subject to variations along different space dimensions, and it is described by partial differential equations [115]. It is quite common, however, to simplify distributed models by neglecting the spacial distribution, if its effect is not relevant to the problem aim, or by implementing a discretization over the space coordinates.

Variable randomness A model is deterministic if the relationships between its variables are completely determined, thus it performs the same way for given initial conditions. It is instead stochastic if the variables are described by probability distributions, which greatly affect the system behavior.

Model type As already mentioned in Section 2.1, black-box models describe systems for which there is no *apriori* information and the relationships between variables are given by empirical correlations. They are typically developed by means of identification procedures with experimental data [117] and do not provide insights on the physical phenomena that characterize the system. On the other hand, in white-box models the relationships between variables are entirely based on known physical principles and, for this reason, can be complex to determine and to solve. Gray-box models lie in-between these two types, as they are described by simpler physics-based correlations (generally identified with data), which carry on knowledge on the underlying dynamic phenomena [118].

3.2 Optimization

"*Optimization is the minimization or maximization of a function subject to constraints on its variables*" [119]. It is a fundamental tool in the analysis of physical systems and in decision-making. Indeed, it makes it possible to identify the values

of the system *variables* that give its best performance according to a quantitative objective, namely *objective function* or *cost function* (e.g. minimum cost or minimum energy consumption). The choice of these optimal values is typically subordinate to a set of limitations, namely *constraints*, which represent the physical or operational boundaries of the system.

A generic optimization problem can be formulated in the following way:

$$\min_{x \in \mathbb{R}^n} J(x) \qquad \text{subject to} \quad \begin{cases} h_{\mathrm{i}}(x) = 0, \ \mathrm{i} = 1, 2 \dots m \\ g_{\mathrm{j}}(x) \geq 0, \ \mathrm{j} = 1, 2 \dots p \end{cases} \tag{3.8}$$

where x is the vector of variables, J is the objective function, and h_{i} and g_{i} are the equality and inequality constraints, respectively.

The first step of an optimization procedure is the development of a suitable model of the system to be optimized (Section 3.1), in order to select the proper variables, constraints and objective. The second step is the solution of the deriving problem by means of an optimization algorithm. This should be able to identify a solution with good accuracy for multiple problems in their class, with a feasible computational time and memory. There is a large variety of techniques suitable for the solution of optimization problems, depending on the problem formulation and on the required computational performance.

A set of possible classifications of optimization problems based on different criteria [119] is reported in Table 3.2 and clarified as follows:

- A problem is **static** if the decision variables are optimized for a given time instant and it is described by Eq. (3.8), while it is **dynamic** if the decision variables actively change in time, and their values are optimized over an entire time interval. In the latter case, the optimal trajectory of the variables used to actively control the system has to be found and a suitable representation is the state-space form (Eq. (3.5)).

- A problem is **continuous** if the variables are allowed to be real numbers, while it is **discrete** or integer if at least one of the variables is integer or binary.

- A problem is **unconstrained** if there are no equality and inequality constraints, while it is **constrained** otherwise. Frequently, the latter can be reformulated as an unconstrained problem in which the constraints are replaced by penalty factors added to objective function, in order to discourage constraint violations.

- A **global** optimization problem seeks the global optimum, which is the point with the lowest value of the objective function among all feasible points. Oftentimes, however, this is difficult to find, especially in problems with complex structures. Hence, in these cases, **local** optimization seeks a local optimum, which is a point with a value of the objective function lower than all other feasible nearby points.

- Similarly to the mathematical model classification, optimization problems can be **deterministic**, if their models are completely known, or **stochastic**, if their models include uncertain quantities and the produced solution optimizes the *expected* performance of the model.

Table 3.2. Classification of optimization problems according to various features.

Feature	Classification	
Optimization time	Static	Dynamic
Variable type	Discrete	Continuous
Presence of constraints	Unconstrained	Constrained
Optimum type	Local	Global
Problem randomness	Deterministic	Stochastic

The analytic solution of the optimization problem Eq. (3.8) by means of a direct method [120] is unfeasible in the vast majority of cases, due to the potential complexity of the functions or to the large computational burden. Therefore, numerical algorithm are exploited to find a numerical solution, by relying on iterative procedures. They usually start from a candidate solution and generate a sequence of improved approximate estimations by means of different methods until a given termination criterion for convergence is satisfied [121].

There are two main classes of numerical optimization algorithms for static problems:

- **Iterative methods** are based on a mathematical approach to the problem. The way in which the iterative procedure estimates the solution relies on an approximation of the objective function and its first and second order derivatives (i.e. gradient and Hessian). This evaluation tends to increase the computational complexity of the techniques. Indeed, for a function with n variables, the gradient approximation requires at least $n + 1$ function evaluations, while the Hessian approximation at least n^2. For these reasons,

such techniques generally provide good accuracy and robustness, but may become ineffective in presence of large nonlinearities. The most common strategies are line search methods and trust region methods. Full details are extensively treated in many textbooks [119, 122].

- **Heuristic methods** are based on a set of simple high level rules and procedures which should direct the iterative search toward the optimum, without any knowledge on the analytic structure of the objective function and constraints. This allows the problem to be solved more quickly than classic methods but, on the other hand, it does not mathematically guarantee convergence to the solution. Hence, this class of methods constitutes a trade-off between accuracy/optimality and computational feasibility. These techniques are classified according to their heuristic rules, which take inspiration from natural phenomena (e.g. genetic algorithms [123]) or social sciences (e.g. Particle Swarm Optimization [124], Ant Colony Optimization [125]). Full details are provided in [126].

In the following sections, a closer look at the three types of optimization problems obtained in the present thesis and to the related algorithms is reported. For each algorithm, the advantages and limitations with regard to the optimization of energy systems are reported.

3.2.1 Dynamic Programming

A dynamic optimization problem consists of determining an optimal control law for the dynamic system which, if implemented, optimizes a given performance criterion over a given time horizon $[t_0; t_\mathrm{f}]$. The system is represented by a state-space model. The resulting problem, called optimal control problem [127], can be written in the following form:

$$\min_{u(t)} J(x_0, u(t)) \qquad \text{subject to} \quad \begin{cases} \frac{dx(t)}{dt} = f\left(x(t), u(t), d(t), t\right) \\ x(t_0) = x_0 \\ x(t_\mathrm{f}) \in X_\mathrm{f} \\ x(t) \in X \quad \forall\, t \in [t_0; t_\mathrm{f}] \\ u(t) \in U \quad \forall\, t \in [t_0; t_\mathrm{f}] \end{cases} \tag{3.9}$$

where x_0 is the initial condition, and X_f, X and U are the feasible sets of final state, states and inputs, respectively. There can be constraints also on the input rate of change, but they are here omitted without losing generality. It is also

possible to notice that the inputs are decomposed into manipulated variables $u(t)$ and disturbances $d(t)$.

The input and state constraints which generate the input and state feasible sets generally include the physical limitations on these variables and can be expressed as box constraints, as follows:

$$u_{\min} \leq u(t) \leq u_{\max} \tag{3.10a}$$

$$x_{\min} \leq x(t) \leq x_{\max} \tag{3.10b}$$

Hence, the solution of this problem consists of calculating the optimal control trajectory u^* that generates the optimal system performance according to optimality criterion J in the form of Eq. (3.11), while considering the constraints on the variables.

$$J(x_0, u(t)) = G(x(t_\mathrm{f})) + \int_{t_0}^{t_\mathrm{f}} H\left(x(t), u(t), d(t), t\right) \tag{3.11}$$

Since this is a cost functional, analytical methods (based on calculus of variations) to find the problem solution are feasible for simplified problem formulations [121].

On the other hand, more complex nonlinear problems can be efficiently solved by means of Dynamic Programming (DP), which is a numerical method with the Bellman's principle of optimality as its foundation [128].

The deterministic DP algorithm requires the discretization of the time scale in N steps. The state function becomes:

$$x_{\mathrm{k}+1} = f_\mathrm{k}\left(x_\mathrm{k}, u_\mathrm{k}, d_\mathrm{k}\right) \qquad k = 0, 1 \ldots N-1 \tag{3.12}$$

while the cost function becomes:

$$J_\pi(x_0) = G_\mathrm{N}(x_\mathrm{N}) + \sum_{\mathrm{k}=1}^{N-1} H_\mathrm{k}\left(x_\mathrm{k}, \mu_\mathrm{k}(x_\mathrm{k}), d_\mathrm{k}\right) \tag{3.13}$$

where $\mu_\mathrm{k}(x_\mathrm{k}) = u_\mathrm{k}$ represents the feasible inputs that can be applied at state x_k. An admissible control law or control policy π comprises a sequence of feasible inputs at each time-step of the optimization horizon:

$$\pi = [\mu_0, \mu_1 \ldots \mu_{\mathrm{N}-1}] \tag{3.14}$$

Hence, the deterministic problem is solved by calculating the optimal policy π^* which minimizes the cost $J_\pi(x_0)$ starting from the initial condition x_0.

The aforementioned principle of optimality states that the tail of an optimal trajectory of an optimization problem is still optimal for the tail subproblem. A

commonly used explanatory example clarifies this principle [121]: if the fastest route between point A and point B passes through a third point C, then the portion of this route from C to B is also the fastest route from C to B (Fig. 3.2). Similarly, if the policy $\pi^* = \left[\mu_0^*, \mu_1^* \dots \mu_{\mathrm{N}-1}^*\right]$ is optimal for the original problem, then the truncated policy $\left[\mu_{\mathrm{k}}^*, \mu_{\mathrm{k}+1}^* \dots \mu_{\mathrm{N}-1}^*\right]$ is optimal for the tail subproblem with cost $J_\pi(x_{\mathrm{k}})$.

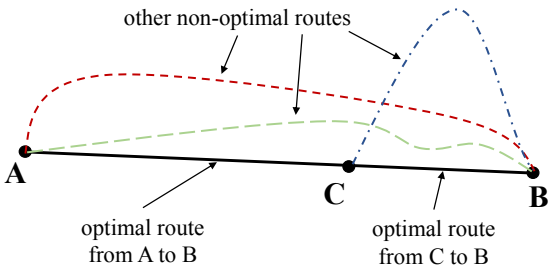

Fig. 3.2. Example of the Bellman's principle of optimality: the optimal route between A and B passes through C, thus the portion of that path between C and B is also the optimal route between C and B.

This concept can be exploited to find an optimal control policy by dividing the global problem into smaller subproblems, which are solved recursively proceeding backward in time (from the final to the initial state). At each iteration, the results from the tail subproblem are stored in memory and exploited for the following step. This allows the computational time to be reduced significantly.

In many cases, it is not possible to obtain an analytical solution. Nevertheless, a fully numerical DP algorithm can be developed and exploited. This relies on the discretization of the whole state-space of the optimization problem. For each time-step k, the feasible states $x_{\mathrm{k,i}}$ are considered, with the index i representing the points of the state grid. The solution is found by means of a time-backward iterative calculation that, at each iteration k, solves the optimal control problem involving the subproblem from time-step k to time-step $N-1$. The optimal cumulative cost $J_{\mathrm{k}}(x_{\mathrm{k,i}})$ (from the current step to the end of the optimization horizon) and the related optimal inputs $u_{\mathrm{k}}(x_{\mathrm{k,i}})$ are evaluated for each feasible state $x_{\mathrm{k,i}}$ and stored in memory:

$$J_{\mathrm{N}}(x_{\mathrm{N,i}}) = G_{\mathrm{N}}(x_{\mathrm{N,i}}) \tag{3.15a}$$

$$J_{\mathrm{k}}(x_{\mathrm{k,i}}) = \min_{u_{\mathrm{k}}} \left[H_{\mathrm{k}}\left(x_{\mathrm{k,i}}, u_{\mathrm{k}}, d_{\mathrm{k}}\right) + J_{\mathrm{k}+1}\left(f_{\mathrm{k}}\left(x_{\mathrm{k,i}}, u_{\mathrm{k}}, d_{\mathrm{k}}\right)\right)\right] \qquad k = N-1, \dots 2, 1 \tag{3.15b}$$

The procedure covers the entire time horizon and returns an optimal control map which contains the optimal inputs $u_{\mathrm{k}}(x_{\mathrm{k,i}})$ that should be applied if the system is in state $x_{\mathrm{k,i}}$ at time-step k. This map is finally exploited to identify the actual optimal control sequence $\left[u_0^*, u_1^* \dots u_{\mathrm{N}-1}^*\right]$ and optimal states $[x_1^*, x_2^* \dots x_{\mathrm{N}}^*]$ through a time-forward calculation that starts from the initial condition:

$$u_0^* = u_0(x_0) \tag{3.16a}$$

$$\begin{cases} x_{\mathrm{k}}^* = f_{\mathrm{k}}\left(x_{\mathrm{k}-1}^*, u_{\mathrm{k}-1}^*, d_{\mathrm{k}-1}\right) \\ u_{\mathrm{k}}^* = u_{\mathrm{k}}(x_{\mathrm{k}}^*) \end{cases} \qquad k = 1, 2, \dots N-1 \tag{3.16b}$$

A simplified example with one state variable T_{k} (i.e. temperature) is provided in Fig. 3.3 to clarify the procedure in an intuitive way. The optimization horizon comprises only three time-steps (i.e. 900 seconds each), at which the state can assume only the values represented in the figures. The input can assume only two directions which have the effect of increasing or decreasing the state of 1 °C. Each state transition is represented by a segment and characterized by a cost. The tail subproblems are solved recursively while the optimal cumulative cost is saved for each feasibe state (Figs. 3.3b and 3.3c). Finally, the optimal trajectory starting from the initial condition is selected (Fig. 3.3d).

The main advantages and limitations of this technique are shown in Table 3.3. One of the main drawbacks is the necessity to discretize the state-space, with consequent reduction in accuracy, though this limit can be overcome by refining the spacial grid. Moreover, the DP algorithm is affected by the so-called "curse of dimensionality" [121]. This indicates that an increase in the number of system states gives a significant increase in computational time and memory, as the number of function evaluations corresponds to the product of numbers of grid points per state, numbers of grid points per input, and number of time-steps.

Nonetheless, the DP is particularly appropriate for dynamic problems in which the objective function is to minimize the total cost, e.g. economic cost or energy consumption over the entire optimization horizon. It is not suitable with other types of objective function, involving e.g. minimization of the maximum value of a variable over the horizon, as in these cases the cumulative cost loses its significance.

A numerical function that solves generic deterministic DP problems with up to five state variables has been proposed by Sundström and Guzzella [129] and used in several applications [130–132]. In Section 4.2, an original fast numerical DP algorithm suitable for multi-agent control applications is presented.

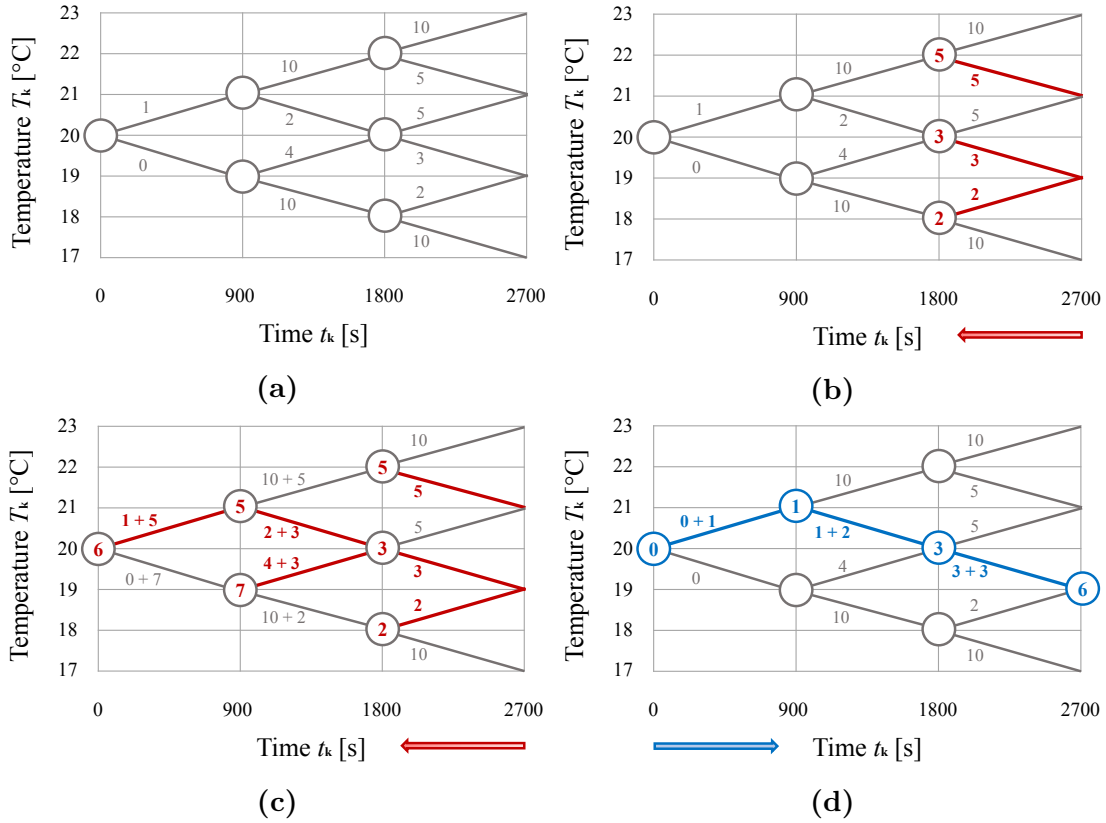

Fig. 3.3. Simplified example of the DP algorithm application. (a) Feasible system states at each time-step with state change and related cost; (b) solution of the optimal control problem of the last time-step; (c) optimal input map obtained from the time-backward calculation; (d) time-forward calculation returning the optimal trajectory.

Table 3.3. Summary of advantages and limitations of the Dynamic Programming algorithm.

Advantages	Limitations
• Global optimum guaranteed • Suitable for economic optimization • Straightforward implementation for dynamic problems • No restrictions on objective function and constraints • Nonlinearities easily handled	• Computational time increases with number of states and inputs • Discretization of states and inputs required for numerical solution • Potential influence of algorithm parameters on the solution

3.2.2 Linear Programming

The specific form of the static optimization problem Eq. (3.8) in which both the objective function and the constraints are linear is called Linear Programming (LP). This problem presents the property of convexity, which makes it significantly easier to solve in theory and practice [119].

LP problems can be written in standard form, regardless of the constraints and variable signs:

$$\min_x c^T x \qquad \text{subject to} \quad \begin{cases} Ax \leq b \\ x \geq 0 \end{cases} \tag{3.17}$$

where c and b are vectors of known coefficients (in $\mathbb{R}^n$ and $\mathbb{R}^m$ respectively), and A is an $n \times m$ matrix of coefficients. Even problems with particular nonlinear objective functions, involving e.g. minmax/maxmin forms and absolute values, can be reported to the previous formulation by introducing *slack* variables.

The solution of this problem can be found through two numerical algorithms [119]:

- The **simplex algorithm** belongs to the class of active set methods and guarantees the global optimum to be found, if it exists. Indeed, the solution is identified as one of the vertices of the feasible polytope, which is the n-dimensional space determined by all feasible points (represented for a generic LP with two dimensions and three constraints in Fig. 3.4). The algorithm formulates reduced versions of the original problem in an iterative way, each containing a subset of the constraints. Eventually, the procedure leads toward the actual problem solution. This algorithm has as its foundation the duality theory, according to which each LP problem (i.e. primal) can be converted into a dual problem providing an upper bound to the optimal solution of the primal, and viceversa.

- The **interior-point algorithm** approaches the boundary of the feasible polytope from the interior or exterior, but never actually lies on the boundary of this region. For this purpose, it approximates the inequality constraints through proper barrier functions able to push the tentative solution inside the feasible polytope. A sequence of iterations progressively relaxes the barrier penalization, until the boundary is met.

These algorithms can be readily tackled by reliable solvers typically available in many commercial softwares [133]. Complete mathematical details are extensively

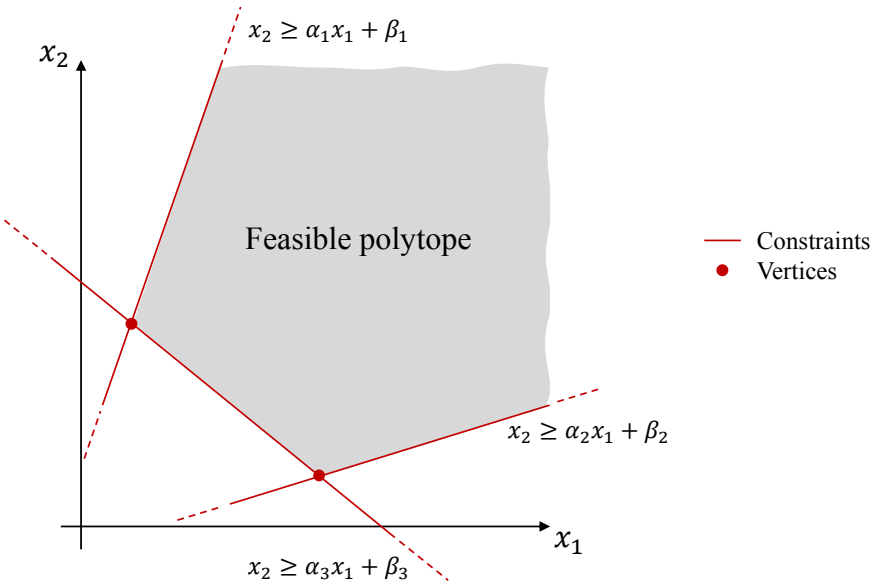

Fig. 3.4. Qualitative representation of the feasible polytope of a generic Linear Programming problem with two variables (x_1 and x_2) and three constraints (red lines).

described in [119] while a summary of advantages and limitations of this technique is reported in Table 3.4.

A noteworthy type of LP problems, particularly common in optimization of energy systems [134], is Mixed Integer Linear Programming (MILP), in which the vector of variables comprises both real and integer quantities. In this case, proper algorithms such as branch and cut or some heuristics are adopted for the solution.

Table 3.4. Summary of advantages and limitations of Linear Programming.

Advantages	Limitations
• Global optimum guaranteed • Discretization of states and inputs not required • Efficient algorithms available in many commercial softwares	• Nonlinearities not handled • Linearization of nonlinear parameters introduces potential errors • Number of optimization variables increases for dynamic problems

3.2.3 Nonlinear Programming

The generic form of the static optimization problem Eq. (3.8) in which both the objective function and the constraints are nonlinear is called Nonlinear Programming (NLP). Its solution presents more challenges compared to LP problems, as the convexity is not guaranteed.

An optimal solution can be reached through many different numerical methods, classified according to the nature of the objective function and constraints. For instance, the original problem can be replaced by a sequence of simplified subproblems obtained by approximating the objective function with a quadratic form and the constraints with linear forms. This method is called Sequential Quadratic Programming. Furthermore, in similarity with LP algorithms, interior-point methods are very effective and they are also included within various softwares [133, 135]. The summary of advantages and limitations of this technique is reported in Table 3.5.

Table 3.5. Summary of advantages and limitations of Nonlinear Programming.

Advantages	Limitations
• Global optimum guaranteed • Nonlinearities handled • Discretization of states and inputs not required	• Number of optimization variables increases for dynamic problems • Available algorithms may not achieve convergence • Potentially high computational time

3.3 Control

Controlling a dynamic system (i.e. plant) deals with developing its *control system*, which is a set of elements that regulate the variables of interest. Generally, the output variables of a system need to follow a certain reference over time, thus the controller manipulates the input variables in order to obtain the desired effect, despite the external disturbances.

In this section, the traditional types of control systems are discussed with reference to dynamic system models in the state-state form outlined in Section 3.1.1. Then, the advanced control strategy of Model Predictive Control, which is applied to district heating networks in this thesis, is described.

3.3.1 Control system classification

Firstly, it is worth reminding that the plant state is characterized by the state variables x. The output variables y are measurable effects which have to follow a reference or set-point y_{SP}. The inputs variables u are also called manipulated variables as they can be actively changed by an actuator in order to control the plant. The disturbances d are external inputs that cannot be manipulated, but in some cases can be measured and disturbance rejection strategies can be activated to improve control performance.

The control systems can be classified with many different criteria, some of which are summarized in Table 3.6 and discussed below.

Table 3.6. Classification of control systems according to various features.

Feature	Classification	
Input computation	Open-loop	Closed-loop
Approach to disturbance	No rejection	Feed-forward
Control architecture	Centralized	Distributed
Problem randomness	Deterministic	Stochastic/Robust

There are two main types of control loops, depicted in Fig. 3.5:

- **Open-loop** control system, in which the control action is defined based only on the set-point, independently from the process output. The input relies on a predefined static correlation (e.g. look-up table) between the set-point and the input value applied to the process. The performance of this controller depends entirely upon the accuracy of this correlation and cannot be corrected if there is any error.

- **Closed-loop** control system, or **feedback** control, in which the control action depends on the measured process output y_{m}. The deviation between the measured output and the set-point is the error e, which is used by the controller to compute the input.

Another distinction can be based on the disturbance rejection property: if this is present, the input is calculated also as a function of the measured disturbance, and the controller is also called **feed-forward**.

The feedback controller that is most widely implemented in industry due to its simplicity is Proportional-Integral-Derivative (PID) control [136], represented in

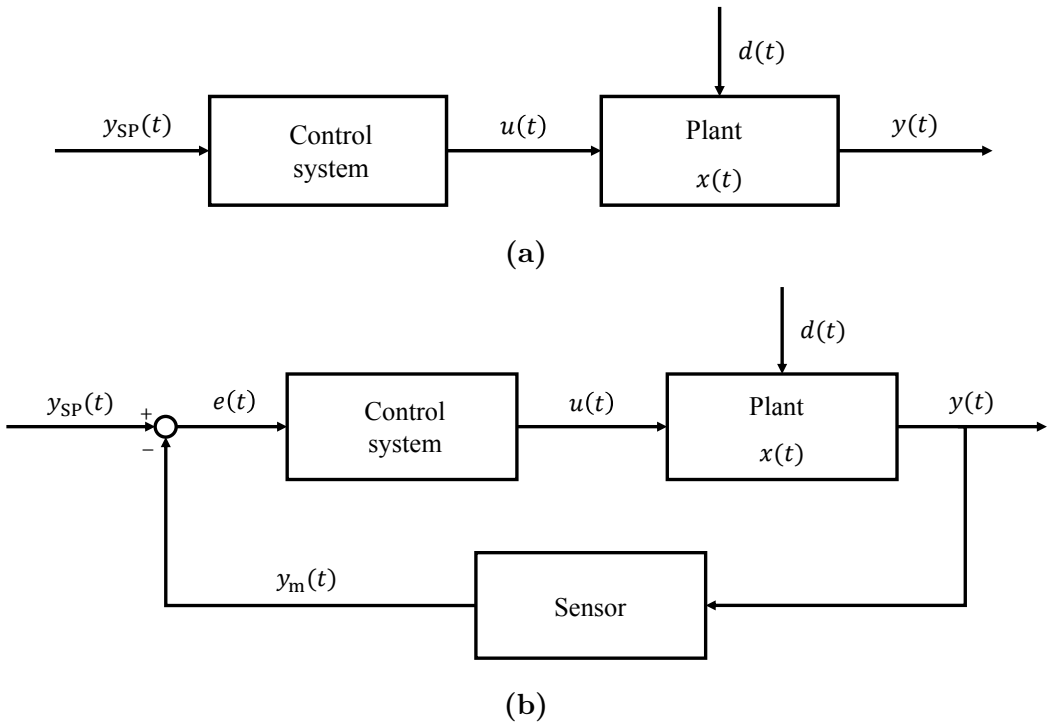

Fig. 3.5. Main types of control loops: (a) open-loop control system and (b) closed-loop control system.

Fig. 3.6. The control action is indeed based on three terms, which are proportional to the error, to its integral (in order to consider the historic cumulative value of the error) and to its derivative (in order to estimate the future trend of the error), respectively, according to Eq. (3.18):

$$u(t) = k_{\mathrm{P}}\, e(t) + k_{\mathrm{I}} \int_0^t e(\tau) d\tau + k_{\mathrm{D}} \frac{de(t)}{dt} \tag{3.18}$$

The controller becomes P and I if there is only the proportional or integral term, respectively, while it is PI if both terms are present.

The PID control presents many limitations. Firstly, it is only able to manage one input at a time and, hence, is not suitable for multi-input-multi-output (MIMO) systems. Secondly, it is not able to include constraints on the variables. Moreover, optimal control according to a performance objective is not allowed. Such drawbacks can be overcome by advanced control strategies such as MPC.

A further classification of control strategies, also illustrated in Fig. 3.7, can be done according to the control architecture:

- In the **centralized** architecture, the plant is entirely managed by a centralized processor which is responsible for all tasks, i.e. data acquisition, contin-

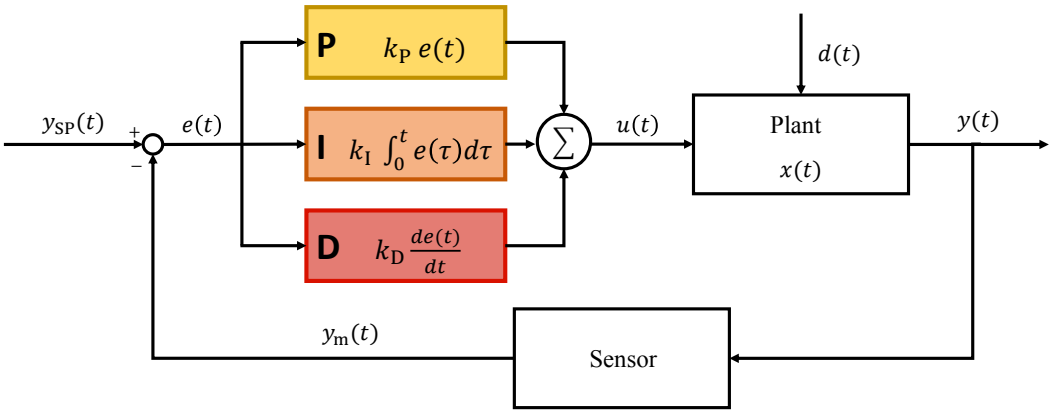

Fig. 3.6. Schematic representation of a PID control system.

uous control, process supervision and scheduling, external communication. However, this approach limits the application of optimal control to large-scale distributed systems, which may impose a significant computational burden as well as high connectivity levels [137]. Moreover, this architecture is less flexible and reliable, as a failure may affect the global plant.

- In the **distributed** architecture, the plant is divided into various subsystems and the related low-level control tasks (i.e. data acquisition and control of actuators) are performed by dedicated processors distributed locally. This mitigates potential failures in individual processors, which affect only a subsystem, and distributes the computational burden. If each processor is independent from the others, the system is horizontally distributed. Otherwise, it is hierarchical (Fig. 3.7b) when there is a supervisory controller that communicates with the low-level controllers and is dedicated to high-level tasks, i.e. system optimization, supervision and scheduling.

The latter architecture can also be referred to as **multi-agent hierarchical**. As a matter of fact, each low-level control module can be seen as an intelligent active agent with given objectives [138, 139], while being coordinated by the supervisory module. This approach is adopted in this work to develop and apply a smart controller for small-scale DHNs.

The last classification operated in this section is a direct consequence of the model and optimization problem classification regarding the system randomness. Indeed, a controller is **deterministic** if perfect knowledge of the variables is assumed. On the contrary, **stochastic** control provides and exploits information about the uncertainty in the evolution of system and disturbances (e.g. through

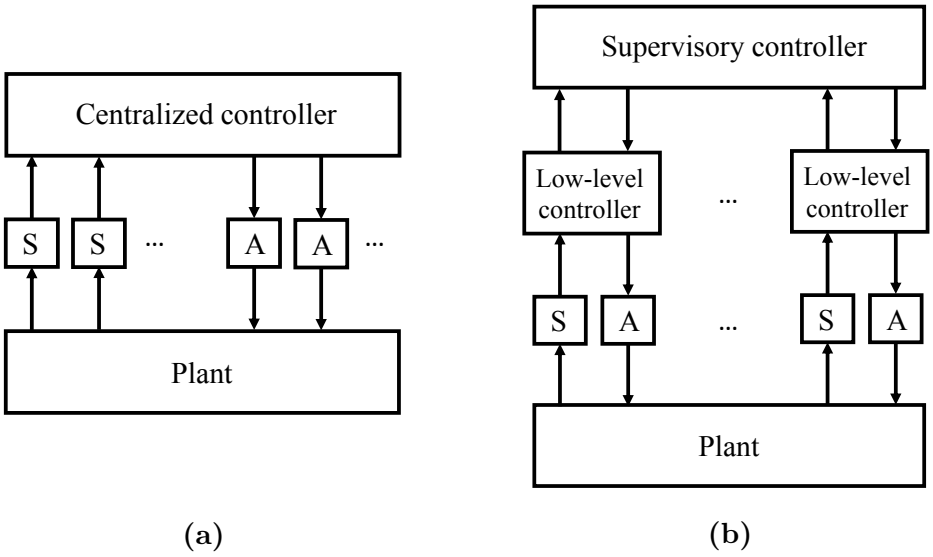

Fig. 3.7. (a) Centralized and (b) distributed hierarchical control architectures. S: sensor, A: actuator.

a stochastic model), while **robust** control only assumes that the uncertainty is subject to an upper boundary and guarantees stability and performance in the worst case scenario.

There are different methods to deal with uncertainty in control and decision making [140]. Here, the approach adopted in the MPC application with uncertainty in Section 5.2 is briefly presented. Basically, a set of scenarios or events is generated with an associated probability of occurrence, based on a model or an estimation of stochastic variables. Then, an optimal control problem is formulated with the same mathematical structure as in Section 3.2.1 but with a different objective. It consists of minimizing the expected value of the objective function by weighting the cost of each scenario s with the related probability ω_{s}, as in Eq. (3.19):

$$\min_{u(t)} \sum_{\mathrm{s}\in S} \omega_{\mathrm{s}}\, J_{\mathrm{s}}\left(x_0, u(t)\right) \tag{3.19}$$

Even though the solution obtained in this way may be suboptimal with respect to the deterministic problem, it allows the most probable events to be effectively considered.

3.3.2 Model Predictive Control

Model Predictive Control is a family of control strategies that uses a dynamic model of the plant to predict its behavior over a defined time horizon in the fu-

ture, namely prediction horizon. The knowledge of the dynamic system evolution is exploited to calculate an open-loop optimal control policy by solving a constrained optimization problem that minimizes the objective function starting from the actual initial condition of the plant. Furthermore, feed-forward MPC is obtained if this optimization relies also on the forecast of external disturbances and anticipates their effects. In the following sections, the described MPC strategies include the feed-forward logic. The main features indicated by the approach's denomination are reported in Fig. 3.8.

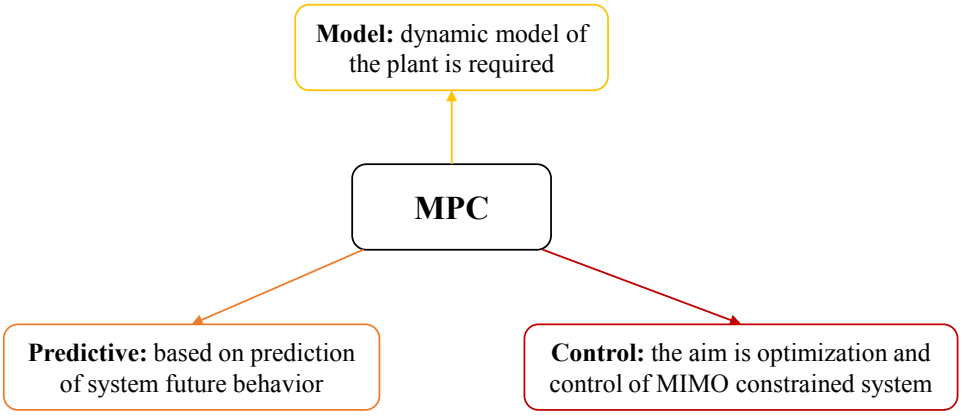

Fig. 3.8. Main features of Model Predictive Control.

If a numerical optimization algorithm is used to solve the problem and, for this reason, the prediction horizon is discretized in N_P time-steps, the output of the MPC is a sequence of control inputs that shall be executed to obtain the optimal behavior of the system. The implementation of this entire open-loop control policy, however, may produce an unsatisfactory performance, as it may be subject to modeling approximations, forecast inaccuracy and even unexpected events. In order to reduce the influence of these factors on the control performance and realize *implicit feedback*, MPC adopts the so-called *receding time horizon* strategy. It consists of implementing only the first element of the optimal control policy (corresponding to the current time-step) and discarding the remaining part. Then, after a time-step, the system variables are updated with new measurements and estimations, the prediction horizon is moved one step forward and the new optimization problem is solved. A schematic representation of the concept with the assumption that the system states are measurable is provided in Fig. 3.9.

In summary, at each control time-step k, the following procedure is continuously repeated:

1. Get the current system state, and new initial condition x_0, by measurements

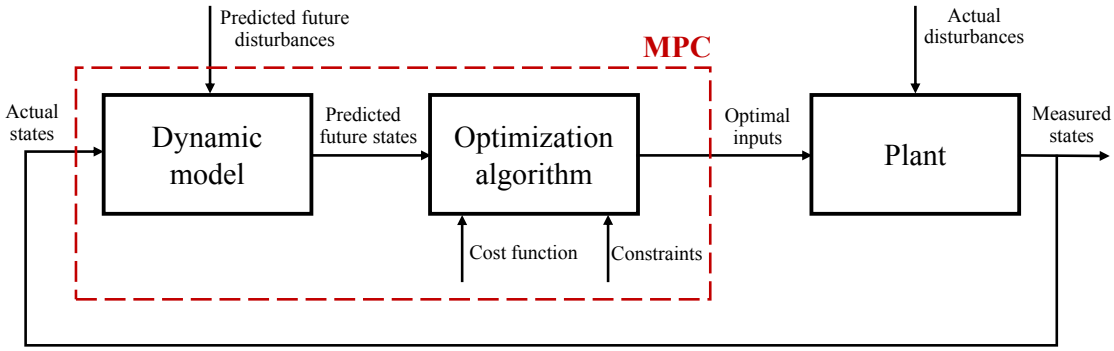

Fig. 3.9. Schematic representation of Model Predictive Control. A constrained optimization problem which relies on prediction of the plant future behavior by a dynamic model is solved. The resulting optimal inputs are used to control the plant until the optimization problem at the following time-step is solved.

or estimation.

2. Obtain the forecast of the external disturbance $d(t_\mathrm{k})$ over the next N_P steps.
3. Solve the dynamic optimization problem Eq. (3.9) in the discretized form, over the horizon $[t_\mathrm{k}; t_{\mathrm{k}+N_\mathrm{P}}]$.
4. Obtain the discrete optimal control policy u^* as a sequence of piecewise constant control signals which minimizes the cost J.
5. Control the real system with the first element u_0^*.
6. Move the prediction horizon to $[t_{\mathrm{k}+1}; t_{\mathrm{k}+N_\mathrm{P}+1}]$ and repeat the procedure with $k = k + 1$.

The computational burden of this strategy can be reduced by optimizing the inputs only for a control horizon of $N_\mathrm{C} \leq N_\mathrm{P}$ time-steps, while the remaining elements of the sequence are kept constant.

MPC presents several advantages over classical PID methods [141]:

- it can deal with MIMO processes;
- it inherently includes constraints on the variables, since they are directly encompassed within the optimization problem, thus avoiding the necessity of counter measures to compensate physical constraints;
- it introduces feed-forward control in a natural way to compensate for measurable or predictable disturbances;

- it provides feedback on the actual evolution of the plant and updates the control action accordingly;
- it needs limited knowledge of control, as its concepts are intuitive, thus it can be exported in practical applications.

The construction of an MPC controller requires, as its fundamental components, a dynamic model of the system and a computationally efficient optimization algorithm that is able to solve the optimization problem within a time-step. The model should be able to capture the main dynamics with good accuracy, but it should also be sufficiently simplified to be computed by the algorithm a large number of times per time-step. Hence, a trade-off has to be found between the model complexity and the necessity to obtain an optimal (or, in some cases, only feasible) control law within the length of a time-step. For these reasons, black-box and gray-box models are generally preferred in spite of detailed white-box models.

These features also give rise to the two main drawbacks of the technique. Firstly, a reliable dynamic model of the system might not be easily available, and its development can be time-consuming and case-specific. Sometimes, the partial knowledge of a system or the unavailability of a process model entail the use of empirical models, which are valid only for the operating conditions considered during the identification phase. Secondly, the MPC online control approach implies a significant calculation effort at every iteration, depending on the dimension of the problem. This has limited the MPC applications to the fields in which the processes are slow enough to enable online optimization [142]. In this regard, the relatively slow dynamics of thermal networks make them particularly suitable for MPC applications.

The method was first introduced during the 1980s [143] gaining relevant success mainly in the chemical and oil industry due to its ability to control and simultaneously optimize multi-variable processes subject to constraints, typical of the industrial field. Over the past decades, many control theory-oriented studies have provided a solid and rigorous foundation for the technique [144, 145].

Since its origins in the chemical field, MPC has mainly been studied and implemented with a **target tracking** configuration. In this problem type, the objective function penalizes the deviation of the system output from a reference set-point or trajectory [88] defined *apriori*, and is formulated as a quadratic function of the error between current and desired conditions (indicated with the subscript ref) as

follows:

$$J(x_0, u) = \sum_{\mathrm{k}=0}^{N_\mathrm{P}} \left(y_\mathrm{k} - y_\mathrm{k,ref}\right)^T Q_y \left(y_\mathrm{k} - y_\mathrm{k,ref}\right) + \sum_{\mathrm{k}=0}^{N_\mathrm{P}-1} \left(u_\mathrm{k} - u_\mathrm{k,ref}\right)^T Q_u \left(u_\mathrm{k} - u_\mathrm{k,ref}\right) \tag{3.20}$$

with Q_y and Q_u being the weights of the output and input deviations from the reference, respectively. The problem can be linear or nonliner depending on the controlled system dynamics (Section 3.1).

On the other hand, high-level controllers in hierarchical control architectures generally adopt **economic MPC** [146], in which the objective function is related to an economic parameter (e.g. process cost or energy consumption) rather than a deviation from the reference [147]. In this case, the supervisory MPC controller optimizes the global system and establishes the set-points for each low-level controller. This, in turn, can be implemented as a traditional feedback or as a target tracking MPC.

The economic MPC problem is usually characterized by nonlinear objectives and constraints, thus the numerical optimization algorithms for its solution are usually based on DP or NLP. Due to its versatility and flexibility of application in energy systems, economic MPC as a supervisory controller is the strategy selected for DHN applications in the present thesis. Its overview is concluded with the summary of advantages and limitations reported in Table 3.7, with specific reference to control of thermal networks.

Table 3.7. Summary of advantages and limitations of Model Predictive Control.

Advantages	Limitations
• MIMO control handled	• High modeling effort
• Constraints inherently handled	• Case-specific design procedure
• Feed-forward included	• High computational effort depending on algorithm and problem dimension
• Implicit feedback produced by receding time horizon	• Discretization of time scale
• Concomitant system optimization	• Unavailability of commercial tools to derive MPC models of thermal networks
• Compatible with relatively slow dynamics of thermal networks	

4 Method development

This section describes the novel methods developed in this thesis with the aim of setting up smart controllers for DHNs. The proposed original elements are:

1. **Small-scale DHNs**: a control-oriented model and a Dynamic Programming optimization algorithm suitable for MPC implementation [74];

2. **Large-scale DHNs**: a scale-free dynamic model for aggregating and characterizing different regions [148] and a two-stage Linear Programming-Nonlinear Programming optimization algorithm suitable for MPC implementation.

4.1 Small-scale district heating: model

The MPC framework requires a dynamic model that has to be computed many times at each time-step. Thus, the mathematical model used to represent each branch of small-scale DHNs within the DP algorithm is the simplified gray-box model of a building connected to the DHN through a substation and the related pipeline.

A schematic representation of a branch of DHN fed by a production unit (e.g. boiler), comprising the substation and end-user, is given in Fig. 4.1. The thermal power is transferred from the production unit to the building substation heat exchanger through underground distribution pipes. A mixing valve recirculates a part of the return water to regulate the mixing temperature.

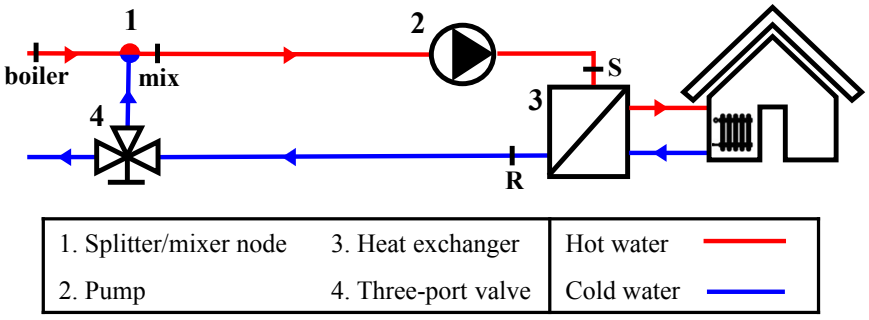

Fig. 4.1. Schematic representation of the distribution pipeline for each building. Pipe sections are defined as follows: **boiler**: boiler; **mix**: mixing; **S**: supply; **R**: return.

4.1.1 Model development

The model is derived from the dynamic energy balance equation that describes the evolution of the indoor temperature T of a single-zone building and is reported in Eq. (4.1):

$$\frac{dT}{dt} = -a\ (T - T_{\text{ext}}) + b\,\dot{Q} \tag{4.1}$$

Heat transfer through the envelope to the external air T_{ext} and the thermal power from the heating system $\dot{Q}$ influence the internal building temperature evolution through the performance coefficients a and b, which also include the building heat capacity [149]. They are the main model parameters and can be identified from real building data. More details on the identification procedure can be found in Section 4.1.2. Forced ventilation is absent and air infiltrations are neglected. Moreover, internal and solar gains are not included within the thermal power transferred to the system. This is due to several reasons:

- when dealing with a whole building, the estimation of the contribution of building occupation and radiation is often inaccurate, since the former depends on the actual number of occupants and the latter depends on the shading of each glazed surface;
- neglecting these aspects shows the feasibility and robustness of the approach also when less knowledge about the system is obtainable;
- the simplicity of the model and the low number of required inputs is an advantage when extending the approach to networks with a large number of connected buildings. This assumption is commonly made in many other studies in the literature [80].

Nonetheless, these contributions can be easily added as model inputs, if available.

The thermal power supplied to the substation heat exchanger and, then, distributed to the building space heaters, is expressed by Eq. (4.2):

$$\dot{Q} = \dot{m}\,c\ (T_{\text{S}} - T_{\text{R,SP}}) \tag{4.2}$$

with $\dot{m}$ and c being the water mass flow rate and specific heat capacity, and T_{S} and $T_{\text{R,SP}}$ being the supply and return water temperature in the primary side of the substation. The latter is a model boundary condition, according to the assumption that it is regulated by the substation heat exchanger controller on the secondary side.

The actual supply temperature of the primary side is calculated from the mixing temperature T_{mix} by Eq. (4.3). The heat losses from the supply and return pipes $\dot{Q}_{\text{loss,S}}$ and $\dot{Q}_{\text{loss,R}}$ are included in Eq. (4.4).

$$T_{\text{S}} = T_{\text{mix}} - \frac{\dot{Q}_{\text{loss,S}}}{\dot{m}\, c} \tag{4.3}$$

$$\dot{Q}_{\text{loss,S}} = (UA)_{\text{S}}\ (T_{\text{mix}} - T_{\text{soil}}) \tag{4.4a}$$

$$\dot{Q}_{\text{loss,R}} = (UA)_{\text{R}}\ (T_{\text{R,SP}} - T_{\text{soil}}) \tag{4.4b}$$

where UA is the overall heat transfer coefficient, including the heat transfer surface, from the water in the pipes to the soil. The heat losses are calculated with respect to the highest temperatures, i.e. T_{mix} for the supply pipe and $T_{\text{R,SP}}$ for the return pipe, in order to have a conservative estimation and simplify the model.

In summary, the end-user behavior can be described by the state equation Eq. (4.5):

$$\frac{dT}{dt} = -a\ (T - T_{\text{ext}}) + b\ [\dot{m}\, c\, T_{\text{mix}} - UA\ (T_{\text{mix}} - T_{\text{soil}}) - \dot{m}\, c\, T_{\text{R,SP}}] \tag{4.5}$$

The total power necessary to operate the given branch of the network consists of the thermal power from the production unit and the pump power. The former is calculated as the sum of the heat transferred to the substation heat exchanger of the considered branch and the related heat losses that have to be compensated:

$$P_{\text{prod}} = \left[\dot{m}\, c\ (T_{\text{S}} - T_{\text{R,SP}}) + \dot{Q}_{\text{loss,S}} + \dot{Q}_{\text{loss,R}}\right] \frac{1}{\eta_{\text{prod}}} \tag{4.6}$$

with η_{prod} being the production unit efficiency, which can be corrected based on the actual load with respect to the nominal efficiency.

The pump power is proportional to the cube power of the circulating mass flow rate, as in Eq. (4.7), which is derived from the Darcy-Weisbach expression of the distributed pressure losses along the pipeline:

$$P_{\text{pump}} = \frac{8 f L}{\pi^2 \rho^2 D^5} \frac{1}{\eta_{\text{pump}}} \dot{m}^3 = k_{\text{pump}}\, \dot{m}^3 \tag{4.7}$$

where f, L and D are the pipe friction factor, length and internal diameter, respectively, ρ is the water density, and η_{pump} is the pump efficiency.

Model discretization From a control point of view, the model variables are the following:

- The system state and controlled variable of this model, namely x, is the building indoor temperature T.
- The inputs and manipulated variables, namely u_1 and u_2, are the water mass flow rate $\dot{m}$ and the mixing temperature T_{mix}, respectively. Indeed, the pump rotational speed regulates the former while the recirculation valve regulates the latter.
- The main disturbances and non-manipulated variables, namely d_1 and d_2, are the outdoor temperature and soil temperature. The former can be obtained by querying real-time weather forecast databases or by adopting forecasting functions that reasonably build the temperature profiles based on available data [150].

As stated later in Section 4.2.1, the selected Dynamic Programming optimization algorithm requires the discretization of the state and input grids. Hence, the model described above is discretized according to the forward Euler method (Section 3.1.2) with time intervals Δt. At the k-th time-step and with the control notation, Eq. (4.5) becomes:

$$\frac{x_{\text{k+1}} - x_{\text{k}}}{\Delta t} = -a\ (x_{\text{k}} - d_{1,\text{k}}) + b\ [u_{1,\text{k}}\, c\, u_{2,\text{k}} - UA\ (u_{2,\text{k}} - d_{2,\text{k}}) - u_{1,\text{k}}\, c\, T_{\text{R,SP}}] \quad (4.8)$$

Thus, the discretized state equation is:

$$x_{\text{k+1}} = (1 - \Delta t\, a)\ x_{\text{k}} + \Delta t\, a\, d_{1,\text{k}} + \Delta t\, b\ [u_{1,\text{k}}\, c\, u_{2,\text{k}} - UA\ (u_{2,\text{k}} - d_{2,\text{k}}) - u_{1,\text{k}}\, c\, T_{\text{R,SP}}] \quad (4.9)$$

The input grid is created according to the lower and upper constraints of the input variables. The state grid is discretized according to the state boundary values. The steps of the input and state grids are algorithm parameters that can be set according to the sensitivity analysis described in Section 4.2.2.

The cost function for each time-step is given by summing the energy for the production unit and the pump over the time interval, as in Eq. (4.10):

$$\begin{aligned} J_{\text{k}} &= (P_{\text{prod,k}} + P_{\text{pump,k}})\ \Delta t + \phi_{\text{k}} = \\ &= \left[u_{1,\text{k}}\, u_{2,\text{k}}\, \frac{c}{\eta_{\text{prod}}} + \frac{(UA)_{\text{R}}}{\eta_{\text{prod}}}\ (T_{\text{R,SP}} - d_{2,\text{k}}) + k_{\text{pump}}\, u_{1,\text{k}}^3\right]\ \Delta t + \phi_{\text{k}} \end{aligned} \quad (4.10)$$

When required by the building occupants, the indoor temperature is constrained according to the lower and upper limits, otherwise it is left unconstrained. The penalty factor ϕ is therefore added to the cost function associated with the unacceptable state values in order to force compliance with the constraints.

Time delays It is necessary to consider pipe dynamics in the simulation and optimization of DHNs as the time delay between production and effective supply to buildings might affect the operation and control of the system [151]. Nevertheless, the pipe dynamics would require the introduction of an additional system state variable. It is preferable to maintain one state variable to match a single-state structure of the Dynamic Programming algorithm. In this way, it is possible to avoid the exponential increase in computational complexity with the number of states. Moreover, MPC implementation requires a simplified and fast model.

For these reasons, the model introduced in this section considers the time delays in a quasi-static way by introducing a factor Δt_d for each calculation. This is defined as the ratio between the pipe length and the current speed, calculated from the current mass flow rate:

$$\Delta t_\mathrm{d} = \frac{L}{\frac{4\,\dot{m}}{\rho\,D^2\,\pi}} \tag{4.11}$$

It represents the delay with which the water mass flow reaches the building. The DP algorithm gives the optimal mixing temperature. In the current time-step, however, the temperature of the water that actually reaches the building remains at the same temperature as the previous time-step for a time interval equal to Δt_d. Hence, the optimal mixing temperature is modified in order to send the same amount of energy required for the current time-step, as in Eq. (4.12):

$$T_\mathrm{mix,new} = \frac{T_\mathrm{mix,DP}\,\Delta t - T_\mathrm{mix,previous}\,\Delta t_\mathrm{d}}{\Delta t - \Delta t_\mathrm{d}} \tag{4.12}$$

where the subscripts *new*, *DP* and *previous* indicate the new input, the optimal DP input and the previous time-step input, respectively. This solution guarantees that the model structure is maintained and that the energy requirements of the users are respected. Eq. (4.12) is valid when $\Delta t_\mathrm{d} < \Delta t$, which represents the typical condition of small-scale DHNs. In other cases, different strategies can be adopted to consider time delays, as presented in Section 4.4.3.

4.1.2 Model identification

The parameters of the presented model for small-scale DHNs can be derived via identification, which is a procedure that builds the mathematical model of a system starting from input and output datasets. As stated in Section 4.1.1, the proposed simplified model can be identified by means of experimental or simulated data. In the latter case, the input and output datasets are produced by detailed simulation of the real system in different conditions. This identification procedure is based

on simulation data collected in [74] by simulating the district heating branch for fourteen days. The input dataset contains the sequences of the water mass flow rate, mixing temperature, and outdoor and soil temperatures, which are imposed as system disturbances. The output dataset contains the sequence of indoor building temperature, which is the system state. All data are obtained with a sampling period of 15 minutes. Random components are added to both the indoor and outdoor temperatures to simulate measurement uncertainty.

These data are divided into a training set for identification of the model parameters and a test set for validation. The training set and the specified model structure defined by Eq. (4.9) are inputs of the identification problem. This consists of estimating the parameters of the model by solving a nonlinear least-squares problem, which operates the minimization of the squared error between the model predictions $x(a, b)$ and the original data $\hat{x}$. The function of the parameters a and b that has to be minimized is described by Eq. (4.13):

$$F(a,b) = \frac{1}{2} \sum_{i=1}^{N_\mathrm{m}} \left[\hat{x}_\mathrm{i} - x_\mathrm{i}(a,b)\right]^2 \tag{4.13}$$

with N_m being the number of samples.

The validation of the procedure is performed by comparing the output of the newly-identified gray-box model with the test set data. Different training set lengths are tested, while the test set is chosen as the last two days of the dataset. With this aim, Fig. 4.2 shows the building temperature predicted by the model identified with two different training sets compared to the original temperature. The results highlight that the identification performed on a relatively short training set (e.g. 0.25 days) provides a model which does not adequately fit the measurements. This happens because the heating up and cooling down building dynamics are not sufficiently represented by the training set and cannot be highlighted.

The performance of the identification can be further evaluated through the Root Mean Squared Error (RMSE) between predicted and original data:

$$RMSE = \sqrt{\frac{\sum_{i=1}^{N_\mathrm{m}} \left[\hat{x}_\mathrm{i} - x_\mathrm{i}\right]^2}{N_\mathrm{m} - 1}} \tag{4.14}$$

Fig. 4.2 illustrates the RMSE with varying training set lengths, showing that acceptable results are obtained with at least one-day-long datasets, provided that they cover typical weekday operation (i.e. with building heating and cooling transients).

This consideration can be helpful when developing an MPC controller for small-scale DHNs, as it enables its application to systems with a limited amount of

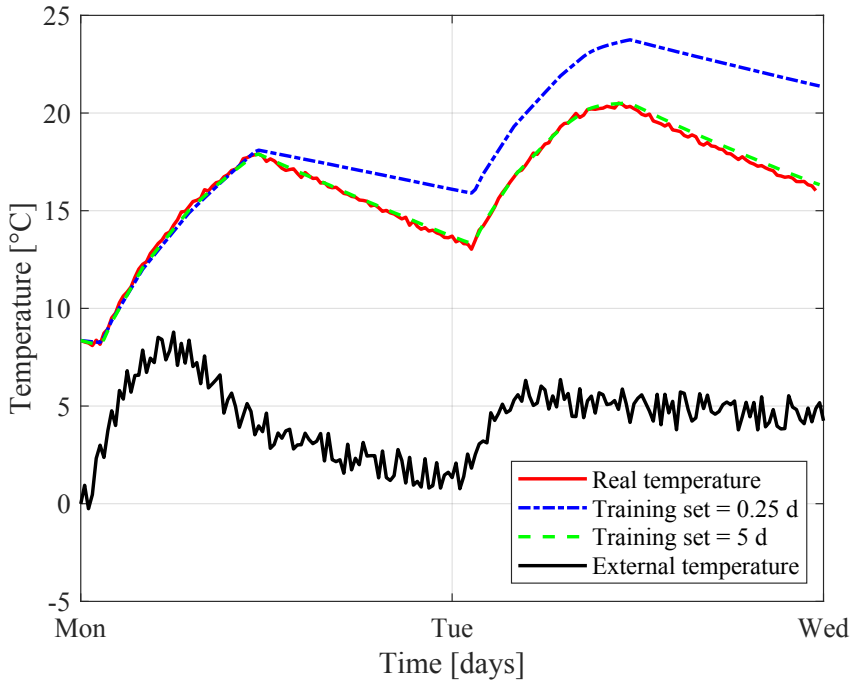

Fig. 4.2. Comparison between identification results with two different training sets and original dataset.

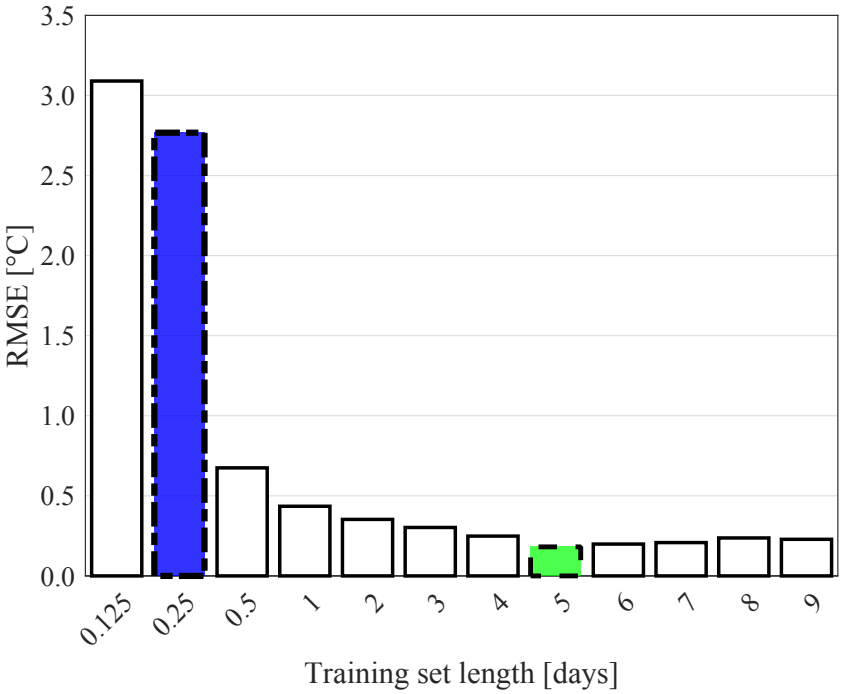

Fig. 4.3. Root Mean Squared Error for different training set lengths.

data available. Furthermore, since the implementation of MPC allows system measurements to be collected real-time, the model parameters can be periodically adapted and identified with new acquisitions.

4.2 Small-scale district heating: optimization algorithm

The MPC framework requires an optimization problem to be solved at each time-step (i.e. minimization/maximization of the cost function) and, thus, an optimization algorithm that combines high computational speed with feasible accuracy.

For small-scale DHNs, the Dynamic Programming algorithm is selected for the reasons discussed in Section 3.2.1:

- it has an exact and inherently dynamic optimization character;
- it easily manages the nonlinearities typical of DHNs in the state and cost functions;
- it is particularly feasible for models with a low number of states and, therefore, for multi-agent application to heating networks with a tractable number of buildings.

The sequence of operations for the development of the MPC elements suitable for small-scale DHNs [74] is illustrated in Fig. 4.4. In the first block, the algorithm architecture is created according to the theoretical background in Section 3.2.1 and suitable parameters are selected through sensitivity analysis. In the second block, the model embedded within the algorithm is developed and identified according to the method presented in Section 4.1.

The application of this algorithm in the framework of a multi-agent hierarchical MPC controller for small-scale district heating is reported in Sections 5.1 and 5.2.

4.2.1 Algorithm

The novel function based on the Dynamic Programming theoretical framework provides a numerical solution to the deterministic DP problem by means of the discretization of the time, input and scale scales. The algorithm is developed in the MATLAB® coding environment, which is one of the most widely used programming languages in engineering.

As depicted in Fig. 4.5, the DP algorithm architecture comprises three main sections, described in detail below:

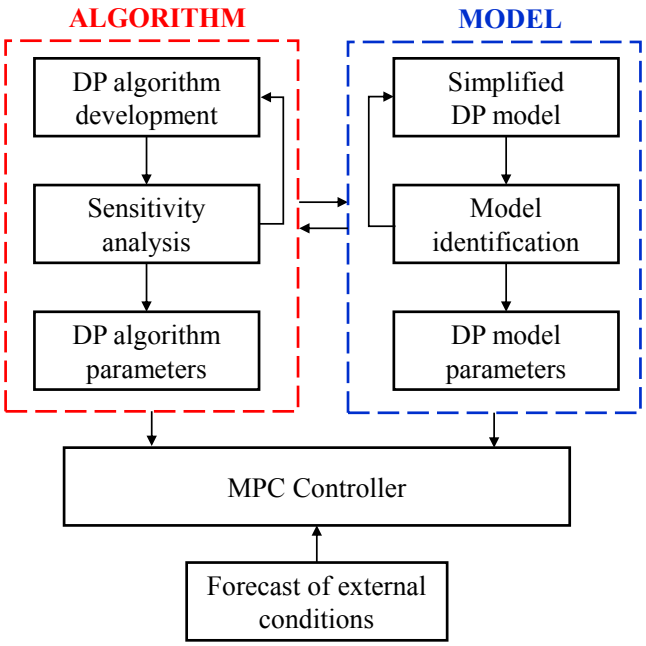

Fig. 4.4. Block diagram of the development of the model and optimization algorithm of the MPC controller.

- the data function;
- the algorithm function;
- the model function.

This structure is modular, as different problems can be tackled by changing only the model and by defining proper data, regardless of the field of application.

The algorithm is suitable for problems with one state, a variable number of inputs and a variable number of disturbances. With reference to the present work, this approach significantly simplifies multi-agent implementation, as the application of the algorithm to different branches supplying each building can be operated in a modular way by changing just building data and parameters.

In addition, the novel function takes approximately one quarter of the time requested by Sundström and Guzzella in [129] to solve the same optimization problem. For these reasons, it is adequate for real-time MPC applications.

Data function The parameters that are necessary for the problem solution are related to the discretization of time scale and state-space and to the algorithm options. For this purpose, the data that has to be firstly defined by the user regard the following aspects:

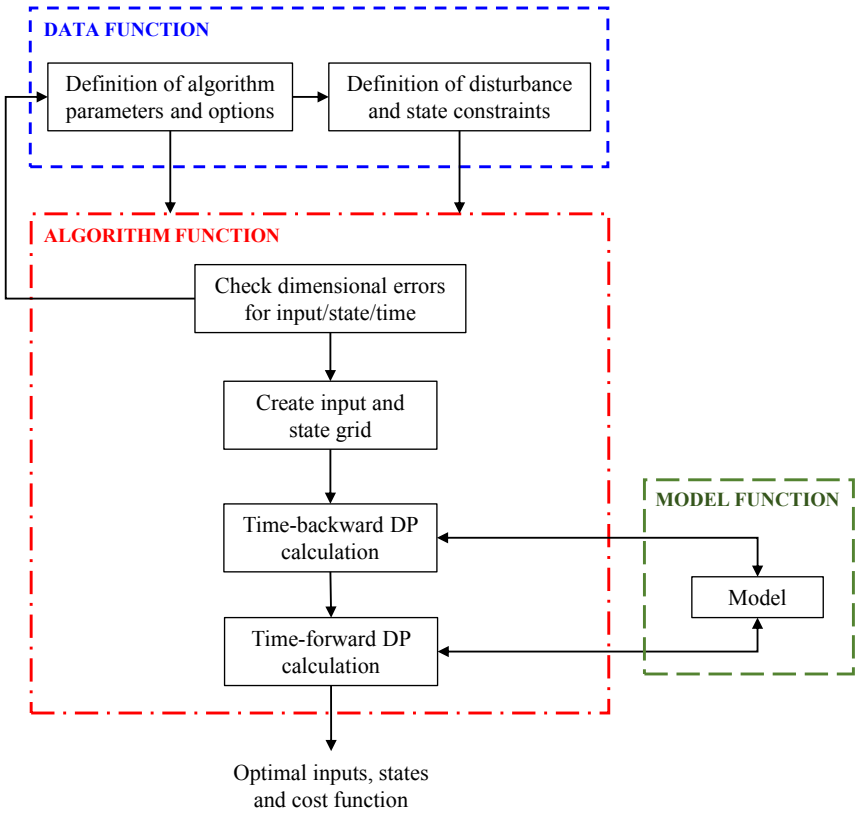

Fig. 4.5. Block diagram of the DP algorithm architecture.

- Problem dimensions: number of inputs, number of states and number of disturbances.
- Parameters of the time grid: in particular the time horizon of the optimization and the amplitude or number of time-steps N.
- Parameters of the input grids: lower and upper boundary for each input, which typically represent the physical constraints of the input signals (e.g. minimum and maximum mass flow rate) and constitute the boundaries of the input grids; amplitude or number of input steps. The input grid discrtization can be non-homogeneous (with variable step sizes), in order to carry out a local grid refinement while keeping a feasible computational effort.
- Parameters of the state grid: lower and upper boundary for the state, which define a plausible range for its variation and constitute the boundaries of the state grid; amplitude or number of state steps; state initial condition. Similarly to the inputs, the state grid can be locally refined in order to improve the calculation accuracy where it is considered noteworthy.

- State constraints: for each time-step of the horizon, a lower and upper boundary for the state feasibility have to be defined or loaded as external functions. The boundaries can be infinite in given time-steps if the state is unconstrained. An explanatory example regards the indoor temperature of office buildings, which is constrained within given limits if the building is occupied and unconstrained otherwise.

- Disturbances: for each time-step of the horizon, the value of the disturbances have to be defined or loaded as external functions.

- Additional options, such as the penalty factor, which is added to the cost function in presence of infeasible states.

Algorithm function This function receives the data defined above as inputs and solves the optimization problem, giving the sequence of optimal control actions over the future time horizon as output. The sequence of operations is detailed as follows:

- **Check dimensional errors**. If the parameters defined in the data function are not coherent with the problem dimensions or if the dimension of the state constraints or disturbance vectors does not correspond to the number of time-steps, a *mismatch error* is returned. It indicates to revise the chosen data, otherwise the optimization problem cannot be solved.

- **Create the grids** of the inputs and state, according to the defined parameters. The grids can have a fixed step or a variable step.

- **Time-backward calculation** that builds the map of optimal inputs for each discretized state at each time-step. This is done through an iterative procedure that starts from the last time-step, proceeds backward in the time scale toward the first time-step and solves the deriving tail subproblems. Firstly, all possible combinations of the discretized states and discretized inputs are created. Then, for each iteration, corresponding to time-step k, which goes backward from $N-1$ to 1:
  Step (i). The model function is evaluated for each combination in order to obtain the new state x_{k+1} and the cost of this operation.
  Step (ii). The cost is added to the cumulative cost obtained at the previous iteration (corresponding to time-step $k+1$) for the new state. Since the cumulative costs of the tail subproblems are evaluated in discrete points of

the state grid, if the new state x_{k+1} does not correspond to a grid point, the actual cumulative cost is obtained by linear interpolation between the closest grid points.
Step (iii). For each discretized state at time-step k, the inputs that minimize the new cumulative cost from Step (ii) are selected and saved in the map.
Steps (i)–(iii) are repeated until the first step of the time scale. Thus, the map that associates the optimal inputs to each discretized state over the time scale is obtained.

- **Time forward calculation** that returns the sequence of optimal inputs for the actual problem. This is done through a successive iterative procedure that starts from the first time-step to the end of the time scale. The initial condition is set as the first time-step state x_1. Then, for each iteration, corresponding to time-step k, which goes forward from 1 to $N-1$:
Step (i). The optimal inputs corresponding to the actual state x_k are taken from the map created previously. Since the map is evaluated in discrete points of the state grid, if the actual state x_k does not correspond to a grid point, the actual inputs are obtained by linear interpolation between the closest grid points.
Step (ii). The model function is evaluated with the optimal inputs from Step (i). In this way, the state x_{k+1} (i.e. at the next time-step $k+1$) and the cost of this operation are obtained.
Steps (i)–(ii) are repeated until the end of the time scale. The results are the sequences of optimal inputs, optimal states verified with those actions and the related values of the cost function.

Model function This function is characteristic of the problem tackled and is responsible to calculate (i) the dynamic response of the system and (ii) the cost of applying given inputs with given disturbances. Hence, it has to contain:

- the state function which, given the state, inputs and disturbances applied at time-step k, calculates the state and output at time-step $k+1$;
- the cost function related to this state change. If the action leads to an infeasible state, a penalty factor is added to prevent constraint violation.

Complete details of the model function developed and exploited for this application have already been reported in Section 4.1.

4.2.2 Sensitivity analysis

The DP algorithm requires the discretization of the state and input grids and the choice of the parameters might affect the algorithm performance. Therefore, detailed sensitivity analysis of the characteristic parameters of the algorithm is presented in this section.

The investigation is based on the model described and identified in Section 4.1. The constraints on the input and state grid as well as the time parameters, which are problem-dependent, are reported in Table 4.1.

Table 4.1. Input, state and time parameters set for the sensitivity analysis of the DP algorithm.

Variable	Description	Symbol	Lower boundary	Upper boundary
Input 1	Mass flow rate	u_1	0 kg/s	12 kg/s
Input 2	Mixing temperature	u_2	60 °C	80 °C
State	Indoor temperature	x	0 °C	30 °C
			Time-step	Time horizon
Time		t	15 min	3 days

The analysis is conducted by varying the state grid steps (i.e. Δx) and the input grid steps (i.e. Δu_1 and Δu_2) independently and by comparing the performance of the algorithm according to the following key performance indicators:

- computational time for one DP algorithm calculation;
- predicted global energy consumption over the time horizon of one DP algorithm calculation;
- number of time-steps in which the compliance with the temperature constraints is not realized (i.e. failures);
- number of time-steps in which the required temperature is reached in advance, since reaching the required comfort conditions some hours before the building is occupied would represent a loss of energy.

The scope of the analysis is to choose the parameter values that give the best trade-off between a low computational time and feasible accuracy (e.g. low predicted energy consumption, low energy loss).

Fig. 4.6 represents the normalized energy consumption (with respect to the minimum) obtained for one DP algorithm calculation over the prediction horizon, for different values of Δu_1 and Δu_2. Each plane refers to a different value of Δx. The influence of the input discretization on the global energy consumption is clearly lower than the influence of the state discretization. In fact, the algorithm results in terms of energy consumption do not vary significantly for a given state grid step. Hence, it is possible to choose feasible values of the input grid steps and focus on the sensitivity analysis of the state grid step.

The calculation time of one algorithm run for different input grid step settings is represented in Fig. 4.7. It is shown that an intermediate value of the input grid step is acceptable for MPC online implementation and, at the same time, it does not affect the algorithm results significantly. Hence, $\Delta u_1 = 0.5$ kg/s and $\Delta u_2 = 0.5$ °C are reasonably assumed to proceed with the analysis.

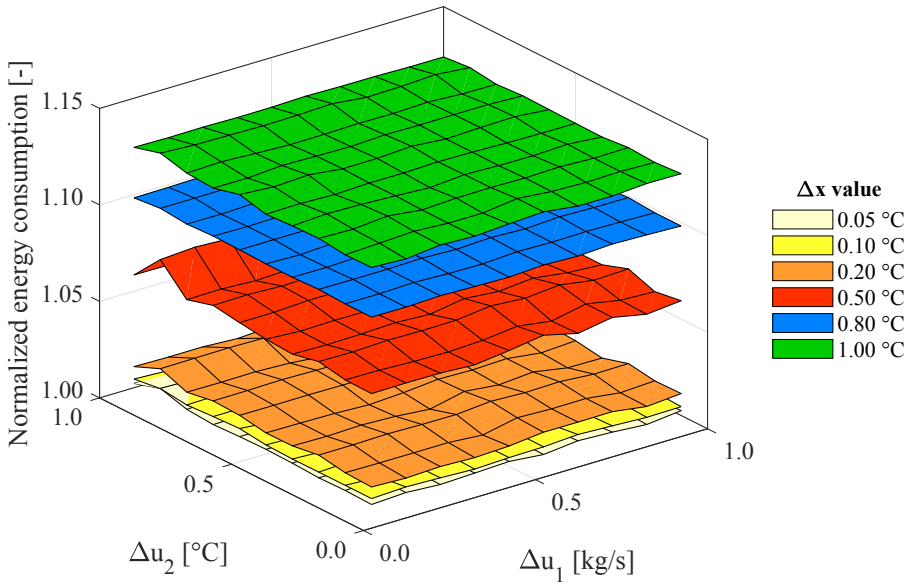

Fig. 4.6. Predicted normalized energy consumption over the prediction horizon for different values of input grid steps. Each plane refers to a different value of the state grid step.

The variation of (a) the predicted global energy consumption, (b) number of time-steps in advance and (c) number of failures with the state grid step Δx is shown in Fig. 4.8. The former increases significantly with Δx. A finer state mesh allows the algorithm to evaluate the cost of each feasible state and select the optimal trajectory more precisely. As a matter of fact, linear interpolation is applied for the states between the grid points (Section 4.2.1) and this may

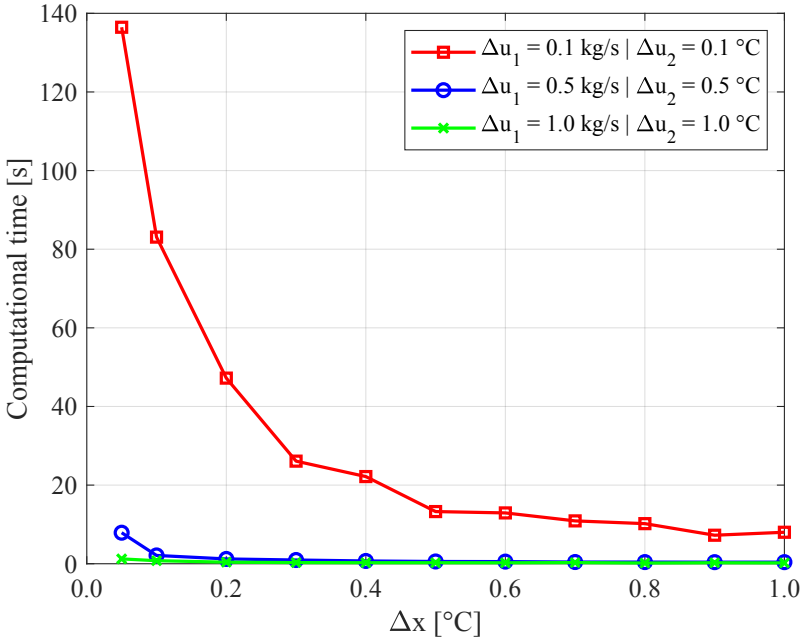

Fig. 4.7. Computational time with varying state grid steps Δx for selected input grid step values Δu_1 and Δu_2.

lead to approximation uncertainties, since the state dependence on inputs and disturbances is not linear. Furthermore, a lower value of Δx guarantees that indoor building temperature requirements are satisfied (i.e. no failures) and the energy losses are minimized (i.e. temperature is not reached several hours before the building is occupied).

A state grid step equal to 0.4 °C leads to a large number of failures in the fulfillment of the required temperature for numerical reasons (Fig. 4.8c). Indeed, that value results (i) in the comfort conditions being reached exactly at the requested time (i.e. maximum advance equal to zero) but also (ii) in the indoor temperature being maintained at a value which is slightly lower than the lower boundary during the maintenance phase. The algorithm returns optimal input values that are not able to keep the state above the lower limit. This happens because the intrinsic discretization nature of the algorithm leads to the need to interpolate the values between the grid points, therefore producing numerical errors. In this case, the linear interpolation gives rise to the large number of failures corresponding to the state grid step of 0.4 °C. Higher values of Δx, on the other hand, allow the fulfillment of the required building conditions several time-steps (i.e. hours) before it is occupied with consequent energy waste. Thus, it is possible to conclude that Δx values lower than 0.4 °C are acceptable for the accuracy of the algorithm.

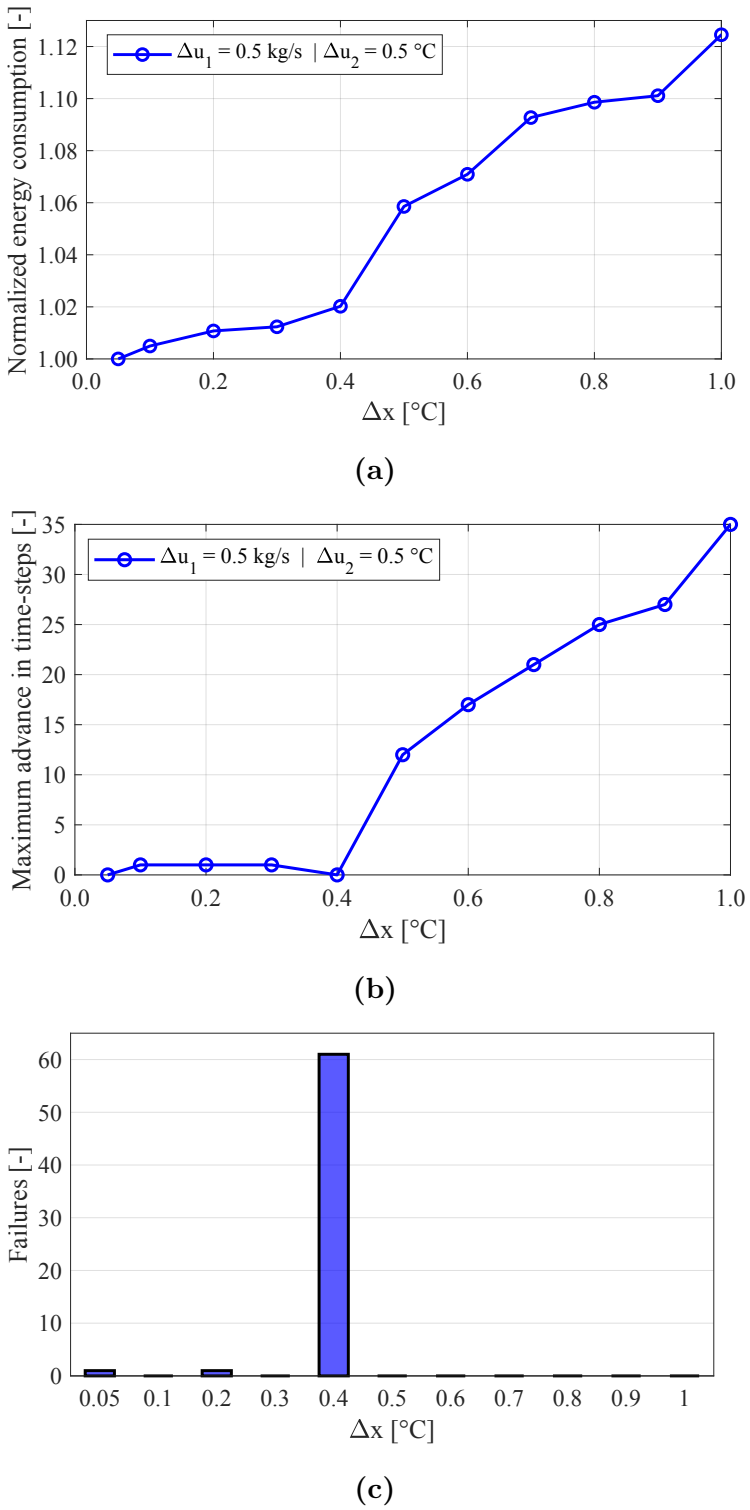

Fig. 4.8. Sensitivity analysis on the state grid step Δx: (a) normalized predicted energy consumption, (b) maximum advance of required temperature achievement in time-steps, (c) number of time-steps in which the required temperature achievement fails.

4.3 Large-scale district heating: model

As mentioned in Section 2.1, the current large-scale DHN modeling framework lacks simplified models of the consumers that (i) include their heat capacity estimation and (ii) do not require extensive and detailed investigations of individual building data and characteristics, which can be time-consuming and expensive. A model with these features can be essential in the application of demand side management and smart control strategies. For this purpose, the present section proposes a novel reduced-order, scale-free, gray-box model of DHN aggregated end-users (i.e. region) that can be built with a limited amount of data which are usually available from the system substations [148]. The procedure for the model development is illustrated in Fig. 4.9.

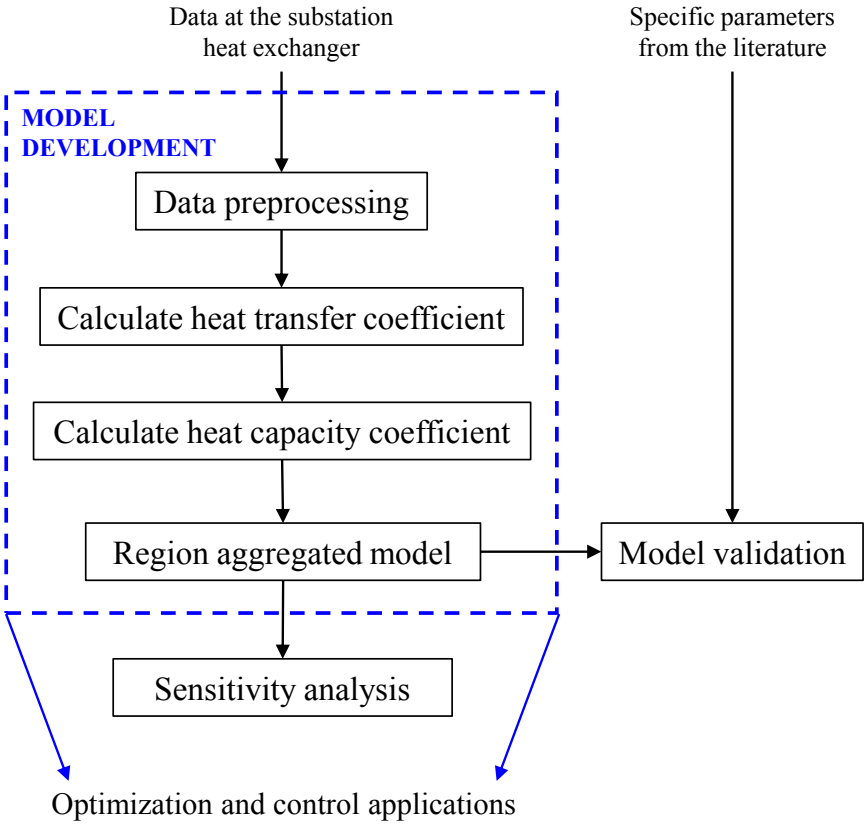

Fig. 4.9. Block diagram of the method for the development of the aggregated region model.

The method is described as an application to the DHN of the city of Västerås, in central Sweden. This network comprises six peripheral regions, namely Surahammar, Skultuna, Rönnby, Tillberga, Barkarö and Hallstahammar, each supplied

by a main substation heat exchanger. More details on network layout and size can be found in Section 5.3.1.

In Sweden, district heating providers are required to measure heat consumption through smart meter devices installed in the substations [53]. The availability of data makes it possible to identify the behavior of the system to a greater extent. However, it is still common that in other contexts the data acquisition devices are only installed in given sections of the network. Hence, it is beneficial to investigate methods that can be implemented in networks where the end-users are not monitored at an individual building scale. The proposed model is able to represent the dynamic behavior of the clusters of buildings connected within each aggregated region. Nevertheless, the method is independent from the size and system characteristic, thus its extension to generic networks and scales is straightforward.

4.3.1 Data preprocessing

In this application, the available data derive from the main substation heat exchangers of the six peripheral regions of the Västerås DHN during the period January 2016–May 2019, with a resolution of one hour. The dataset includes the following quantities:

- water mass flow rate of the primary side of the substation heat exchanger, $\dot{m}$;
- supply and return temperature of the primary side of the substation heat exchanger, T_{S} and T_{R}, respectively;
- outdoor temperature, T_{ext}.

The thermal power actually transferred to each region $\dot{Q}$, which covers the heat demand of the aggregated end-users, can be calculated according to the energy balance in Eq. (4.15):

$$\dot{Q} = \dot{m}\, c\, (T_{\mathrm{S}} - T_{\mathrm{R}}) \tag{4.15}$$

This entire thermal power dataset together with the outdoor temperature are illustrated in Fig. 4.10.

Since the data are collected automatically [53], there might be connection issues resulting in missing data or values that are not significant in the dataset. Hence, a proper preprocessing phase is carried out to remove the acquisitions corresponding to missing sensor readings.

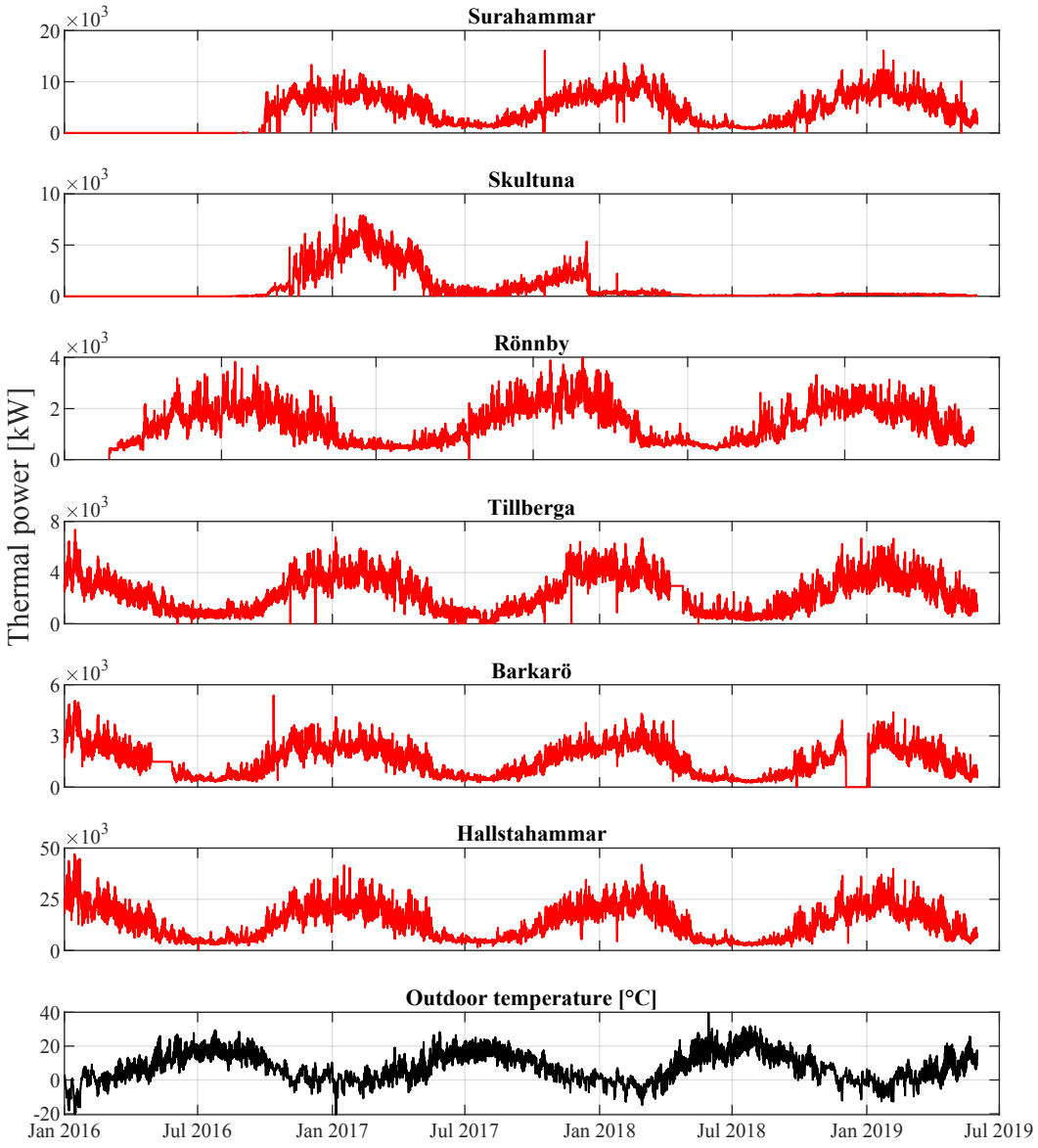

Fig. 4.10. Original dataset of thermal power transferred to the regions and outdoor temperature.

Firstly, the data referred to heating seasons (i.e. from October of each year to March of the following year) are extracted from the initial dataset. This is because the analysis aims to create a model that represents the consumers and their heat capacity when there is a significant thermal demand. The datasets of thermal power, mass flow rate, and supply and return temperature of one heating season for the region of Surahammar, chosen as an illustrative example, are reported in Fig. 4.11. It can be noted that, as expected, while the outdoor temperature

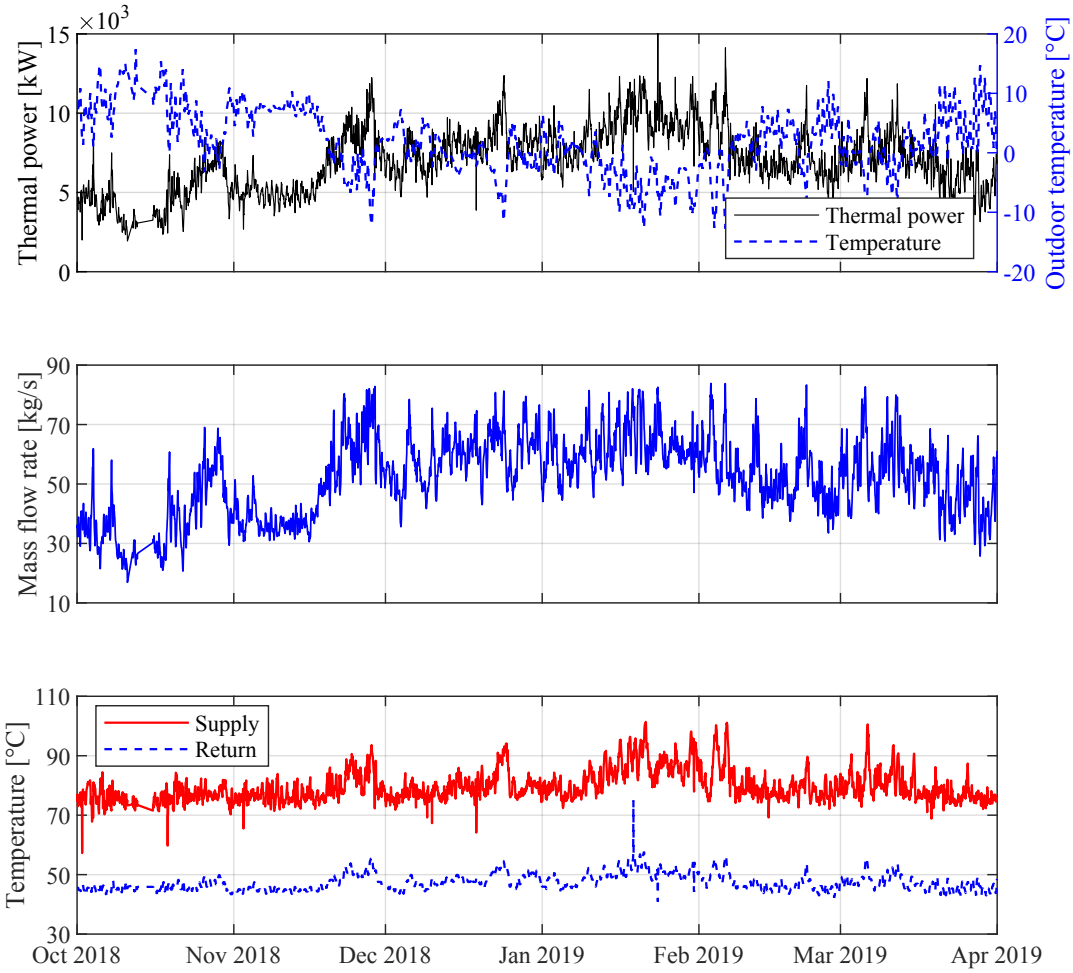

Fig. 4.11. Thermal power, outdoor temperature, mass flow rate, and supply and return temperatures of the region of Surahammar during the 2018–2019 heating season.

decreases the thermal power increases almost symmetrically, as a consequence of a higher demand to keep end-user comfort.

Secondly, days during which acquired data show one of the following features are eliminated from the dataset:

- the thermal power is zero or negative;
- the supply temperature is lower than a given threshold (i.e. 40 °C);
- the difference of temperature at the primary side of the substation is lower than a given threshold (i.e. 10 °C);
- the outdoor temperature is higher than 19 °C.

The latter cases are excluded because they represent a condition in which the heat demand is not relevant, usually far from the typical pattern of a heating season in Sweden.

4.3.2 Model development

The data are visualized in order to identify load profiles and typical behaviors. Generally, each day of the heating season shows a double peak behavior in heat load, in which the load increase in the early morning is followed by a maintenance period and then a second peak in the evening. The approach is similar to that proposed by Guelpa et al. [80] for the DHN of Turin, Italy. The authors calculate the coefficients that characterize a compact model based on the energy balance of each building starting from seasonal data.

In the present thesis, without other information concerning the individual end-users and the network specific configurations, the dataset related to each region is used to identify a simplified dynamic model that represents the sum of the buildings of the given area as a single aggregated consumer, represented in Fig. 4.12.

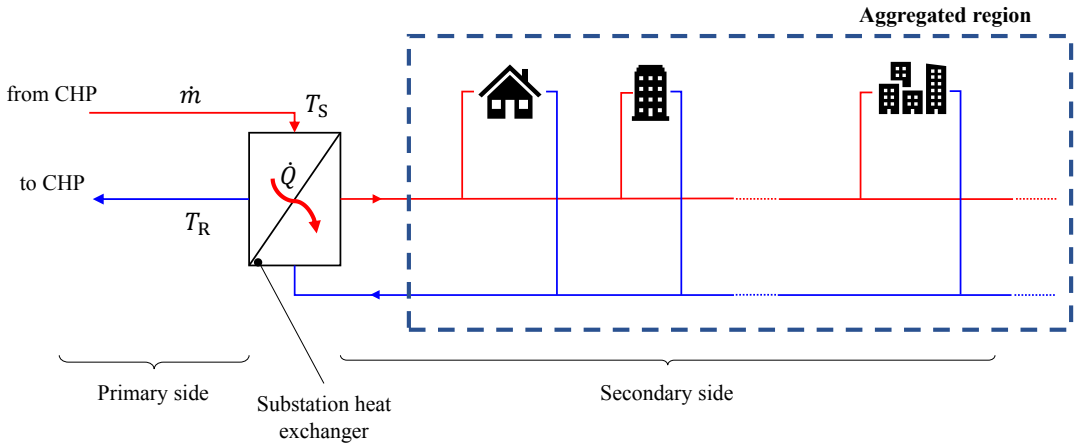

Fig. 4.12. Schematic representation of the assumption of aggregated region.

For this purpose, the region is considered as a system with a given mass at a uniform temperature T, which is an equivalent representation of the energy content of the aggregated consumer. The main factors that affect its thermal behavior are (i) the heat dissipation through the envelope, determined by the difference between indoor and outdoor temperatures, and (ii) the thermal power supplied by the DHN. The model is therefore represented by the thermal balance in Eq. (4.16):

$$\frac{dT}{dt} = -\frac{U}{C}\,(T - T_{\text{ext}}) + \frac{1}{C}\,\dot{Q} \tag{4.16}$$

Since this is a gray-box model, the parameters maintain a precise physical meaning. In particular, U is the aggregated heat transfer coefficient, while C is the aggregated heat capacity coefficient.

4.3.3 Model identification

This section describes the procedure to identify the model from Section 4.3.2 by means of the available data from Section 4.3.1.

Heat transfer coefficient In order to calculate the heat transfer coefficient U, the following assumptions are made:

- The indoor thermal conditions of the aggregated region are constant and, thus, the variation of T over time is not significant. This assumption is unavoidable since, in the most part of large DHNs actual indoor temperatures are rarely acquired, and significant mean values are difficult to estimate.
- T is assumed equal to 21 °C [152].

Eq. (4.17) is calculated for each data point and the mean of the obtained values gives the estimation of the average U.

$$U = \frac{\dot{Q}}{T - T_{\text{ext}}} \tag{4.17}$$

Four different calculation methods are compared to challenge the reliability of the assumption:

1. All data related to the heating seasons are selected for the calculation of the average U.
2. The data corresponding to the hours from 10 a.m. to 6 p.m. on weekdays are selected for the calculation of the average U. Indeed, that is considered as a maintenance phase, in which the indoor conditions of the buildings are kept constant. In residential dwellings this phase can last longer, however, the present model includes a large variety of additional generic end-users (e.g.commercial and education buildings). Hence, in order to include all users, the assumption of constant indoor temperature is presumably more reliable during the mentioned hours of the day.
3. The data corresponding to the days on which the percentage variation between maximum and minimum daily thermal power is close to the percentage

variation between maximum and minimum indoor-outdoor temperature difference are selected for the calculation of the average U:

$$\frac{\dot{Q}_{\max} - \dot{Q}_{\min}}{\dot{Q}_{\max}} \times 100 \approx \frac{(T - T_{\text{ext}})_{\max} - (T - T_{\text{ext}})_{\min}}{(T - T_{\text{ext}})_{\max}} \times 100 \tag{4.18}$$

This means that the daily variation of the outdoor temperature can potentially justify the daily variation of the heat load as well as the initial assumption.

4. Both sides of Eq. (4.17) are integrated in order to obtain the coefficient as the integral mean over each day. The average of these values over the heating season is selected for the calculation of the average U.

The results obtained for the six regions of the network are reported in Table 4.2. The average values and standard deviations (absolute and relative to the average) are also shown.

Table 4.2. Calculation of the heat transfer coefficient with different methods, average value and standard deviation (std) for the six regions of the Västerås network.

Region	Method				Average	Std	Std
	1	2	3	4	1–4	1–4	1–4
	[kW °C^{-1}]						[%]
Surahammar	367.2	390.2	392.0	366.8	379.0	13.9	3.7
Skultuna	219.4	239.5	250.4	218.7	232.0	15.6	6.7
Rönnby	99.3	101.8	101.9	99.3	100.6	1.5	1.5
Tillberga	177.0	200.3	201.6	176.6	188.9	13.9	7.4
Barkarö	114.3	117.0	117.0	114.2	115.6	1.6	1.4
Hallstahammar	1046.0	1104.7	1106.6	1046.0	1075.8	34.5	3.2

The standard deviation is lower than 8 % in all cases, so all the methods can be considered almost equivalent. However, methods 1 and 4 tend to return lower values of the coefficients. This might be due to the inconsistency between the initial assumption (i.e. constant indoor temperature) and considering all the daily measurements. The coefficients obtained with method 2 are used to proceed with the model development, since they are expected to better comply with that assumption. Moreover, it is more convenient to overestimate the coefficient that

affects the heat losses to the environment, in order to reduce the risk of adopting new management solutions that do not comply with the comfort requirements.

Heat capacity coefficient Starting from the heat transfer coefficient calculated above, the heat capacity C is evaluated by assuming that the indoor temperature of the aggregated region is subject to periodic variations over the days. Indeed, in most buildings in Sweden the indoor temperature set points are 21 °C during the day and 17 °C during the night [152]. The typical daily profile of the indoor building temperature is subject to an increase up to approximately the former temperature and then a decrease to the latter. It is reasonable to assume that the evolution of the region equivalent temperature over each day resembles this profile.

Therefore, this temperature (i) has to be maintained within the set-point boundaries (i.e. between 17 °C and 21 °C) and (ii) also has to show a variation during each day: the daily maximum and minimum temperatures shall lie within given acceptability bands (e.g. 20 °C to 22 °C and 17 °C to 18 °C for the maximum and minimum temperatures, respectively). A feasible daily behavior, with the temperature extreme values contained within the acceptability bands, is shown in a qualitative way in Fig. 4.13.

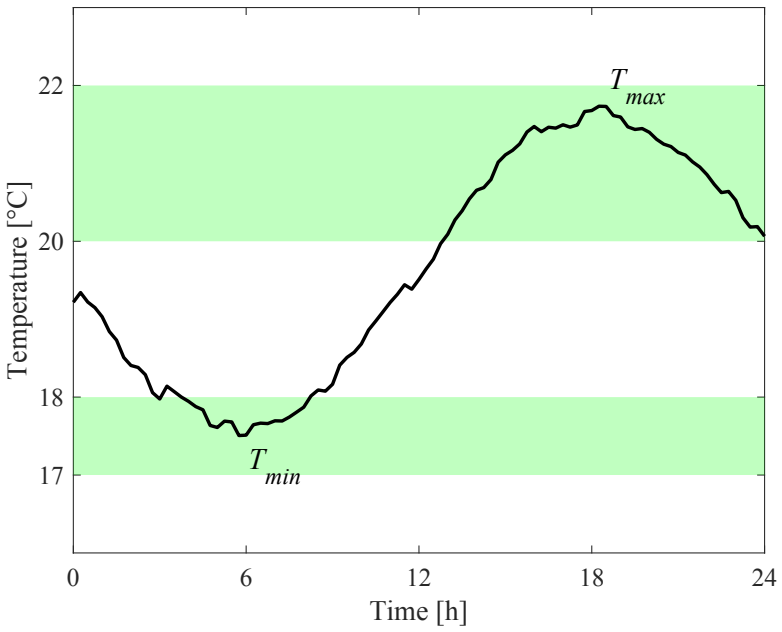

Fig. 4.13. Qualitative representation of a feasible daily behavior of the region equivalent temperature. The shaded areas are the acceptability bands for the maximum and minimum daily values.

With these assumptions, the coefficient of each region is estimated by solving the following optimization problem:

- the equivalent indoor temperature of the aggregated region is simulated with the input data over a defined period as a function of C;
- the aforementioned set-points and acceptability bands for the maximum and minimum daily temperatures are given as constraints;
- a penalty is added to the cost function if these constraints are not met;
- the resulting cost function is minimized and, therefore, the value of C that leads to the most reasonable behavior of the system is obtained.

This procedure is adopted to guarantee that the value of C is coherent with the expected daily periodical variation. A low C leads to sharp oscillations in the temperature and, consequently, to underestimating the storage potential of the given region. On the contrary, a high C leads to a nearly constant temperature behavior and to overestimating the storage capability.

4.3.4 Sensitivity analysis

The results of the estimation of the heat transfer coefficient and heat capacity coefficient carried out in Section 4.3.3 are reported in Table 4.3. The influence of these parameters on the behavior of the model are here investigated through sensitivity analysis.

The six regions are simulated for three representative days of January with the historical data of thermal power and outdoor temperature. The simulations

Table 4.3. Results of the identification of heat transfer coefficient U and heat capacity coefficient C for the six external regions of the Västerås network.

Region	U [kW °C^{-1}]	C [kJ °C^{-1}]
Surahammar	390.2	$13.750 \cdot 10^6$
Skultuna	239.5	$11.974 \cdot 10^6$
Rönnby	101.8	$5.350 \cdot 10^6$
Tillberga	200.3	$10.550 \cdot 10^6$
Barkarö	117.0	$3.875 \cdot 10^6$
Hallstahammar	1104.7	$39.350 \cdot 10^6$

are carried out firstly with the calculated coefficients (full lines in the following figures) and then with the coefficients that are increased and decreased by a given percentage (dashed and dashed-dotted lines in the following figures). Fig. 4.14 and Fig. 4.15 represent the equivalent indoor temperature when U is varied by $\pm 10\,\%$ and when C is varied by the same percentage, respectively. Since the standard deviation of U calculated with different methods (Table 4.2) is lower than 8 % in all cases, it is reasonable to assume that value as an uncertainty parameter.

It can be noted that an increase in U has a greater effect than an equal increase in C. Nonetheless, it is also possible to state that the calculated coefficients (Table 4.3) lead to an acceptable behavior of the equivalent temperature (full lines), while the curves obtained with lower and higher values of U tend to diverge due to the dynamic nature of the model. The effect of varying U is reduced when the outdoor temperature is higher (e.g. autumn and spring). This is given by the fact that the rate of variation of the equivalent temperature is proportional to U

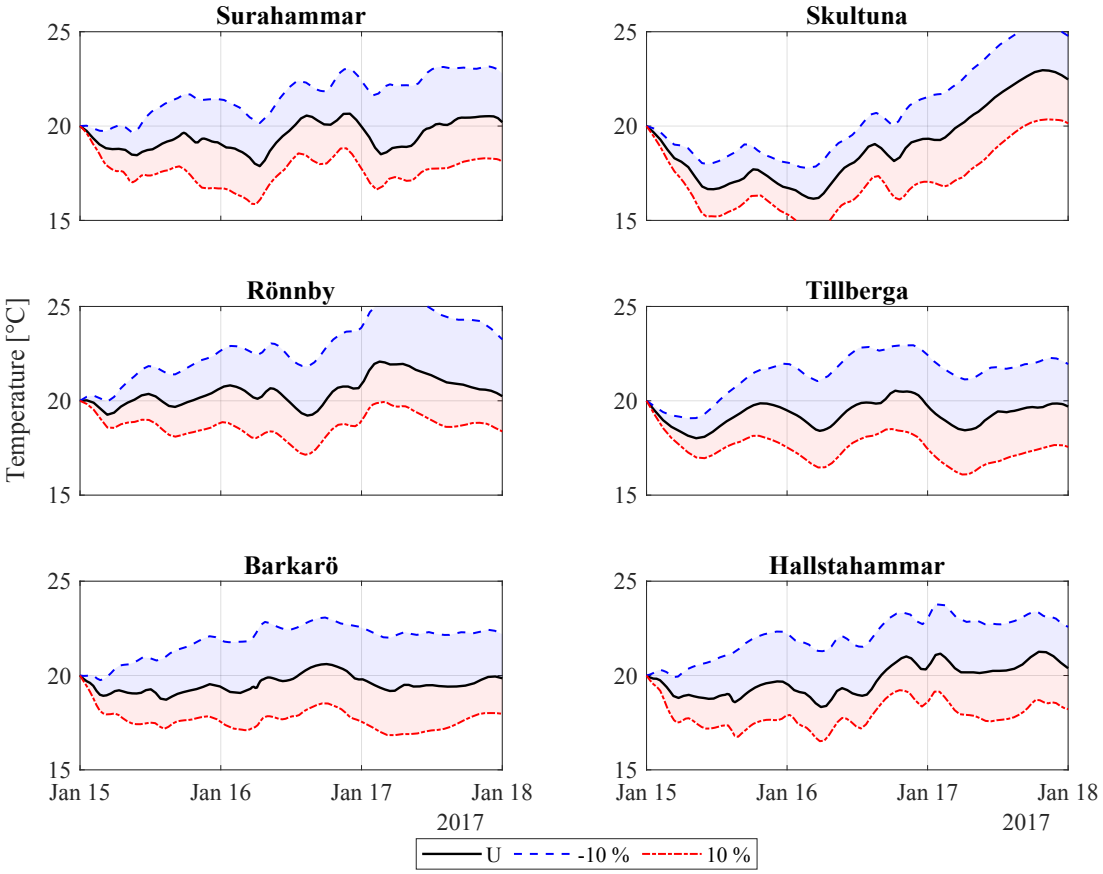

Fig. 4.14. Sensitivity analysis of the behavior of the model with the heat transfer coefficient U, considering a $\pm 10\,\%$ increase.

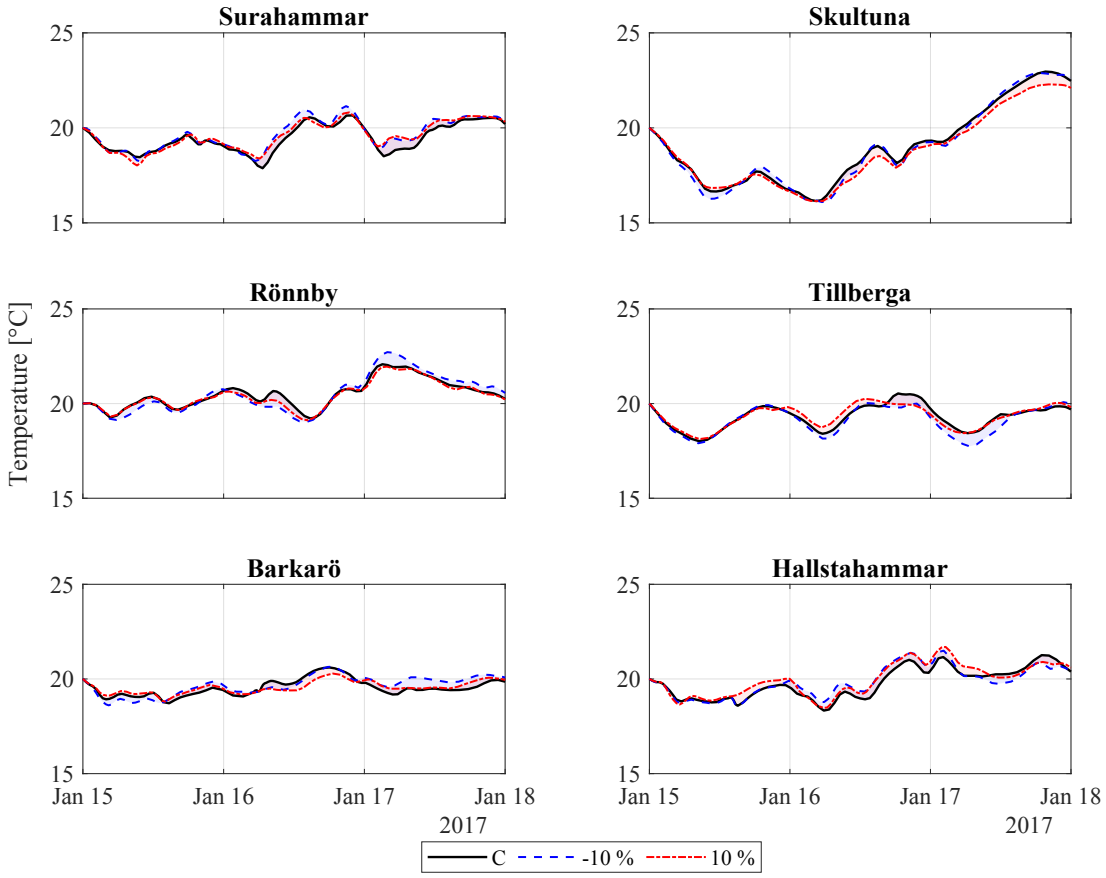

Fig. 4.15. Sensitivity analysis of the behavior of the model with the heat capacity coefficient C, considering a $\pm 10\,\%$ increase.

and to the difference between the temperature itself and the outdoor temperature, as in Eq. (4.16). For this purpose, Table 4.4 reports the average deviation between $-10\,\%$ and $+10\,\%$ curves (Fig. 4.14) in three different seasons, confirming that the deviation is significantly lower during middle seasons.

On the other hand, the deviation obtained by varying the heat capacity coefficient is not appreciable. The influence of this parameter on the model is further explored by increasing and decreasing it by up to one order of magnitude. Table 4.5 reports the maximum and minimum value, and the maximum difference of the equivalent temperature profile of Surahammar. It is demonstrated that a lower C leads to significant daily temperature variations (i.e. up to two times higher than that obtained with the calculated baseline coefficient C_0), while a higher C leads to a flat temperature profile. Since both conditions are not acceptable, the baseline C_0, which leads to daily temperature oscillation with an amplitude of around 2 °C to 3 °C, is considered reasonable for the presented model.

Table 4.4. Influence of the heat transfer coefficient U on the model behavior: average temperature deviation in [°C] between the two temperature curves (i.e. $-10\,\%$ and $+10\,\%$) on three representative days in different seasons.

Region	November [°C]	January [°C]	March [°C]
Surahammar	2.98	4.02	2.42
Skultuna	2.00	3.61	2.41
Rönnby	2.69	4.18	2.18
Tillberga	2.72	3.95	2.26
Barkarö	3.40	4.20	2.54
Hallstahammar	2.90	4.14	2.43

Table 4.5. Influence of the heat capacity coefficient C on the model behavior for the region of Surahammar on three representative days (January 15–17, 2017). C_0 is the baseline heat capacity coefficient (see Table 4.3), which leads to the parameters presented in **bold**.

C/C_0	$T_{\max}$ [°C]	$T_{\min}$ [°C]	$\Delta T_{\max}$ [°C]	$\Delta T_{\max}$ compared to baseline [%]
0.1	23.57	14.30	9.26	+208
0.2	23.19	15.53	7.66	+148
0.5	21.83	17.33	4.50	+47.4
1	**20.65**	**17.88**	**2.78**	**0**
2	20.21	18.84	1.37	-25.7
5	20.00	19.16	0.84	-59.1
10	20.00	19.63	0.37	-73.7

4.3.5 Model validation

The model is validated by comparing its parameters, converted to specific values per unit of heated space, with data from the literature.

Since the total heated area of the regions supplied by the Västerås DHN is unknown, it is firstly estimated based on the energy statistics published by the Swedish Energy Agency [153]. The document reports the values of the average yearly energy consumption per square meter of heated surface for different Swedish

counties. The total heated area of the i-th region is:

$$A_{\mathrm{tot,i}} = \frac{Q_{\mathrm{tot,i}}}{Q_{\mathrm{avg}}} \tag{4.19}$$

where $Q_{\mathrm{tot,i}}$ and Q_{avg} are the total and average yearly consumption, respectively. The model parameters are then scaled with the estimated area and with an average height of the heated environment (i.e. $z = 3\,m$) to obtain the specific coefficients per unit of the heated volume:

$$U_{V,\mathrm{i}} = \frac{U_{\mathrm{i}}}{A_{\mathrm{tot,i}}\, z} \tag{4.20a}$$

$$C_{V,\mathrm{i}} = \frac{C_{\mathrm{i}}}{A_{\mathrm{tot,i}}\, z} \tag{4.20b}$$

The statistics for the Västmanland county, where Västerås is located, report a Q_{avg} between $135\,\mathrm{kWh\,m^{-2}}$ and $165\,\mathrm{kWh\,m^{-2}}$ [153]. The specific coefficients U_V and C_V obtained by varying the average consumption within these limits are depicted in Fig. 4.16. The characteristic time τ of each region, calculated as the ratio between the heat capacity and the heat dissipation to the environment, is also represented:

$$\tau_{\mathrm{i}} = \frac{C_{\mathrm{i}}}{U_{\mathrm{i}}} \tag{4.21}$$

The values of U_V and C_V calculated in [80] for individual buildings of the Turin DHN are around $0.85\,\mathrm{W\,m^{-3}\,°C^{-1}}$ and $5 \cdot 10^4\,\mathrm{J\,m^{-3}\,°C^{-1}}$, respectively. The characteristic times vary significantly depending on building type: most values are around $7 \cdot 10^4\,\mathrm{s}$, while some are even smaller than $5 \cdot 10^4\,\mathrm{s}$.

Results obtained in this work are slightly lower than the literature values, however, the order of magnitude is the same. The fact that the characteristic times are comparable shows that the heat transfer and heat capacity coefficients are coherent. Moreover, it is worth stating that the literature values have been obtained for individual buildings in the city of Turin, which is characterized by old multi-story dwellings. The regions of Västerås are likely to be characterized by aggregations of newer or more energy-efficient dwellings, thus a lower loss coefficient can be reasonably expected. This is confirmed by a research stating that the average temperature loss of Italian houses (when the indoor and outdoor temperatures are 20 °C and 0 °C, respectively) is 1.5 °C, while in Sweden this parameter drops to 1.2 °C [154]. Hence, lower values of the heat loss coefficient for networks in Sweden compared to Italy are justified by the different characteristics of the connected dwellings. In addition, another work [71] reports that the values of internal

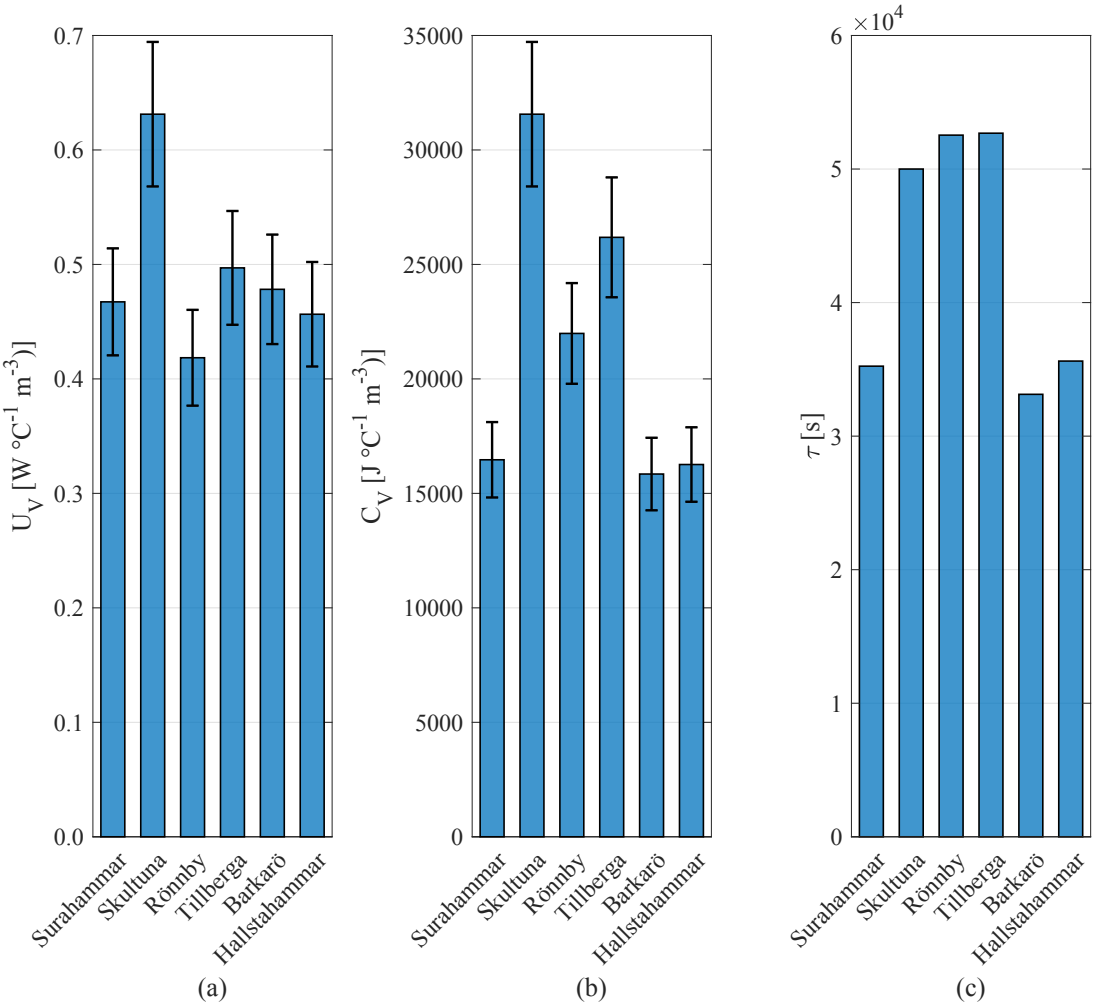

Fig. 4.16. Specific coefficients of (a) heat transfer and (b) heat capacity per unit of heated volume by varying the average yearly consumption, and (c) characteristic time: external regions of the Västerås network.

heat capacity of light-weight buildings drop to $8 \cdot 10^4\,\mathrm{J\,m^{-2}\,°C^{-1}}$, corresponding to around $3 \cdot 10^4\,\mathrm{J\,m^{-2}\,°C^{-1}}$. This is coherent with the results in Fig. 4.16.

Fig. 4.17 represents a further validation with a study by Leśko et al. [54], who conclude that the aggregated Demand Side Management actions performed (i.e. storage of thermal energy in consumer capacity) are limited to 1.4 % of the total heat demand over the period analyzed. The potential daily heat storage of the Västerås regions obtained with this assumption is comparable with that obtained with the model proposed in this work, considering an acceptable variation in the equivalent temperature of $\pm 0.5\,°\mathrm{C}$.

Finally, a preliminary test of the model feasibility is performed through a sim-

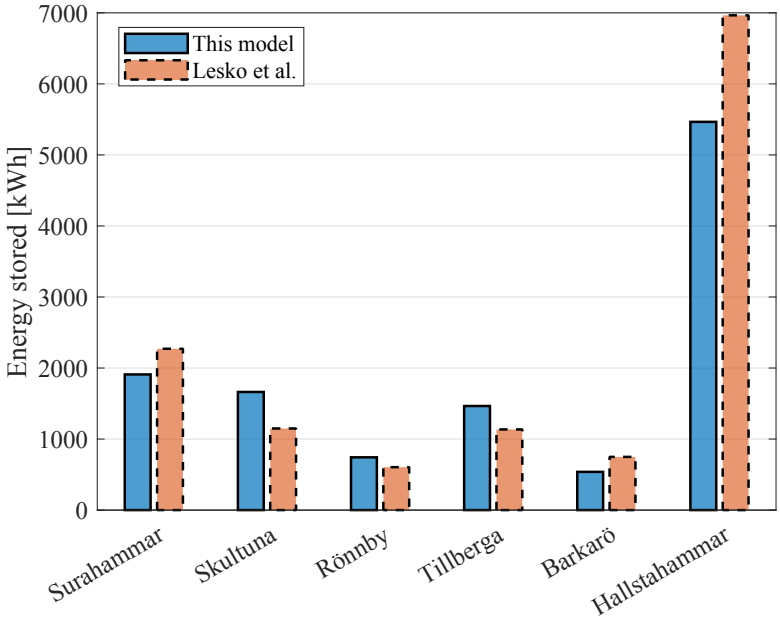

Fig. 4.17. Energy stored in the region's thermal capacity: comparison between this model and that proposed by Leśko et al. [54].

ple dynamic application with the components of the DHN library described in Appendix A, comprising a pipeline loop, a pumping station, a heat exchanger representing the substation and a building representing the aggregated consumer. Thermal power from the historical dataset is supplied to the substation heat exchanger and the equivalent indoor temperature is visualized. An exemplifying result concerning the simulation of the region of Surahammar for the heating season from October 2018 to March 2019 is depicted in Fig. 4.18. It can be noticed that the temperature is maintained around 21 °C and is subject to daily variations between 2 °C and 4 °C, which are compatible with the expected profile. Additional weekly periodical variations in the temperature evolution are visible. They can be justified by the different behavior typically observed on weekends and during holidays (when commercial, industrial or third-sector end-users seldom require heating). This has an influence on the temperature of the aggregated region, which is a representation of its total energy content. Similar results can be derived for other regions and other heating seasons.

4.3.6 Discussion

The developed model does not depend on the scale of the region, which can be viewed as an entire neighborhood as well as an individual dwelling. Therefore, it

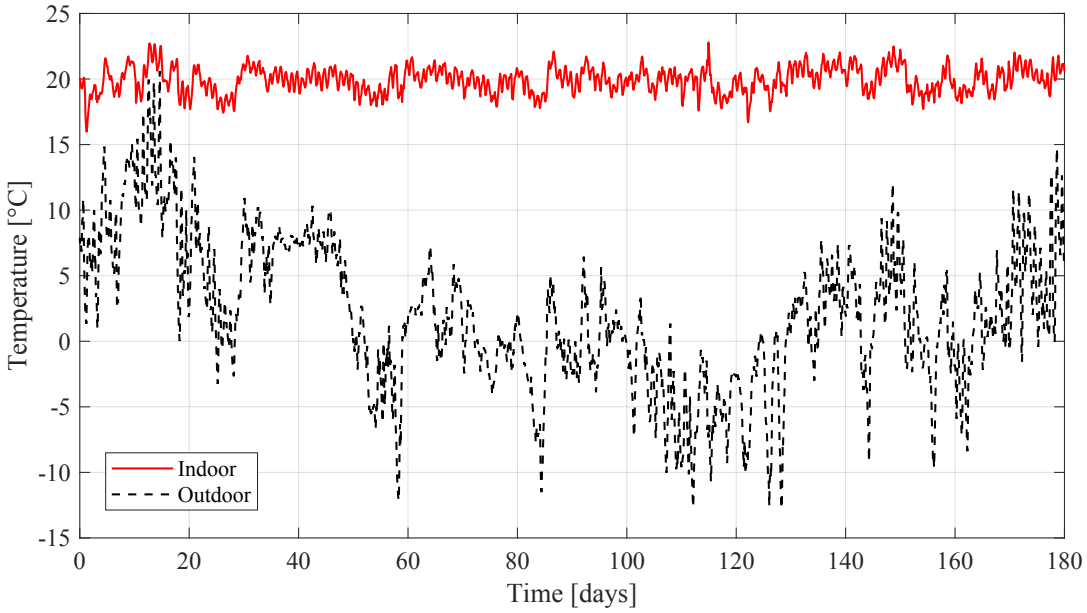

Fig. 4.18. Preliminary test of the model feasibility performed with a Simulink application: region of Surahammar during the heating season October 2018–March 2019.

is versatile and can be exploited for several purposes:

- estimation of heat storage potential of generic DHN areas;
- investigation of innovative management strategies that exploit the region heat capacity as thermal storage;
- Linear Programming optimization problems, due to the model linearity;
- control-oriented applications, such as MPC, where the computational speed is of primary importance, due to the simplified approach adopted.

A potential limitation of the model is the low level of detail in the representation of individual buildings, as they are aggregated with equivalent properties and parameters. Nevertheless, the experimental definition of a significant value of the actual indoor temperature of the buildings in large-scale DHNs is not straightforward and a management solution based on its detailed monitoring may not be applicable. Hence, a region-level view can be beneficial, especially in real-time control. Moreover, the proposed estimation of the heat capacity is conservative, as shown in Section 4.3.5, and leads to a negligible risk of hindering end-user comfort.

In this thesis, the model is the core of a novel optimization algorithm to be embedded in an MPC for large-scale DHNs. The algorithm is detailed in Section 4.4.

4.4 Large-scale district heating: optimization algorithm

The application of DP algorithms to large-scale networks can be particularly challenging due to the "curse of dimensionality" (Section 3.2.1).

Moreover, the DP is ideal when the objective function is an economic or energy cost, which can be cumulated over the considered time horizon. It is, however, not applicable when other problem types such as maxmin or minmax are involved.

In this regard, this section develops another novel deterministic optimization algorithm, designed to achieve new management strategies and MPC control for large-scale DHNs with three main objectives:

- exploit the heat capacity of the connected buildings, without the need for additional investments;
- reduce the peaks in the thermal demand, in order to avoid switching on backup generation devices, which are expensive and inefficient;
- reduce the distribution temperature to lower the heat losses from the pipelines.

The algorithm's general architecture is illustrated in Fig. 4.19. The model of DHN aggregated regions developed in Section 4.3 is used to assign a State of Charge (SoC) variable to each region. This gives a representation of the amount of heat that can be stored in the heat capacity of the region or retrieved from it at all times, without jeopardizing indoor comfort. This concept is exploited by the optimization algorithm, which comprises two stages, namely LP-NLP:

1. Optimization of the thermal power delivered to each region over a future prediction horizon with the goal of peak shaving, achieved by varying the SoC coherently with the indoor comfort constraints. The sequences of optimal thermal power to each region are passed to step 2, where they become constraints.
2. Optimization of (i) the water mass flow rates throughout the network and (ii) the supply temperature from the production plant, with the goal of minimizing the network temperature while keeping pumping costs down.

4.4.1 Region State of Charge

In the literature, there are numerous methods to accurately predict the thermal load of the consumers in a DHN, extensively outlined in Section 2.1. Nowadays,

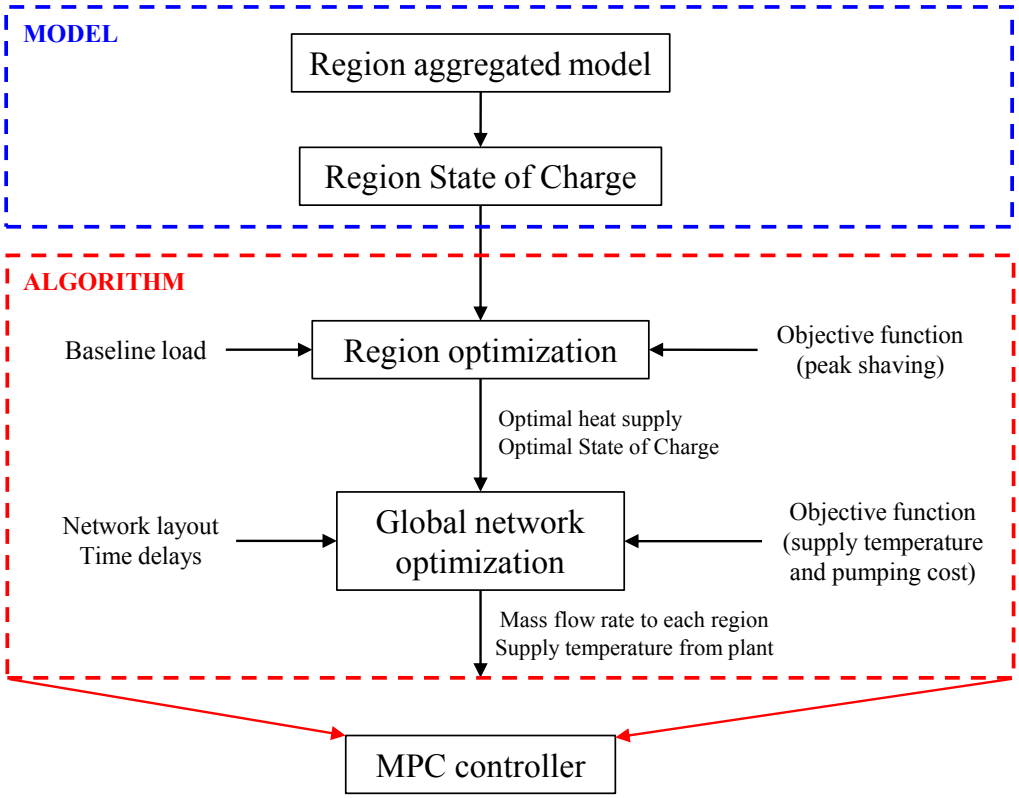

Fig. 4.19. Block diagram of the method for the development of the two-stage LP-NLP optimization algorithm for large-scale DHNs.

black-box models based on historical data are among the most common [56, 57, 155, 156].

In the light of this, the assumptions that define the SoC concept are detailed as follows:

- each region is an aggregated set of end-users characterized by an equivalent temperature, according to the model;
- the historical or predicted load of each region (hourly historical data of the main substations of the network, in this case) is defined as the baseline thermal power and guarantees indoor comfort by maintaining the set-point temperature, which can vary over the day depending on customer requirements;
- the possibility to store/retrieve thermal energy in/from the aggregated region's mass is based on the deviation from this comfort temperature, generated by the deviations from the baseline thermal load, similarly to [69];

- the baseline thermal load corresponds to a region SoC equal to 0.5;
- maximum acceptable deviations from the comfort temperature are limited to $\pm 0.5\,^{\circ}\mathrm{C}$ and are related to variations in the SoC in the range 0 to 1;
- these variations are obtained by regulating the heat supplied to each region and, consequently, storing energy in or retrieving energy from its heat capacity, without altering thermal comfort.

It is worth noting that the acceptable temperature deviation chosen provides a conservative estimation of the region storage capability, since it is lower than the values adopted in other studies (e.g. 1 °C in [69]).

The SoC variable is built by the region aggregated model. Firstly, the model equation Eq. (4.16) is rewritten with the incremental ratio as follows:

$$\dot{Q} = C\,\frac{\Delta T}{\Delta t} + U\;(T - T_{\mathrm{ext}}) \tag{4.22}$$

Secondly, the supplied thermal power is split into two contributions: the baseline load $\dot{Q}_{\mathrm{base}}$ which leads to a rise in temperature equal to ΔT_{base}, and the stored thermal power $\dot{Q}_{\mathrm{stored}}$ which leads to an additional rise (compared to baseline) equal to $\Delta T_{\mathrm{stored}}$. Thus, Eq. (4.23) is obtained:

$$\dot{Q}_{\mathrm{base}}\,\Delta t + \dot{Q}_{\mathrm{stored}}\,\Delta t = C\;(\Delta T_{\mathrm{base}} + \Delta T_{\mathrm{stored}}) + U\,\Delta t\;(T - T_{\mathrm{ext}}) \tag{4.23}$$

The heat that is actually stored in the region (i.e. Q_{stored}), compared to the baseline heat (i.e. Q_{base}), is calculated by Eq. (4.24):

$$Q_{\mathrm{stored}} = \dot{Q}_{\mathrm{stored}}\,\Delta t = \left(\dot{Q} - \dot{Q}_{\mathrm{base}}\right)\,\Delta t = Q - Q_{\mathrm{base}} \tag{4.24}$$

where Q is the actual heat supplied by the DHN through the substation heat exchanger over a time-step.

The maximum heat that can be stored/taken in/from each region is defined by the maximum deviation from the temperature baseline that is acceptable to the users (i.e. that does not compromise the indoor comfort), namely $\Delta T_{\mathrm{stored,max}}$, as follows:

$$Q_{\mathrm{stored,max}} = C\,\Delta T_{\mathrm{stored,max}} \tag{4.25}$$

$$Q_{\mathrm{stored}} = C\,\Delta T_{\mathrm{stored}} \tag{4.26}$$

The SoC of each region is therefore defined by Eq. (4.27):

$$\mathrm{SoC} = \frac{Q_{\mathrm{stored}}}{Q_{\mathrm{stored,max}} - (-Q_{\mathrm{stored,max}})} + 0.5 = \frac{Q_{\mathrm{stored,max}} + Q_{\mathrm{stored}}}{2Q_{\mathrm{stored,max}}} \tag{4.27}$$

In this way, as depicted in Fig. 4.20, the SoC is equal to:

- zero, when the maximum heat in absolute value has been retrieved and a greater subtraction of heat would lead to the violation of thermal comfort constraints;
- 0.5, when no additional heat (compared to baseline) has been stored;
- 1, when the maximum heat has been stored and a further indoor temperature increase cannot be accepted.

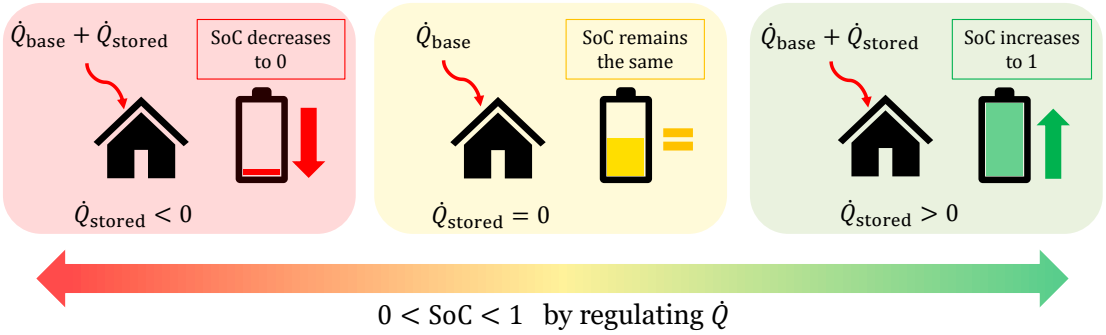

Fig. 4.20. Representation of the concept of State of Charge of a region.

The SoC is the state of the system and is influenced by the amount of incoming thermal power that is stored and by the heat losses to the environment. Its variation in time is expressed by the following differential equation:

$$\frac{d(\mathrm{SoC})}{dt} = \frac{\dot{Q}_{\mathrm{stored}}}{2\,Q_{\mathrm{stored,max}}} - \frac{\dot{Q}_{\mathrm{loss}}}{2\,Q_{\mathrm{stored,max}}} \tag{4.28}$$

The second term $\dot{Q}_{\mathrm{loss}}$ represents the additional heat losses compared to baseline: it is positive if the SoC is higher than the baseline, and negative if it is lower. This is due to the fact that the indoor temperature, together with the SoC, is increased or decreased by $\Delta T_{\mathrm{stored}}$. It is possible to formulate these additional losses by combining Eqs. (4.25) to (4.27):

$$\Delta T_{\mathrm{stored}} = \Delta T_{\mathrm{stored,max}}\ (2\,\mathrm{SoC} - 1) \tag{4.29}$$

$$\dot{Q}_{\mathrm{loss}} = U\,\Delta T_{\mathrm{stored}} = U\,\Delta T_{\mathrm{stored,max}}\ (2\,\mathrm{SoC} - 1) \tag{4.30}$$

The state function Eq. (4.28), together with Eqs. (4.24), (4.25) and (4.30) can be written in a discretized form at the k-th time-step as follows:

$$\mathrm{SoC}_{\mathrm{k+1}} = \mathrm{SoC}_{\mathrm{k}} + \frac{\left(\dot{Q}_{\mathrm{k}} - \dot{Q}_{\mathrm{base,k}}\right)\Delta t}{2\,C\,\Delta T_{\mathrm{stored,max}}} - \frac{U\,\Delta t}{C}\left(\mathrm{SoC}_{\mathrm{k}} - \frac{1}{2}\right) \tag{4.31}$$

This discretized state function, representing the evolution of the SoC of each region, is the core of the optimization problem formulation outlined in Section 4.4.2.

4.4.2 Region optimization

The first stage of the optimization problem aims to optimize the thermal power supplied separately to each region of the DHN. The problem is written in a state-space form for a given prediction horizon. Since the thermal dynamics in large-scale DHNs is relatively long and can reach several hours, a time horizon of at least one day is required to capture all its effects. In order to illustrate the results of the optimization algorithm more extensively, a prediction horizon of three days is considered in this section.

Problem formulation The discretized state function that represents the variation of the SoC for a time-step is given by Eq. (4.31). The initial condition of the problem is the known value of the SoC at the beginning of the prediction horizon SoC_0. The input (i.e. manipulated variable) of the system is the actual thermal power sent to the region $\dot{Q}_\mathrm{k}$ over the prediction horizon, while the baseline load (which depends on the external conditions) $\dot{Q}_\mathrm{base,k}$ is the disturbance. The state and input constraints are given by Eq. (4.32):

$$0 \leq \mathrm{SoC}_\mathrm{k} \leq 1 \tag{4.32a}$$

$$\dot{Q}_\mathrm{k} \geq 0 \tag{4.32b}$$

By renaming SoC as x, $\dot{Q}$ as u and $\dot{Q}_\mathrm{base}$ as d, and by using the following coefficients for the sake of readability:

$$\alpha = \frac{\Delta t}{2\, C\, \Delta T_\mathrm{stored,max}} \tag{4.33a}$$

$$\beta = \frac{U\, \Delta t}{C} \tag{4.33b}$$

it is possible to write the dynamic problem in the state-space form:

$$\begin{cases} x_\mathrm{k+1} = (1-\beta)\; x_\mathrm{k} + \alpha\, u_\mathrm{k} - \left(\alpha\, d_\mathrm{k} - \frac{\beta}{2}\right) \\ x_0 = \mathrm{SoC}_0 \\ 0 \leq x_\mathrm{k} \leq 1 \\ u_\mathrm{k} \geq 0 \end{cases} \qquad \forall\, k = 1 \ldots N \tag{4.34}$$

with N being the number of time-steps of the prediction horizon. This is a Dynamic Linear Programming problem that can be transformed [157] into the following LP

problem with the vector of variables $[u_0, x_1, u_1, x_2 \dots x_{\mathrm{N}-1}, u_{\mathrm{N}-1}, x_{\mathrm{N}}]$:

$$\begin{cases} \min_{u,x} J(u,x) \\ -\alpha\, u_0 + x_1 = (1-\beta)\; x_0 - \left(\alpha\, d_0 - \frac{\beta}{2}\right) \\ (1-\beta)\; x_{\mathrm{k}} - \alpha\, u_{\mathrm{k}} + x_{\mathrm{k+1}} = -\left(\alpha\, d_{\mathrm{k}} - \frac{\beta}{2}\right) \\ -x_{\mathrm{k}} \leq 0 \\ x_{\mathrm{k}} \leq 1 \\ -u_{\mathrm{k}} \leq 0 \end{cases} \quad \forall\, k = 1 \dots N \tag{4.35}$$

This problem consists of calculating the values of the states and inputs for the time-steps of the prediction horizon that minimize the cost function $J(u,x)$. It can be readily solved with the standard algorithms of LP (Section 3.2.2).

Analysis The LP problem in Eq. (4.35) is analyzed by implementing different cost functions and comparing the output. The region of Surahammar of the Västerås DHN is taken as case study. The problem is solved for three representative days (i.e. January 2017) with time-steps of one hour.

Firstly, a preliminary test, namely Case 0, is performed by minimizing the total thermal energy supplied to the region over the prediction horizon. Fig. 4.21 illustrates (i) the optimal thermal power according to this objective function compared to the historical data and (ii) the SoC in both cases. It is worth remembering that the latter is constant and equal to 0.5 in the historical condition, as it represents the baseline in which the indoor temperature is maintained at exactly the set-point required for comfort. The obtained solution is trivial: the SoC of the region is brought to the lower boundary as soon as the simulation starts, in order to reduce the required heat as well as the loss to the environment. This is equivalent to lowering the set-point temperature by 0.5 °C, and is impracticable and non relevant.

Here, the main interest is to achieve peak shaving but also a smooth evolution of the thermal power supplied, in order not to put the production and distribution systems under stress with rapid changes in the operating parameters. For this purpose, four different cost functions are implemented and compared. These cases and the related results are reported in Table 4.6 and illustrated in Fig. 4.22 in terms of sequences of optimal inputs and optimal states. Despite their nonlinearity, these cost functions have particular structures that can be reported to linear functions, as indicated in Section 3.2.2. The percentage peak shaving (PS) and total energy reduction (ER), calculated in Eq. (4.36) with reference to the historical baseline,

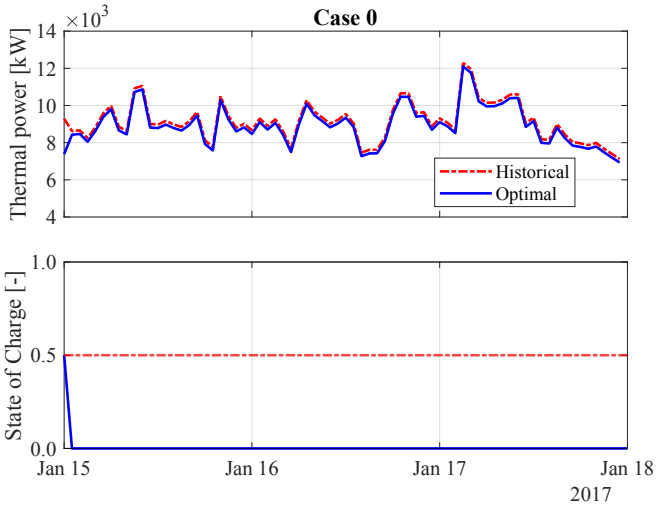

Fig. 4.21. Historical and optimal thermal power and State of Charge as solutions of the Linear Programming problem: Case 0 minimizes the total heat.

Table 4.6. Results of the optimization of the region heat supply with different objective functions. PS: Peak Shaving — ER: Energy Reduction.

Case	Objective to minimize	Function	PS [%]	ER [%]
0	Total heat	$\min_{u,x} \sum_{\mathrm{k}} u_{\mathrm{k}}$	1.59	2.26
1	Maximum heat over horizon	$\min_{u,x} \max_{\mathrm{k}} u_{\mathrm{k}}$	16.21	0.13
4	Maximum consecutive input variation	$\min_{u,x} \max_{\mathrm{k}} \lvert u_{\mathrm{k}} - u_{\mathrm{k}-1} \rvert$	13.17	-0.37
3	Maximum range of input variation	$\min_{u,x} (\max_{\mathrm{k}} u_{\mathrm{k}} - \min_{\mathrm{k}} u_{\mathrm{k}})$	16.21	0.42
4	Total variation of input	$\min_{u,x} \sum_{\mathrm{k}} \lvert u_{\mathrm{k}} - u_{\mathrm{k}-1} \rvert$	16.21	0.25

are the indicators considered for comparing the outcome of the analysis. It should also be remembered that energy reduction is not an objective of the optimization.

$$\mathrm{PS_i} = \left(1 - \frac{\dot{Q}_{\mathrm{i,max,new}}}{\dot{Q}_{\mathrm{i,max,hist}}}\right) \times 100 \tag{4.36a}$$

$$\mathrm{ER_i} = \left(1 - \frac{\sum_{\mathrm{k}} \dot{Q}_{\mathrm{i,k,new}}}{\sum_{\mathrm{k}} \dot{Q}_{\mathrm{i,k,hist}}}\right) \times 100 \tag{4.36b}$$

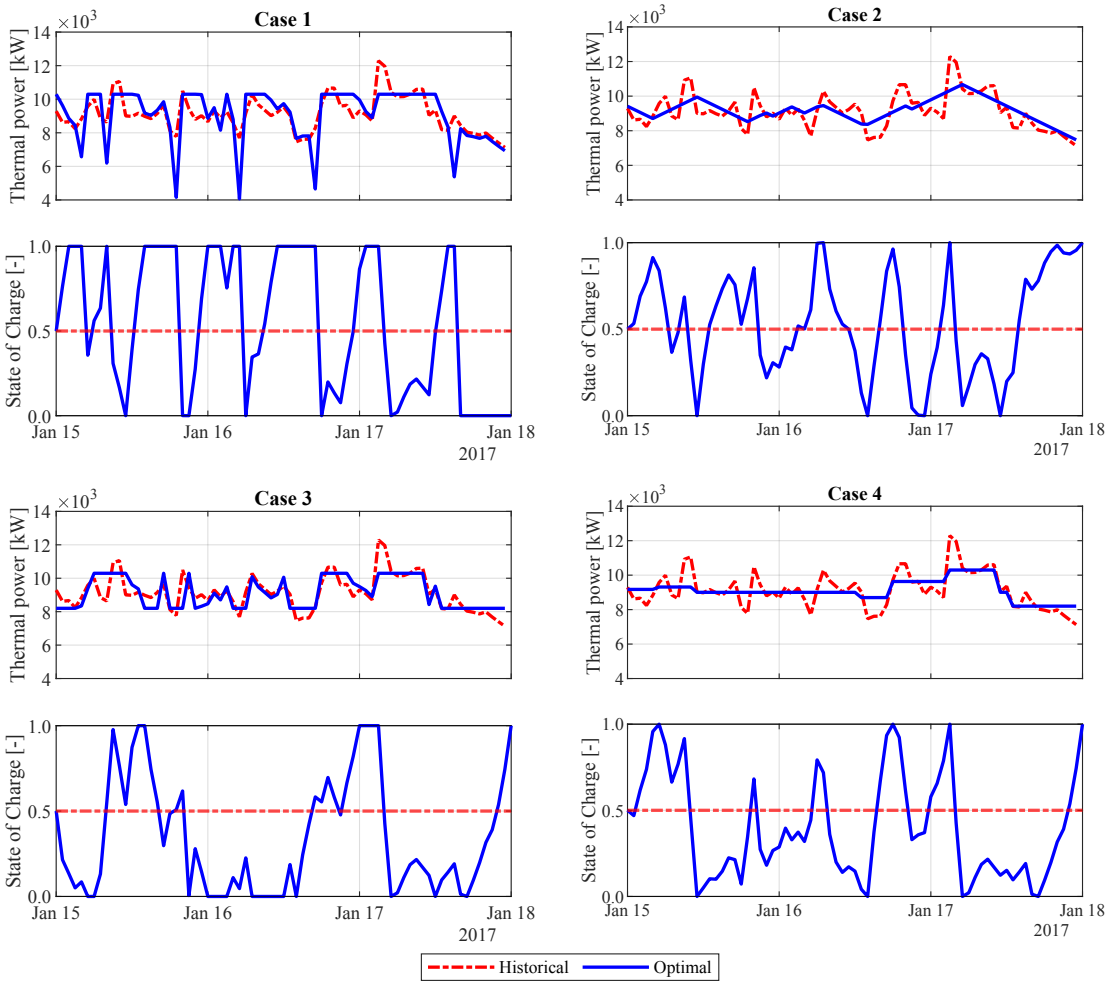

Fig. 4.22. Historical and optimal thermal power and State of Charge as solutions of the Linear Programming problem: Cases 1–4 (the details are reported in Table 4.6).

The optimization allows the thermal peaks to be reduced to different degrees by exploiting the heat capacity of the region. As a matter of fact, the SoC fluctuates between the lower and upper boundaries when it is necessary to store or retrieve heat. Cases 1, 3 and 4 achieves a reduction in peak demand of more than 16 % with no additional energy consumption (with the exception of Case 2 for which, nevertheless, the increase in consumption is negligible).

Some useful conclusions that can be drawn for each case are as follows:

- In Case 1, the input and, consequently, the system state are subject to rapid fluctuations leading to the modulation of thermal power to 40 % of the maximum value in a few hours. This is coherent with the aim of minimizing the maximum input without including any information on its variation in the

cost function. This behavior, however, is not preferable due to the practical difficulties in performing such regulation.

- The sequence of inputs in Case 2 avoids fast changes of the parameters from one step to the next, but the peak shaving obtained is lower than the others.
- In Case 3, input fluctuations are reduced to 80 % of the maximum input in one-hour steps, since the scope is to keep the range of variation of the thermal power as low as possible.
- In Case 4 the evolution of the optimal thermal power is smoother than before, providing slower changes in the supply by regulating the SoC accordingly. Moreover, the same peak shaving and the same range of variation as Case 3 are achieved with additional benefits.

In the light of these reasons, the cost function of Case 4 is chosen in order to proceed with the implementation. Nonetheless, this problem can be adapted with different objectives or combinations of them, depending on the need.

This optimization, if extended to the whole network, can prevent the occurrence of global peaks and, consequently, allow the system operator to avoid turning on backup boilers at the production site. Hence, the LP problem, which constitutes the first stage of the global optimization algorithm, is applied to all the six regions of the Västerås DHN. The sequence of optimal values of thermal power that should be supplied at the substation heat exchanger, hereinafter defined as $\dot{Q}_{\mathrm{LP}}$, and the optimal SoC of each region, defined as $\mathrm{SoC}_{\mathrm{LP}}$, are obtained and passed to the second stage of the algorithm (Section 4.4.3).

4.4.3 Network optimization

The second stage of the optimization algorithm aims to optimize the control variables of the global DHN in order to reduce the supply temperature without increasing pumping costs. This has to be achieved in compliance with $\dot{Q}_{\mathrm{LP}}$ as a constraint.

Problem formulation The optimization variables are the mass flow rates sent to the six regions and the supply temperature at the power plant at each step of the prediction horizon, which comprises N time steps as before. The number of variables is $(6 + 1)\, N$.

The equality constraints are the actual supply of the optimal heat $\dot{Q}_{\mathrm{LP,i,k}}$ to the i-th region at the k-th time-step, as defined by Eq. (4.37):

$$\dot{m}_{\mathrm{i,k}}\, c\, (T_{\mathrm{S,i,k}} - T_{\mathrm{R,SP}}) - \dot{Q}_{\mathrm{loss,i,k}} = \dot{Q}_{\mathrm{LP,i,k}} \tag{4.37}$$

where $\dot{m}_{\mathrm{i,k}}$ is the mass flow rate to the i-th region at the k-th time-step, and $T_{\mathrm{S,i,k}}$ is the temperature that the water reaching the i-th region at the k-th time-step had when it left the power plant, some time before. The return temperature from the substation $T_{\mathrm{R,SP}}$ is assumed equal to a set-point of 35 °C, as achieved in [23]. The approach to calculate heat losses from the pipelines is the same adopted in Section 4.1.1 and recalled in Eq. (4.38):

$$\dot{Q}_{\mathrm{loss,i,k}} = \frac{T_{\mathrm{S,i,k}} - T_{\mathrm{soil}}}{R_{\mathrm{tot,i}}} \tag{4.38}$$

with $R_{\mathrm{tot,i}}$ being the thermal resistance of the pipeline path that conducts to the i-th substation [23, 74].

In this regard, the actual configuration of the network is considered by adopting an automatic approach borrowed from the graph theory (Section 2.1). The N_{r} regions are considered as nodes, while the N_{s} pipeline segments are considered as arcs. The network layout is represented by an $N_{\mathrm{r}} \times N_{\mathrm{s}}$ matrix, namely incidence matrix In, in which the generic element In_{ij}:

- is 1 if arc j belongs to the path from the production plant to node i;
- is 0 otherwise.

A database collects the properties (e.g. diameters, lengths and insulation) of the arcs. The total thermal resistance of the path to each region is then evaluated according to the incidence matrix. More details on the actual configuration of the Västerås DHN are reported in Section 5.3.1. Nevertheless, any generic network can be treated likewise.

It is also important to notice that the temperature that is actually supplied to each region at time k is not the supply temperature at the power plant at the same time k, since there are significant time delays (e.g. several hours) from production to actual delivery in large-scale networks. Since the low computational cost is paramount for this optimization, this network model has to include a simplified representation of the phenomena to avoid an increase in computational complexity. While the authors of [23] select a fixed time delay as an approximation derived from historical data, the present work adopts a procedure to calculate the actual time delays to each region, which depend on the mass flow rates in the different

positions of the network and at different time-steps. The basic assumption is that the temperature front moves at the same speed as the water inside the pipelines, similarly to the model in Section 4.1.1. At each calculation step, the position in the network corresponding to the supply temperature front sent at the previous time-steps is saved and continuously updated in a global matrix. Once this is known, it is possible to evaluate the actual temperature of the water that reaches the different regions at the current step and, therefore, to create the proper constraints for the optimization.

The inequality constraints of the optimization are given in Eq. (4.39):

- the mass flow rate $\dot{m}_{\mathrm{j,k}}$ circulating in the j-th segment at the k-th time-step has to be positive but lower than the maximum mass flow rate allowed;
- the supply temperature has to be higher than the set-point return temperature.

$$0 \leq \dot{m}_{\mathrm{j,k}} \leq \dot{m}_{\mathrm{max,j}} \tag{4.39a}$$

$$T_{\mathrm{S,i,k}} \geq T_{\mathrm{R,SP}} \tag{4.39b}$$

The goal of this stage of the problem is to minimize the maximum value of supply temperature over the prediction horizon. This leads to a reduction in heat losses to the soil while meeting the constraints. Under the same heat supply, as the temperature decreases, the mass flow rate increases and so do the pumping costs, which depend on the third power of the mass flow rate itself. For this reason, a penalty factor proportional to the total pumping power over the prediction horizon is added to the cost function in order to discourage impracticable flow rates. The approach to calculate the pumping power is the same adopted in Section 4.1.1 and recalled in Eq. (4.40):

$$P_{\mathrm{pump,k}} = \sum_{\mathrm{j}} \left(\frac{8 f_{\mathrm{j}} L_{\mathrm{j}}}{\pi^2 \rho^2 D_{\mathrm{j}}^5} \frac{1}{\eta_{\mathrm{pump,j}}} \dot{m}_{\mathrm{j,k}}^3 \right) \tag{4.40}$$

Hence, the overall objective to realize is the following minmax:

$$\min J = \min \max \left(T_{\mathrm{S}} + \Phi \sum_{\mathrm{k}} P_{\mathrm{pump,k}} \right) \tag{4.41}$$

with Φ being the penalty weight for the pumping power (i.e. 10^{-4} in this case).

The optimization problem comprising Eqs. (4.37), (4.39) and (4.41) is an NLP problem and is solved with the Interior Point algorithm (Section 3.2.3) available in MATLAB®.

Analysis The two-stage LP-NLP optimization algorithm that involves the entire network of Västerås is analyzed by solving the problem for three representative days (i.e. January 2017) with time-steps of one hour. The LP problem and the NLP problem are solved in sequence.

Fig. 4.23 represents (i) the supplied thermal power according to the historical dataset and (ii) the thermal power that is actually delivered to the six regions with the new mass flow rates and supply temperature, as calculated by the optimization algorithm. The maximum difference between the actual thermal power supplied with these parameters and that separately calculated by the LP and given as a constraint to the NLP is, in all cases, lower than 0.25 % (Fig. 4.24).

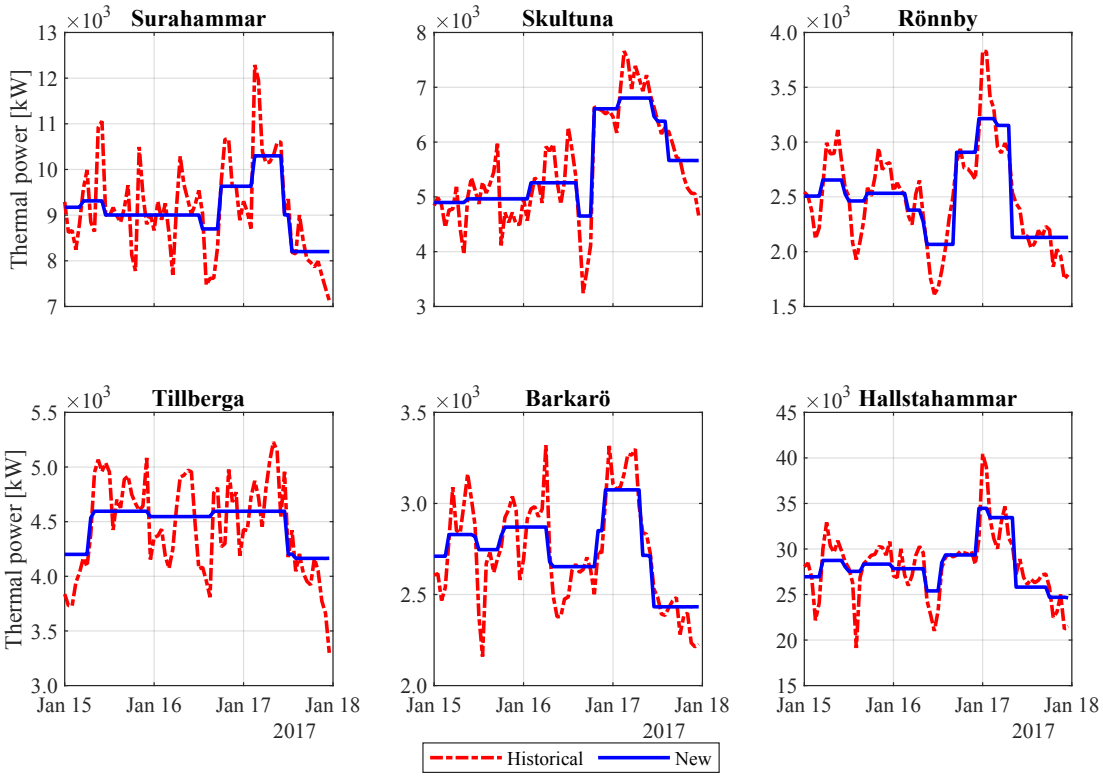

Fig. 4.23. Thermal power supplied according to the historical dataset and to the optimization algorithm.

Moreover, as expected, for all network regions the peak of the actual thermal power is significantly reduced compared to that before the optimization. Table 4.7 reports the peak shaving achieved for each region and the percentage reduction in the thermal power variation range (RVR), calculated by Eq. (4.42) as the difference between maximum and minimum values over the given horizon, compared to the

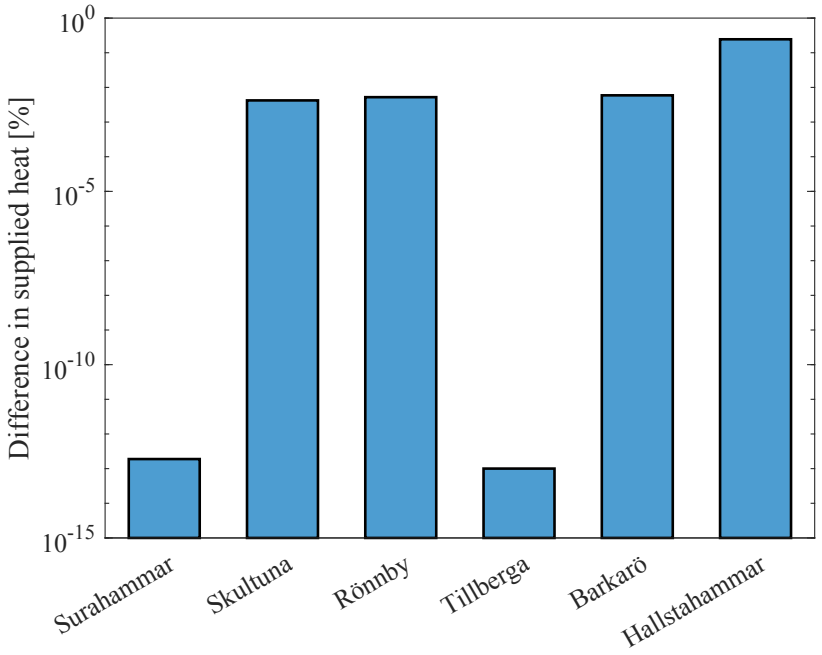

Fig. 4.24. Maximum percentage difference between optimal heat given as a constraint and actual heat supplied with the new operating parameters of the network.

Table 4.7. Results of peak shaving (PS) and reduction in variation range (RVR) of the six external regions of the Västerås district heating network as obtained with the optimal operating parameters.

Region	PS [%]	RVR [%]
Surahammar	16.2	59.3
Skultuna	11.2	51.3
Rönnby	16.1	48.3
Tillberga	12.1	77.6
Barkarö	7.3	44.5
Hallstahammar	14.8	53.9

historical case:

$$RVR = \left(1 - \frac{\dot{Q}_{\text{max,new}} - \dot{Q}_{\text{min,new}}}{\dot{Q}_{\text{max,hist}} - \dot{Q}_{\text{min,hist}}}\right) \times 100 \tag{4.42}$$

The optimization leads to a smoother and more regular operation, which is desirable for managing the production plant more efficiently.

Furthermore, the range of variation of the mass flow rates in the nine main

distribution pipelines of the network (see Fig. 5.15), as well as their boundaries given by historical data, are represented in Fig. 4.25. It is further confirmed that the operating constraints are respected, and the flows are not subject to impracticable variations.

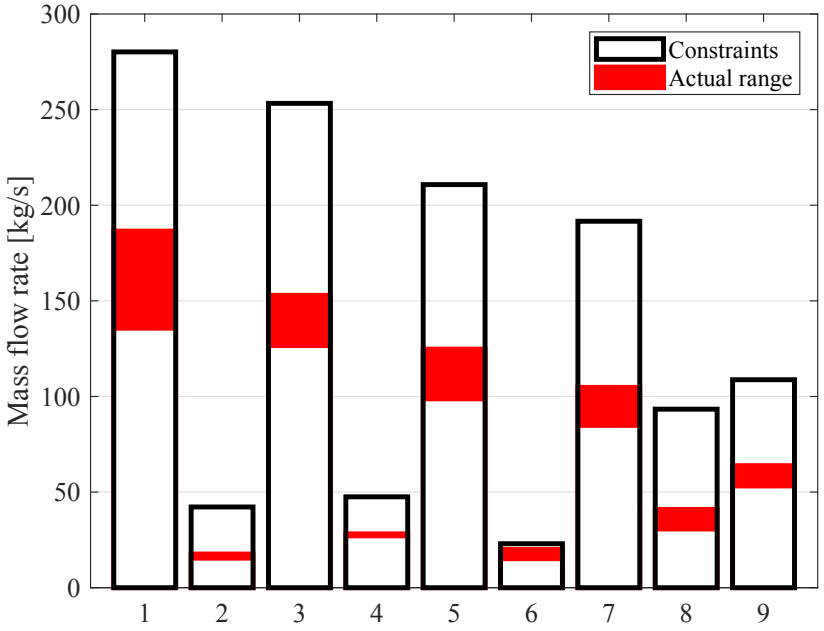

Fig. 4.25. Actual range of variation of the mass flow rate compared to the constraints for nine pipeline segments of the district heating network.

4.4.4 Discussion

The outcomes discussed above show that the results of the optimization are coherent with the constraints and objectives. The computational time necessary for a single run of the entire two-stage optimization algorithm with different prediction horizons is reported in Table 4.8.

Table 4.8. Computational time of the two-stage optimization algorithm.

Length of prediction horizon [h]	Computational time [s]
24	10
48	50
72	120

Other measures might be adopted to further reduce this computational effort. For instance, the nonlinearities introduced by the temperature propagation in the network could be eliminated by introducing instruments such as look-up tables to calculate the network delays depending on the flows. This would require detailed sensitivity analysis of the algorithm performance.

Nonetheless, the implementation of the proposed algorithm as part of an MPC controller that updates its variables and performs the calculation every hour is feasible. Its application to the large-scale Västerås DHN is presented in Section 5.3.

5 Applications and results

The innovative methods developed in this thesis are fundamental elements of novel smart controllers based on Model Predictive Control for small-scale and large-scale DHNs. These new strategies are all tested in a Model-in-the-Loop configuration.

Detailed models that emulate complex energy systems, such as DHNs, are indeed fundamental for the development of efficient management and control strategies. Experimental investigations on proper test rigs can be rarely carried out for several reasons:

- the system size and complexity are not suitable for laboratory-scale experimental setups;
- the characteristic time scale of heating networks (e.g. days) would require relatively large experimental times;
- the high variability of the disturbances over the year does not allow different solutions to be compared in a consistent way and with the same boundary conditions;
- demonstration of new control strategies in a real network might jeopardize the fulfillment of comfort requirements of the energy system customers.

All these issues highlight the importance of conducting a detailed evaluation and refinement of management and control strategies in a simulation environment before implementing them in real systems.

According to the MiL concept [158], a detailed mathematical model, also called system *digital twin*, which reproduces the system dynamics typically faster than real-time, is controlled by a model of the controller, in which the control algorithm code is integrated. In this way, the controller logic is tested and verified on a simulated model without affecting the real system.

This is the aim of the MiL platforms exploited in this thesis to test real-time MPC controllers on DHNs. As illustrated in Fig. 5.1, the MPC controller, which comprises the simplified system model and the optimization algorithm, controls the simulator of the system (i.e. MiL model). With the information available at time-step k, the MPC calculates the optimal control action, which is applied to the MiL model. This, in turn, gives the actual system variables at time-step $k+1$, used to provide the new initial condition to the controller. A new optimization is repeated at time-step $k+1$ to give the new optimal control action. This procedure of control and state update is carried out until the end of the simulation.

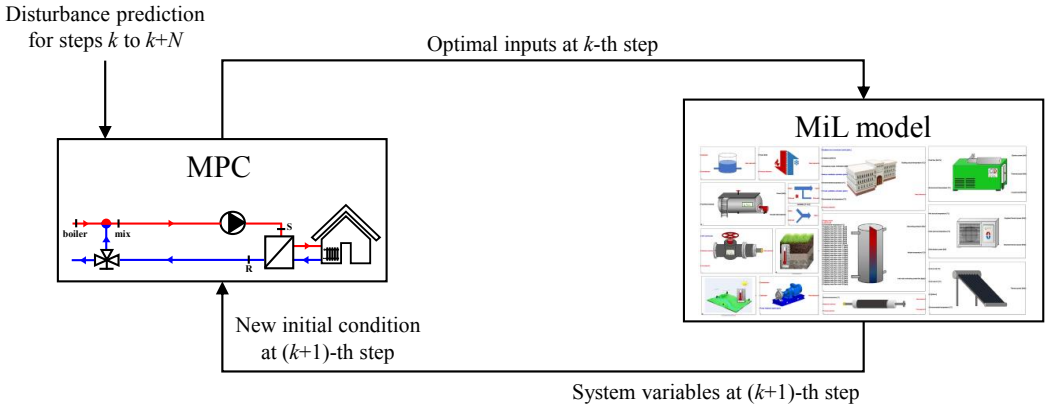

Fig. 5.1. Schematic representation of a generic MPC test in an MiL application.

In particular, the proposed applications are:

- Smart control of a small-scale DHN powered by an Organic Rankine Cycle (ORC) system. In this case, the MPC has a multi-agent hierarchical architecture and adopts the model and DP algorithm described in Sections 4.1 and 4.2, respectively. The test is performed within the MiL platform described in Appendix A. A customized robust version of this application is further investigated, aiming to control a CHP plant to perform flexibility service to the power grid in presence of uncertainty.

- Smart control of a large-scale DHN. The MPC is a high-level controller that builds the set-points of the main parameter of the distribution network. It adopts the aggregated region model and two-stage LP-NLP optimization algorithm described in Section 4.3 and Section 4.4, respectively. The test is performed on the network simulator developed by Zimmerman et al. [23].

All applications and analyses are carried out in the MATLAB®/Simulink® environment.

5.1 Smart control of small-scale district heating

The DP algorithm has firstly been tested in preliminary simple applications [159]. For instance, the heat distribution network of an individual building of the service sector has been modeled within the MiL platform and controlled by a dedicated MPC [160]. One of the most important achievements is that the smart controller rationalizes the energy consumption by supplying the right amount of heat to the building in order to keep the indoor temperature within the constraints only

when it is occupied. In this way, the required comfort is guaranteed without the energy waste that would derive from reaching the temperature set-point before the building is occupied.

The full capability and replicability of this MPC for small-scale networks, however, has to be demonstrated in a more complex case. To this end, this section presents the smart control of the small-scale DHN in a multi-agent hierarchical architecture [161]. The investigation includes the entire system, from energy production, to its distribution and final consumption.

The main objectives of the control for this application are:

- to minimize energy supplied to each network branch;
- to minimize power plant operating cost and electricity purchase.

It also aims to analyze profitable management strategies for production plants that are not conventional for these types of systems, e.g. ORCs.

5.1.1 System description

The case study is the DHN of a school complex comprising three education buildings (i.e. a sports hall, a secondary school and a primary school), located in the Emilia-Romagna region, in northern Italy.

The network is supplied by an ORC plant in cogeneration mode. This type of energy conversion device is versatile due to the possibility of exploiting a wide variety of heat sources [162] in the evaporator (e.g. waste heat recovery, biomass boilers and solar thermal collectors). Moreover, they can meet the electrical demands and, at the same time, supply heat distribution networks in an efficient way. In this case, the ORC is powered by a biomass boiler. Nevertheless, this does not hinder the generality of the approach, as any other low-temperature source can be considered.

The plant produces electrical power to supply the building appliances. A bidirectional connection the power grid allows electricity to be sold when the production exceeds the demand or to be purchased otherwise.

The plant works with a condenser temperature equal to 90 °C [163] and the heat transferred from this component is recovered and directly supplied to a Thermal Energy Storage tank (TES) in two inlets-two outlets configuration [164]. The latter element acts as a buffer by decoupling production and utilization. A supply manifold collects hot water from the TES and dispatches it to the the three buildings, each fed by a branch of the distribution network. Once the thermal

power has been transferred to the building substation heat exchangers, the water is partly recirculated to the building itself, if required, and partly collected by the return manifold of the TES. The internal temperature of the buildings has to be maintained at the comfort value of 20 °C when the buildings are occupied.

The MiL model of the system, used to emulate the behavior of the real system, is created by means of the in-house library of energy system components described in Appendix A. The model is schematized in Fig. 5.2. According to the modeling approach of the library, the heat exchanger model is exploited to simulate the interactions between the energy conversion device (the ORC condenser, in this case) and the heat transfer fluid. The substation heat exchangers of the end-users are included within the building submodel itself.

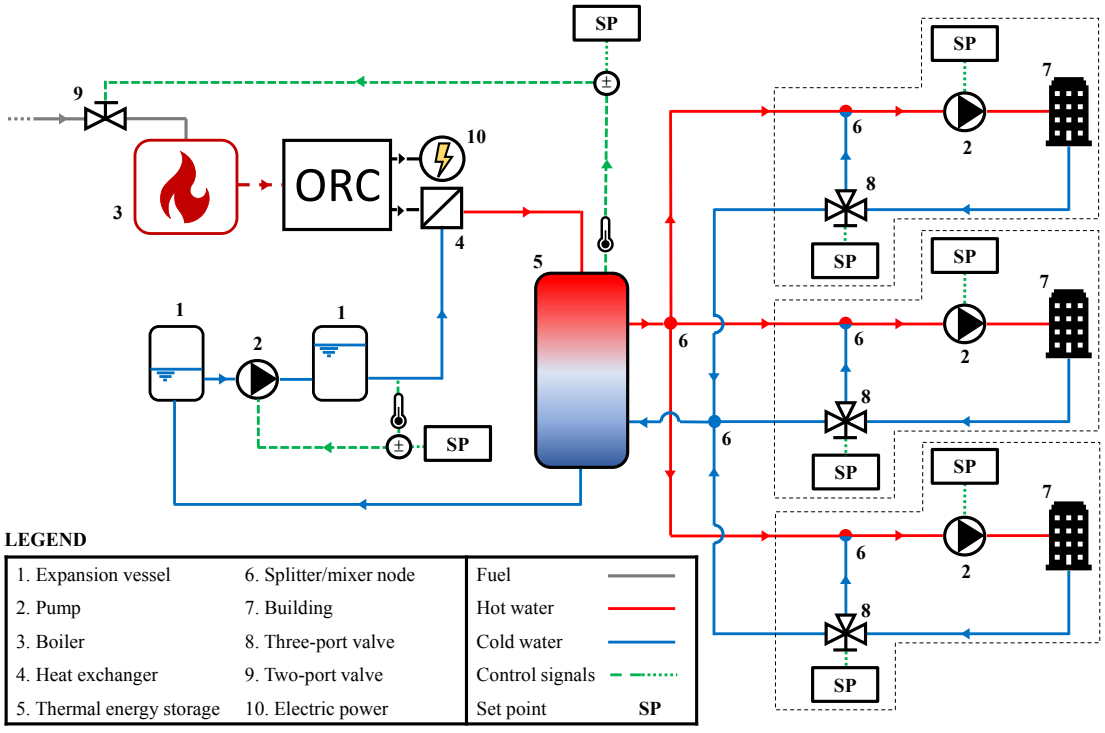

Fig. 5.2. Schematic representation of the small-scale district heating network.

The values of the system main parameters are reported in Table 5.1. The ORC system is sized according to [165], in which the thermal power recovered from a Rankine cycle is around two thirds of the overall end-user thermal peak demand. This is the sum of the maximum thermal power that each distribution branch can delivered, calculated by considering the maximum mass flow rate and the design supply and return temperatures. The efficiency parameters of the ORC are taken from [166]. The size of the TES is also designed according to [165], which indicates

that a profitable sizing is given by the storage ability to fulfill the circuit peak load for 1.5 hours to 2 hours. The TES model is discretized into five nodes.

Table 5.1. System main parameters.

Element	Parameter	Value
Biomass boiler	Nominal thermal power	2500 kW
	Nominal efficiency	0.90
	Biomass LHV	17 MJ kg^{-1}
ORC unit	Nominal electric power	400 kW
	Nominal thermodynamic efficiency	0.16
	Minimum load electric power	60 kW
	Minimum load thermodynamic efficiency	0.10
TES tank	Internal diameter	6 m
	Height	6 m
	Tank thickness	10 mm
	Insulation thickness	50 mm
Sports hall	Envelope heat loss coefficient	0.0262 h^{-1}
	Supplied power coefficient	$7.53 \cdot 10^{-7}$ °C kJ^{-1}
	Pipeline length	100 m
Secondary school	Envelope heat loss coefficient	0.0126 h^{-1}
	Supplied power coefficient	$9.08 \cdot 10^{-7}$ °C kJ^{-1}
	Pipeline length	50 m
Primary school	Envelope heat loss coefficient	0.0081 h^{-1}
	Supplied power coefficient	$1.35 \cdot 10^{-7}$ °C kJ^{-1}
	Pipeline length	200 m

5.1.2 Control architecture

The control architecture of the network comprises two types of controller:

- high-level controllers, which establish the set-points for system operation according to predefined rules or optimal strategies;
- low-level controllers, which regulate the actuators in order to track the set-points.

A conventional control strategy (hereinafter referred to as PID) is used as a term of comparison for evaluating the performance of the MPC. The two approaches differ as regards the high-level control, which defines the set-points for the pumps and valves of the system, i.e. optimized in the MPC and predefined in the PID. The latter constitute the most common operational strategy adopted nowadays in district heating.

PID control strategy The PID control is based on the following features:

- A PI controller (i.e. proportional integral) regulates the pump rotational speed of the ORC condenser cooling circuit in order to guarantee that the thermal power is correctly retrieved, and the temperature of the water supplied to the TES is kept at 80 °C.
- A proportional controller regulates the fuel to the biomass boiler in order to maintain a minimum state of charge of the TES at all times, i.e. the temperature in the upper fifth of the tank is kept between 70 °C and 80 °C.
- A feedback closed-loop regulates the water mass flow rate sent to each building substation through the pump rotational speed (Fig. 5.3) in order to control the building indoor temperature. The recirculation is disabled, thus the supply temperature is that exiting the TES upper node. This control is activated according to time-scheduled set-points that send the maximum thermal power five hours before the building is occupied.
- A proportional controller regulates the building space heaters in order to maintain the water return temperature at the design value of 60 °C (Fig. 5.3).

MPC control strategy In the innovative control approach, the ORC condenser cooling circuit and the building space heaters are regulated as in the PID method. The other set-points at each time-step are calculated by different MPCs, which are designed in a multi-agent hierarchical architecture, as illustrated in Fig. 5.4.

The multi-agent approach consists of splitting the demand side of the system into smaller sub-systems (i.e. the network branches supplying the buildings), each managed by a representative agent and communicating with a central agent, which operates the production side. The features of the agents are explained below:

1. The MPC controller of each network branch is defined *building-MPC*. At each time-step, it receives the actual building temperature and returns the optimal

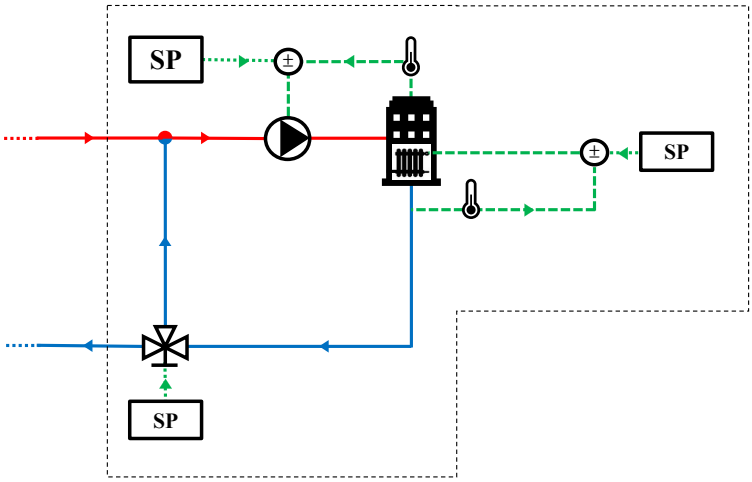

Fig. 5.3. Conventional control strategy of each distribution branch.

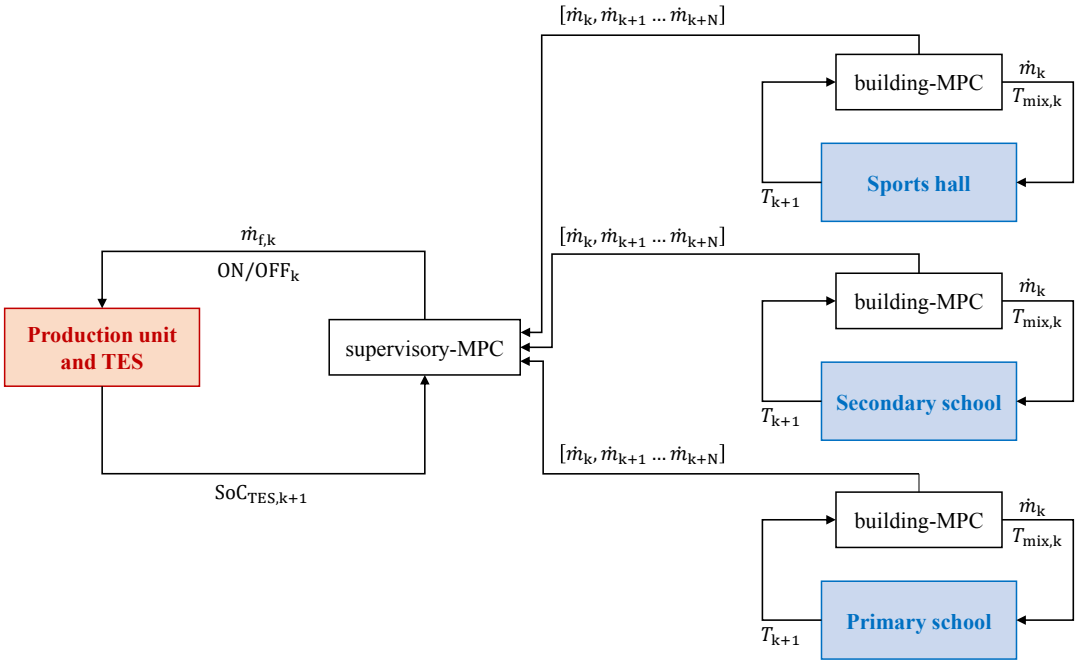

Fig. 5.4. Global architecture of the multi-agent hierarchical control strategy.

set-points for water mass flow rate and supply temperature (Fig. 5.5). The former is tracked with the feedback loop on the pump rotational speed while the latter is tracked by setting the recirculation valve with an open-loop controller (e.g. look-up table). Each building-MPC adopts the DP algorithm and model in the configuration described in Section 4.2. Hence, its objective is to minimize the total heat supplied to each branch and pump energy over the prediction horizon.

2. The MPC controller of the production side is defined *supervisory-MPC*. At each time-step, it receives (i) the State of Charge (SoC) of the TES and, (ii) as disturbances, the predicted thermal demands over the prediction horizon as calculated by the building-MPCs. It then calculates the optimal set-points to operate the plant in order to minimize the total operating cost while guaranteeing that the TES is able to fulfill the downstream thermal demand. The supervisory-MPC adopts the same DP algorithm with a different model, detailed below.

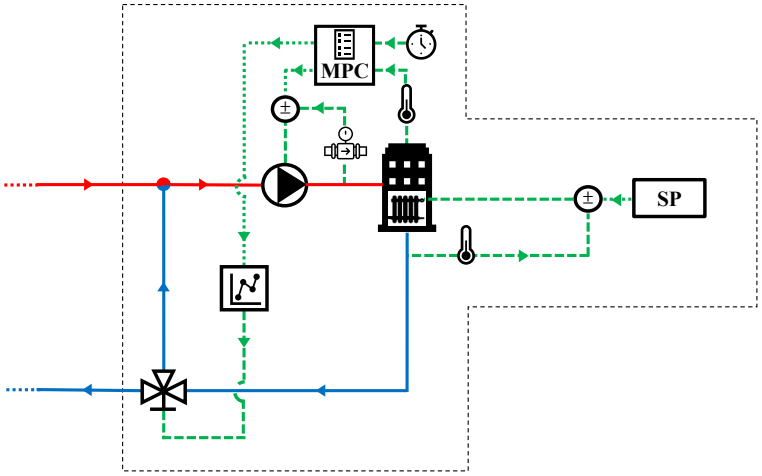

Fig. 5.5. Building-MPC of each distribution branch.

Supervisory-MPC model Since it controls the energy production side, the supervisory-MPC requires a simplified model of the boiler, ORC and TES. In order to comply with the DP algorithm main requirement, the model has one state.

The thermocline assumption [167] represented in Fig. 5.6 is adopted for the TES model: the tank is split into two zones at a defined high temperature T_{h} (80 °C) and low temperature T_{l} (60 °C). The position of the virtual separation surface, with reference to the top of the tank, between the zones is called thermocline and represents the TES State of Charge and system state X_{TES}, constrained between 0 and the TES total height H_{TES}. The state function describes the evolution of the thermocline depending on TES characteristics and incoming and outgoing flow rates:

$$\rho\, c\, A_{\mathrm{TES}}\, (T_{\mathrm{h}} - T_{\mathrm{l}})\, \frac{dX_{\mathrm{TES}}}{dt} = \dot{Q}_{\mathrm{rec}} - \dot{m}_{\mathrm{tot}}\, c\, (T_{\mathrm{h}} - T_{\mathrm{R}}) - \dot{Q}_{\mathrm{loss}} \tag{5.1}$$

where A_{TES} is the tank base surface, $\dot{m}_{\mathrm{tot}}$ is the total mass flow rate requested by

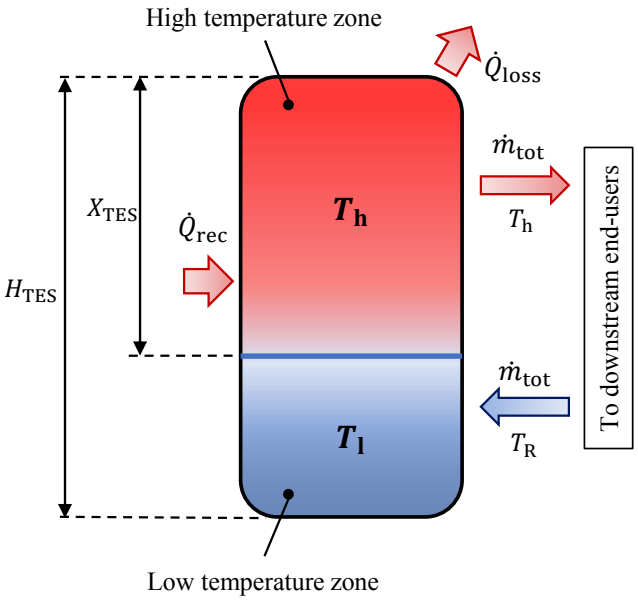

Fig. 5.6. Thermal Energy Storage tank model with thermocline assumption.

the end-users downstream, and $\dot{Q}_{\text{rec}}$ is the heat recovered from the ORC condenser. The heat lost to the environment $\dot{Q}_{\text{loss}}$ is given by:

$$\dot{Q}_{\text{loss}} = \pi \, D_{\text{TES}} \, U_{\text{TES}} \, [X_{\text{TES}} \, (T_{\text{h}} - T_{\text{ext}}) + (H_{\text{TES}} - X_{\text{TES}}) \, (T_{\text{l}} - T_{\text{ext}})] \tag{5.2}$$

Apart from $\dot{m}_{\text{tot}}$, the other disturbances are the electrical demand P_{dem} and the ambient temperature T_{ext}.

The inputs are the fuel mass flow rate $\dot{m}_{\text{f}}$ and the power bought from the electric grid P_{bg}. Since the boiler and ORC are switched off for loads lower than minimum load conditions, it is necessary to include the boiler on-off signal SW as third input variable. This is an integer variable equal to 0 or 1 if the boiler is operating or not, respectively. The recovered heat is defined by Eq. (5.3) according to the boiler and ORC algebraic models, with the corresponding efficiencies η_{b} and η_{th}:

$$\dot{Q}_{\text{rec}} = \dot{m}_{\text{f}} \, LHV \, \eta_{\text{b}} \, (1 - \eta_{\text{th}}) \, SW \tag{5.3}$$

The electrical power produced by the ORC and the electrical energy balance that has to be satisfied at all times are calculated as follows:

$$P_{\text{ORC}} = \dot{m}_{\text{f}} \, LHV \, \eta_{\text{b}} \, \eta_{\text{th}} \, \eta_{\text{m}} \, \eta_{\text{el}} \, SW \tag{5.4}$$

$$P_{\text{ORC}} + P_{\text{bg}} = P_{\text{dem}} + P_{\text{sg}} \tag{5.5}$$

with η_{m} and η_{el} being the ORC mechanical and electrical efficiencies, respectively, and P_{sg} being the power sold to the grid. The model is written in a time-discrete form with forward Euler method, similarly to the DP model in Section 4.1. The details are not reported for the sake of brevity.

The cost function for each time-step of the algorithm is given by the sum of the costs of the biomass, electricity bought from the grid and the revenues resulting from the sale of electricity to the grid, when present:

$$J = (C_{\mathrm{bg}}\, P_{\mathrm{bg}} - C_{\mathrm{sg}}\, P_{\mathrm{sg}} + C_{\mathrm{f}}\, \dot{m}_{\mathrm{f}})\ \Delta t + \phi \tag{5.6}$$

with C_{bg}, C_{sg} and C_{f} being the specific costs of the bought and sold electric power and of the fuel, respectively. In this application, these parameters are considered constant (Table 5.2) without hindering the generality of the approach. Indeed, it is possible to include them as predicted disturbances, variable over time. The penalty factor ϕ is added when the state constraints are not met and when the TES energy content is not able to comply with the downstream thermal demand. An additional penalty as start-up cost is given do discourage frequent plant start-ups and shut-downs.

To sum up, Table 5.3 reports the model variables for the DP algorithms of this application while Table 5.4 reports the discretization parameters, which comply with the sensitivity analysis carried out in Section 4.2.2.

Table 5.2. Specific costs of electricity and biomass.

Bought electricity	Sold electricity	Biomass
0.16 € kWh^{-1}	0.08 € kWh^{-1}	0.16 € kg^{-1}

5.1.3 Results

The network is simulated for four days in January. The prediction horizon and time-step for the MPCs are three days and 15 min, respectively. The results of the MiL simulations concerning the indoor temperature of the schools are depicted in Fig. 5.7. The sports hall is not shown for the sake of brevity, but similar results can be obtained.

When the buildings are occupied (shaded areas), the indoor temperature is kept within the constraints while it is left unconstrained otherwise. The average temperatures in the constrained periods are reported in Table 5.5, showing that the difference between the PID and MPC control methods is negligible as far as indoor

Table 5.3. Variables of the DP algorithms embedded in the building-MPC and supervisory-MPC.

	Building-MPC	Supervisory-MPC
State	Building temperature	TES thermocline
Inputs	Water mass flow rate	Fuel mass flow rate
	Water mixing temperature	Electricity bought
		Boiler on-off
Disturbances	Outdoor temperature	Outdoor temperature
	Soil temperature	Total mass flow rate to buildings
		Electrical demand
Cost	Total heat and pump energy	Total electricity and fuel cost

Table 5.4. State and input discretization parameters of the DP algorithms.

		Building-MPC	Supervisory-MPC
State	Δx	0.1 °C	0.05 m
	Δu_1	0.5 kg s^{-1}	0.001 kg s^{-1}
Inputs	Δu_2	1 °C	10 kW
	Δu_3	-	Integer [0,1]

thermal comfort is concerned. It is also possible to notice that the conventional controller generally results in the required temperature being reached several hours before it is needed with consequent energy wastage, as it is based on set-points established by a predefined rule. Whereas, the MPC controller can send the exact amount of energy required to keep comfort at the minimum allowed temperature. At the same time, when necessary, it manages the thermal inertia of the building by establishing the right time to supply heat and by using the heat capacity as storage. This confirms the capability of the MPC controller to efficiently control buildings with different thermal characteristics, fulfilling the indoor comfort requirements while reducing heat losses.

The two control approaches show significant differences also in the management of the production plant. Fig. 5.8 depicts the electrical output of the ORC power plant compared to the power demand of the whole school complex. The electrical power produced by the plant is not always enough to fulfill the electrical demand, but it should be remembered that the main goal of the plant is to fulfill the

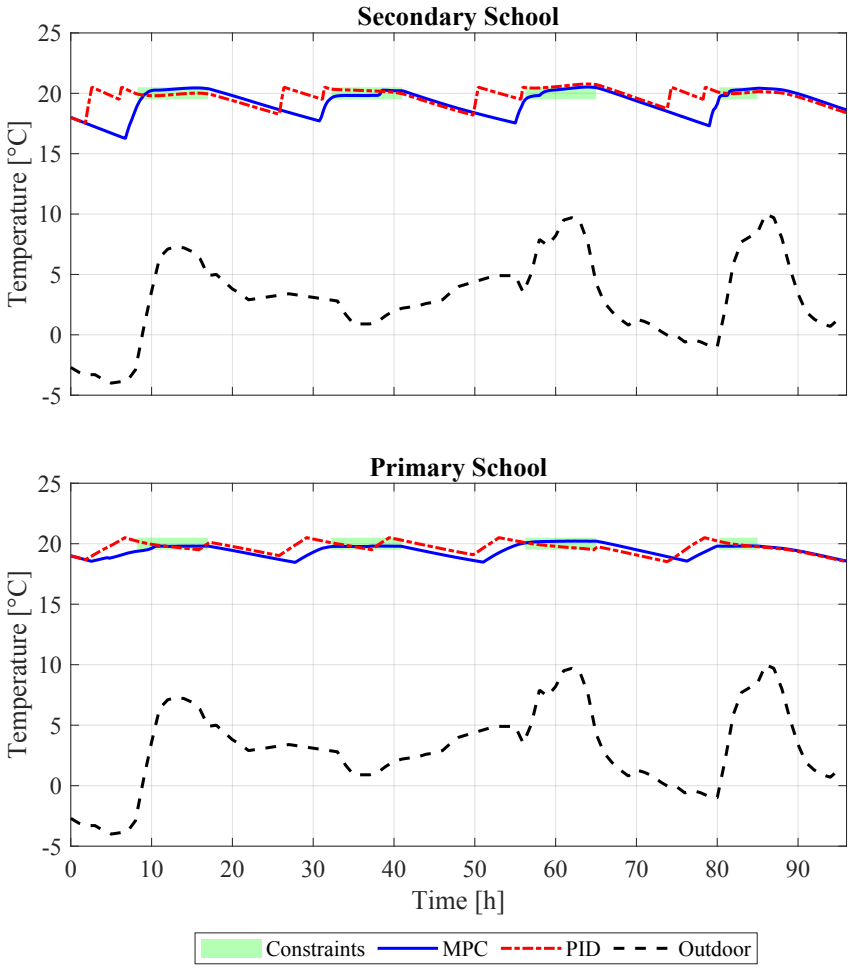

Fig. 5.7. Indoor temperature of two buildings with the MPC and conventional (PID) controllers.

Table 5.5. Average indoor temperatures when buildings are occupied (i.e. contrained periods).

Building	PID average T [°C]	MPC average T [°C]
Secondary school	20.20	20.12
Primary school	19.86	19.88

downstream thermal demand. The electricity is bought from the power grid to cover the demand when self-production is not sufficient, while it is sold to the grid when in excess. The graph shows that the ORC is managed in an on-off way by the PID control, while the MPC is able to define the operating strategy that

minimizes the total cost and modulates the plant output. Indeed, when the indoor comfort of the building is maintained, the production is regulated in order to cover as much electrical demand as possible, while avoiding the complete charge of the storage.

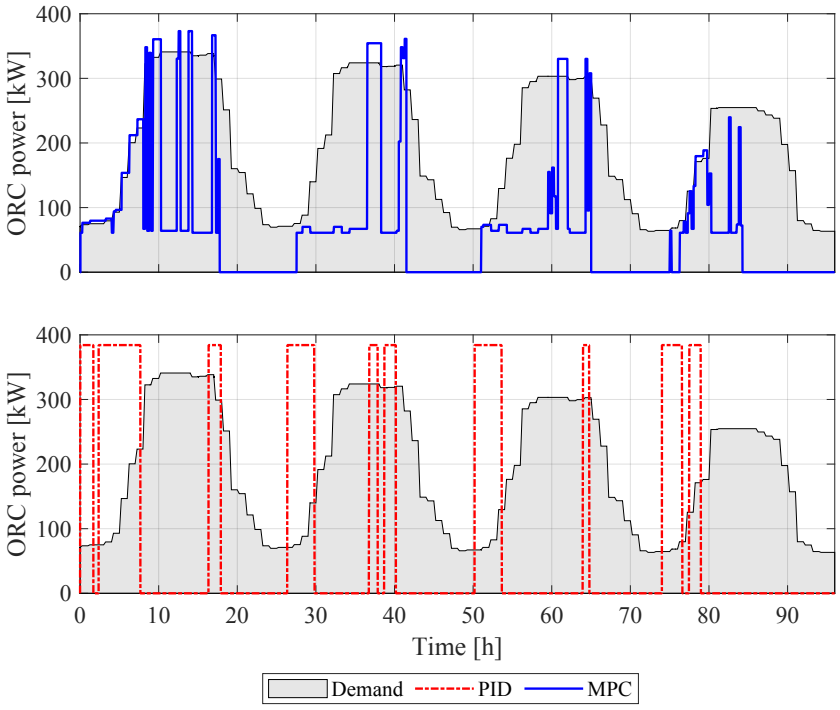

Fig. 5.8. ORC electrical power output and electrical demand with the MPC and PID controllers.

The MPC also optimizes the management of the TES to make sure that, at each calculation step, there is enough stored thermal energy to guarantee the energy supply to the circuits downstream over the prediction horizon, while minimizing the thermal losses from the tank. Fig. 5.9 represents the temperature of the five nodes in which the TES model is discretized. The comparison between the TES temperature evolution in the two control strategies shows that the MPC charges the storage when there is thermal request from the end-users while trying to keep the temperature as low as possible to reduce energy loss.

The economic and energy results of the analysis are reported in Table 5.6. The following key considerations can be drawn:

- As expected, the MPC shows a 7 % reduction in total energy cost.
- Fuel consumption is reduced by 13 %.

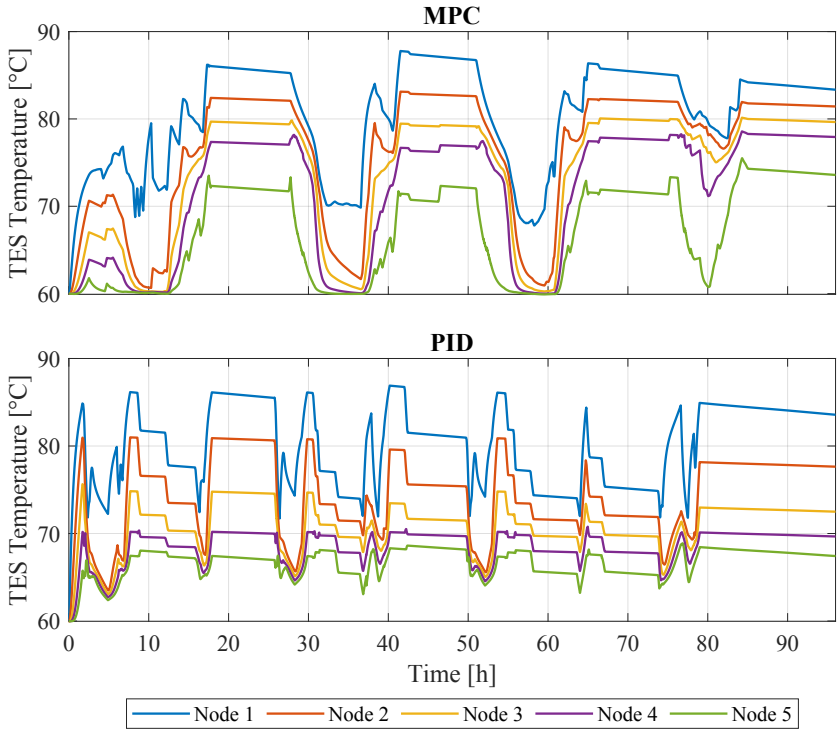

Fig. 5.9. Node temperatures of the thermal energy storage tank with the MPC and PID controllers.

- It is not considered cost-effective to produce and sell electricity to the grid, due to the low thermodynamic efficiency of the ORC. Thus, the produced and sold electricity decrease.
- The total primary energy, obtained by considering an overall efficiency of the national grid equal to 0.41 [168], slightly increases with the new control strategy. Other promising results might be obtained by choosing the total energy consumption as objective function.
- The self-consumed electricity, which is the percentage of the total electric demand satisfied by the ORC production, is increased by more than 70 % in the case of the MPC. Therefore, less electricity is bought from the grid. Moreover, it is produced from biomass which can be considered a renewable primary energy source.

Table 5.6. Energy and economic results of the simulation.

Parameter	PID	MPC	MPC compared to PID
Total cost [€]	4360	4053	-7.0 %
Bought electricity [kWh]	15043	12627	-19 %
Sold electricity [kWh]	5398	667	-87 %
Produced electricity [kWh]	8773	6457	-23 %
Self-consumed electricity [kWh]	3375	5791	+72 %
Self-consumed electricity compared to user demand [%]	18.3	31.5	+72 %
Fuel mass [kg]	14905	13039	-13 %
Total primary energy [kWh]	87553	88697	+1.3 %

5.1.4 Discussion

The multi-agent hierarchical MPC control presented in this section has shown good performance in terms of cost reduction in the simulation environment. This method has proved to be effective also in two real case studies in operational conditions [161], which are beyond the scope of the present disseration. The main results are reported for completeness:

1. **School complex in Podenzano (Italy)**: the application of the multi-agent MPC control has been assessed for an entire winter season, reducing the specific energy consumption by 13 % compared to the previous year;
2. **Parma University Campus (Italy)**: the application of the MPC to a branch of the network for two months has reduced the specific energy supplied by 34 % compared to the previous months.

Significant cost reduction has also been obtained for both cases. Hence, the integrated framework comprising the development of an innovative control algorithm, its application and analysis in an MiL platform and, finally, its demonstration in operational case studies can be useful to foster smart control in small-scale DHNs.

Nonetheless, several further investigations can be carried out in order to improve the method and address its critical issues. Some examples are discussed below:

- The implementation of variable electricity costs during the day might increase cost saving, as the MPC receives the predicted evolution of the cost parameters and updates the system management accordingly.

- The controller can be easily adapted to the cases in which waste heat is recovered as heat source for the ORC evaporator. This might lead to remarkable cost saving and environmental benefits.
- The approach could be applied to multi-energy systems [98, 169–171], which comprise different energy carriers and energy conversion devices (including renewables), in order to optimize their management and explore flexibility options. This is feasible as long as suitable system model, states and cost function are selected.
- The proposed controller is deterministic and relies on a perfect prediction of the disturbances. However, this is not feasible in reality. Future studies will focus on the investigation of stochastic [172, 173] and robust control methods [174], which explicitly consider the uncertainty on disturbance prediction. The following application (Section 5.2) brings ahead the proposed MPC by including one source of uncertainty to improve system flexibility.
- The proposed control architecture separates consumption optimization from production optimization, as the minimization of energy supplied to each end-users does not consider the power plant operation. In some conditions, however, it might be beneficial to change the management of the downstream end-users (e.g. pre-heating the building thermal capacity, despite higher losses) in order to improve plant flexibility or further reduce the cost. Hence, future developments will regard the implementation of bidirectional communication between the building-MPCs and the supervisory-MPC. This might let different solutions emerge. The application presented in Section 5.3 takes a step forward on this road by investigating the potential of the thermal capacity of the end-users in large-scale DHNs.

5.2 Smart control of CHP with uncertainty for grid flexibility

The significant growth in renewable energy penetration by a variety of discontinuous, grid-connected devices over the last few decades has resulted in the introduction of a significant degree of uncertainty in managing the power system [175]. This represents an important technical challenge for the grid operator, which has to guarantee grid stability and balance at all times. In this context, the aggregation of several producers or consumers is a promising solutions, since it allows distinct devices to act as a single entity when interacting with the grid.

In Italy, the Transmission System Operator (TSO) has recently adopted a specific regulation for a pilot project [176] involving the so-called UVAMs (Mixed Virtual Aggregated Units). These are grid-connected devices or aggregators entitled to provide ancillary services such as congestion resolution, supplemental reserve and grid balancing. The UVAMs declare in advance their availability to perform grid services during a defined time interval. Thus, each unit has to be ready to produce (or consume) a given amount of power, regardless of whether or not this power is actually required by the TSO.

Under these circumstances, cogeneration represents a suitable and flexible technology to face this demand uncertainty, if properly managed by a smart controller. A suitable strategy has to be economically optimal but also robust enough to consider compliance, at any given time, with the potential requests from the TSO as well as with the thermal demand of the connected end-users.

This section demonstrates an additional property in terms of robustness of the multi-agent hierarchical MPC control for small-scale DHNs. It is illustrated by means of the previous application with a CHP in UVAM configuration, in order to address the uncertainty on the electricity request and provide power grid flexibility.

5.2.1 System description

The case study as well as the control architecture are the same as in Sections 5.1.1 and 5.1.2. The only exception is that the production plant is an internal combustion gas engine acting as a CHP unit, with the main parameters reported in Table 5.7. This is chosen as it is a mature technology with higher efficiency and flexibility potential.

Table 5.7. CHP main parameters.

Parameter	Nominal condition	Minimum load condition
Electrical power	2160 kW	220 kW
Electrical efficiency	0.43	0.31
First principle efficiency	0.93	0.84
Natural gas LHV	47.1 MJ kg^{-1}	

The fuel supply and, consequently, the CHP operation are determined by a dual controller: the supervisory-MPC generates the set-point of the fuel mass flow rate, which is then corrected by a proportional controller based on the actual electricity

request from the TSO. The plant operator (PO) makes 1600 kW available to the power grid as a flexibility service from 07:00 to 12:00 each day. However, this is not actually exploited at all times, as exemplified by Fig. 5.10, because the TSO plans and requests power production from the dispatchable UVAM units coherently with the actual system and market conditions.

In this case, the system's flexibility regards only the production of electrical power for grid services. The electrical and thermal demands of the end-users has to be met at all times.

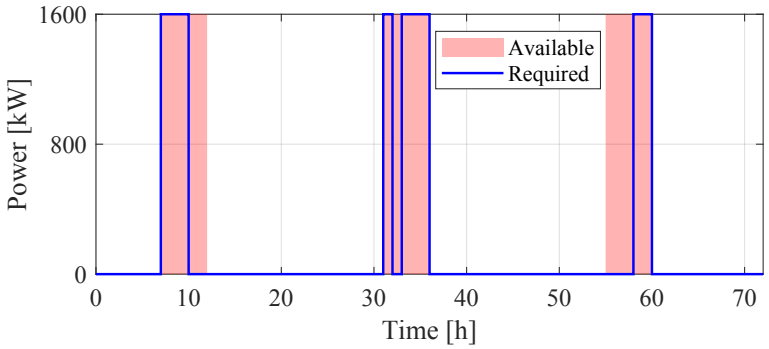

Fig. 5.10. Schematic representation of the small-scale district heating network.

5.2.2 Uncertainty implementation

The supervisory-MPC is customized for including the uncertainty of the request for electricity from the TSO. This is implemented by considering that, when the power availability has been assigned, two events may occur:

- E1: the TSO does not require the available power;
- E2: the TSO requires the entire amount of available power from the dispatchable generation plant.

In the former case, the objective of the optimization is defined by Eq. (5.6). On the contrary, the occurrence of E2 is associated with a modified cost function (Eq. (5.7)) in which the amount of electricity required by the TSO and actually dispatched is rewarded more (i.e. $C_{\mathrm{sg,TSO}} = 0.4\ €\,\mathrm{kWh}^{-1}$) than in the usual case, since the power plant is providing a service.

$$J(\mathrm{E2}) = \left[C_{\mathrm{bg}}\, P_{\mathrm{bg}} - C_{\mathrm{sg,TSO}}\, P_{\mathrm{sg,TSO}} - C_{\mathrm{sg}}\, \left(P_{\mathrm{sg}} - P_{\mathrm{sg,TSO}}\right) + C_{\mathrm{f}}\, \dot{m}_{\mathrm{f}}\right] \Delta t + \phi \quad (5.7)$$

As mentioned in Section 3.3.1, the global cost function of the controller is obtained by weighting the cost functions of E1 and E2 with the respective probability of occurrence:

$$J_{\text{tot}} = \omega_1 \, J(\text{E1}) + \omega_2 \, J(\text{E2}) \tag{5.8}$$

The assessment of MPC with uncertainty is carried out by simulating and comparing four different scenarios, depending on the knowledge of the actual TSO request (Table 5.8):

- Scenario 0 (S0): this is the baseline scenario in which the supervisory-MPC considers the occurrence of E1 only. The potential TSO request is not included in the model prediction and optimization.
- Scenario 1 (S1): the PO knows the exact occurrence of E1 or E2 (i.e. weight equal to 1) with a time advance of three hours, presumably when the TSO plans the production. In the rest of the prediction horizon, E1 and E2 are considered equally probable events (i.e. weight equal to 0.5). This scenario is expected to be the most similar to reality.
- Scenario 2 (S2): the PO has no exact information regarding the occurrence of E1 or E2. The events are equally probable over the entire prediction horizon.
- Scenario 3 (S3): the PO assumes that the available power is always requested by the TSO and, thus, E2 occurs over the entire prediction horizon.

Table 5.8. Summary of the four simulated scenarios and related weights of the cost functions of E1 and E2.

Scenario	Short description	ω_1	ω_2
S0	E1 considered over prediction horizon	1	0
S1	E1 or E2 occurrence known three hours before, equally probable over rest of prediction horizon	$1 \vee 0 \vert 0.5$	$0 \vee 1 \vert 0.5$
S2	E1 and E2 equally probable	0.5	0.5
S3	E2 occurs over prediction horizon	0	1

5.2.3 Results

The network is simulated for three days in January. The prediction horizon and time-step for the MPCs are three days and 15 min, respectively.

As in the previous case, the required indoor temperature of the buildings are kept within the limits. Fig. 5.11 shows that a similar behavior is obtained for one of the schools in all scenarios. This is reasonable because the control of the downstream part of the network is not varied over the various cases.

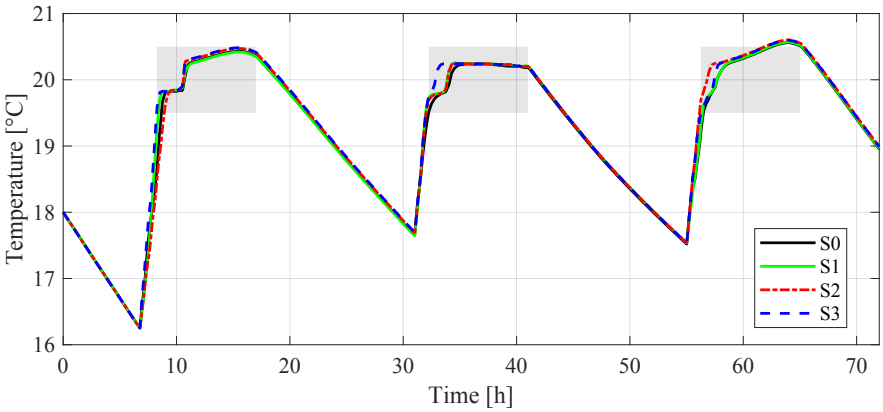

Fig. 5.11. Indoor temperature of the primary school in the in the four scenarios.

On the other hand, the management of the production side is influenced by the knowledge of the scenario. The TES State of Charge (i.e. percentage of energy content of the water in the tank with reference to the maximum) is represented in Fig. 5.12. The graph shows that, when the optimization considers the possibility to produce electric power to provide flexibility to the grid (S1–3), the TES is charged in advance compared to the baseline scenario, in order to increase electricity production and operate the dispatching service. Moreover, its SoC does not reach the maximum so as to leave a safe margin to store heat when CHP production is required. In each case, however, the TES is almost full at the beginning of each operating day, as it has to correctly pre-heat the buildings in order to fulfill indoor comfort. In addition, it collects the heat produced by the CHP to meet the electrical demand of the previous day.

In Fig. 5.13, the power produced by the CHP is compared to the actual electricity required (shaded area), which is the sum of the power demand of the school complex and the actual TSO request. Moreover, Table 5.9 reports:

1. the operating cost as the sum of the fuel cost and electricity bought from the grid (without including sold electricity);

2. the TSO request compliance as the percentage of the total electrical energy required by the TSO that is actually produced and fed to the grid. This can be seen as an indicator of the flexibility provided to the power grid.

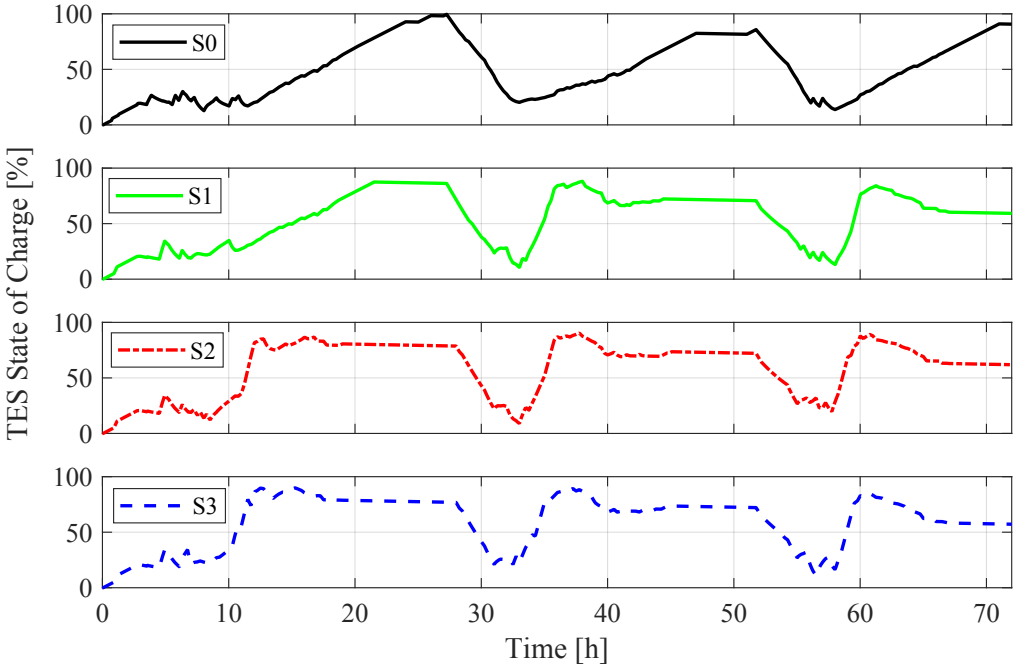

Fig. 5.12. State of charge of the TES in the four scenarios.

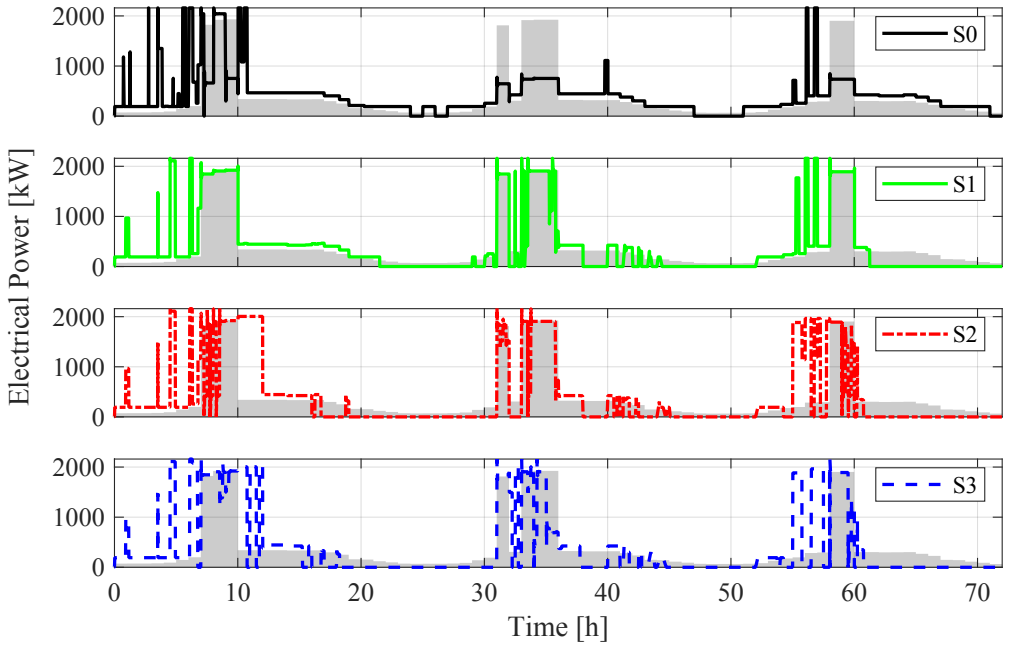

Fig. 5.13. Electrical power produced by the CHP in the four scenarios. The shaded area represents the actual total power requested by the consumers and the grid operator.

Table 5.9. Operating cost and TSO request compliance in the four scenarios.

Scenario	Operating cost [€]	TSO request compliance [%]
S0	1190	36.7
S1	2580	92.3
S2	1523	78.5
S3	1946	81.6

It is possible to observe that S1 is the case that gives better results in meeting the TSO request. Indeed, at each time-step the controller knows precisely the constraints of the successive three hours, thus it is able to react and operate the system in order to maximize the fulfillment of power demand up to 92.3 %. A poorer performance is obtained when there is uncertainty over the entire prediction horizon (S2) and when there is the assumption that it is always necessary to produce electricity (S3). The latter scenario overestimates the time in which power production is considered necessary and, given the limitations on the TES capacity, the actual production is planned in less profitable hours.

As regards the economic performance, S1 leads to a higher operating cost, as it produces more electricity. However, the actual profit is underestimated, as the gain of the flexibility service performed, which is significant in S1 and lower in S2 and S3, is not included in the economic indicator.

5.2.4 Discussion

As discussed above, the uncertainty on the disturbance plays a significant role in the global performance of this control strategy.

It can also be useful to define an upper boundary, represented by the ideal scenario of perfect knowledge of the actual request over the prediction horizon. In this specific application, this would lead to a TSO request compliance of 94 %. This means that, in the current system configuration, it is not possible for the PO to fulfill the TSO request to a greater extent. This happens because, in some cases, the power is made available when the TES is unable to store enough energy. As a consequence, in this condition it is not possible to operate the CHP, as heat cannot be dissipated.

In the light of these considerations, some management or design changes can be suggested for this case study:

- The period in which electrical power is made available to the grid should be

revised in order to better match the thermal demand. In this way, it is likely that the electricity is dispatched when the TES is not full.

- The current system configuration, which does not allow the electrical and thermal power production to be regulated independently, should be rearranged with more degrees of freedom, for instance by supplying heat directly to the users or by enabling heat dissipation.

Overall, since S1 is expected to represent the real conditions more closely, this MPC pledges good performance and replicability to other cases. Moreover, it can be helpful to the PO by providing insights regarding operation and management in presence of uncertainty and, therefore, in revising production planning and considering cost-effective design choices.

The proposed controller, however, includes only a basic uncertainty estimation of one of the disturbances. Future research will include additional sources of uncertainty, such as the variability of external environment conditions and electricity market prices. Furthermore, other methods for scenario generation (e.g. Monte Carlo Simulation [177]) and uncertainty analysis [178–180] will be investigated in order to create a more robust MPC.

5.3 Smart control of large-scale district heating

As extensively discussed in Section 2.1, there are few cases of smart controllers for large-scale DHNs which, due to their high complexity and size, are currently controlled with obsolete non-optimal strategies.

With the aim of demonstrating a scalable smart controller for these systems, this application presents an MPC built with the novel two-stage LP-NLP optimization algorithm developed in Section 4.4 and tested on the large-scale DHN of the city of Västerås, in central Sweden. The main objectives of the algorithm are briefly remembered:

- exploit the heat capacity of end-users as thermal storage, by means of the aggregated region model (Section 4.3);
- achieve peak shaving;
- reduce distribution temperature without increasing pumping costs.

5.3.1 System description

The Västerås DHN is supplied by a centralized production site, comprising a waste-to-energy Combined Heat and Power plant, back-up boilers and thermal energy storage tanks. The network distributes hot water to the city center and to the six main peripheral regions (already introduced in Section 4.3) with an yearly heat supply of around 1800 GWh. Since the center is relatively close to the power plant, it is easier to control its heat supply and comfort fulfillment, compared to the farthermost areas. Therefore, it is considered to be supplied according to the historical heat consumption and is not included in the innovative control.

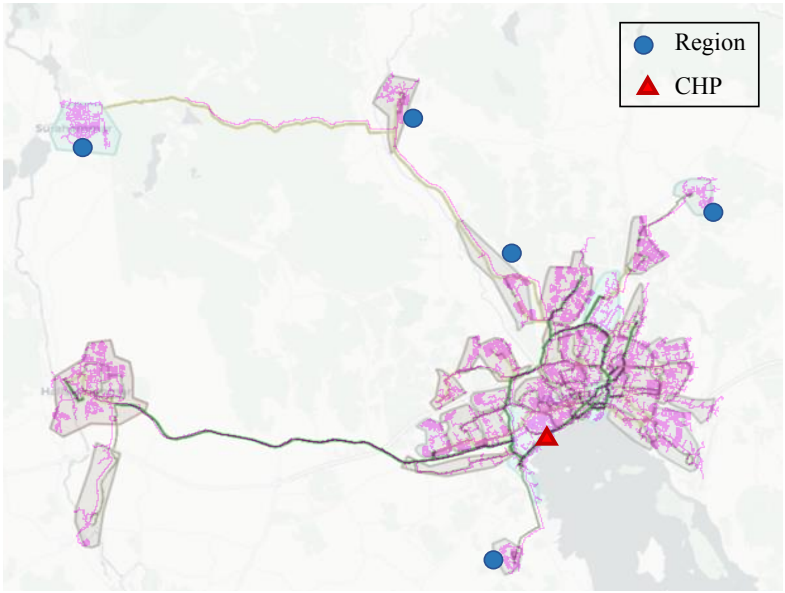

Fig. 5.14. Västerås district heating network.

A schematic representation of the system is given in Fig. 5.15. It is possible to notice that the distribution network can be split into nine main pipelines.

The network can be further schematized with six nodes and nine arcs (Fig. 5.16) in order to comply with the simplified network representation required by the optimization algorithm. For this purpose, the incidence matrix of this network is:

$$In = \begin{bmatrix} 0 & 0 & 1 & 0 & 1 & 0 & 1 & 0 & 1 \\ 0 & 0 & 1 & 0 & 1 & 0 & 1 & 1 & 0 \\ 0 & 0 & 1 & 0 & 1 & 1 & 0 & 0 & 0 \\ 0 & 0 & 1 & 1 & 0 & 0 & 0 & 0 & 0 \\ 0 & 1 & 0 & 0 & 0 & 0 & 0 & 0 & 0 \\ 1 & 0 & 0 & 0 & 0 & 0 & 0 & 0 & 0 \end{bmatrix} \tag{5.9}$$

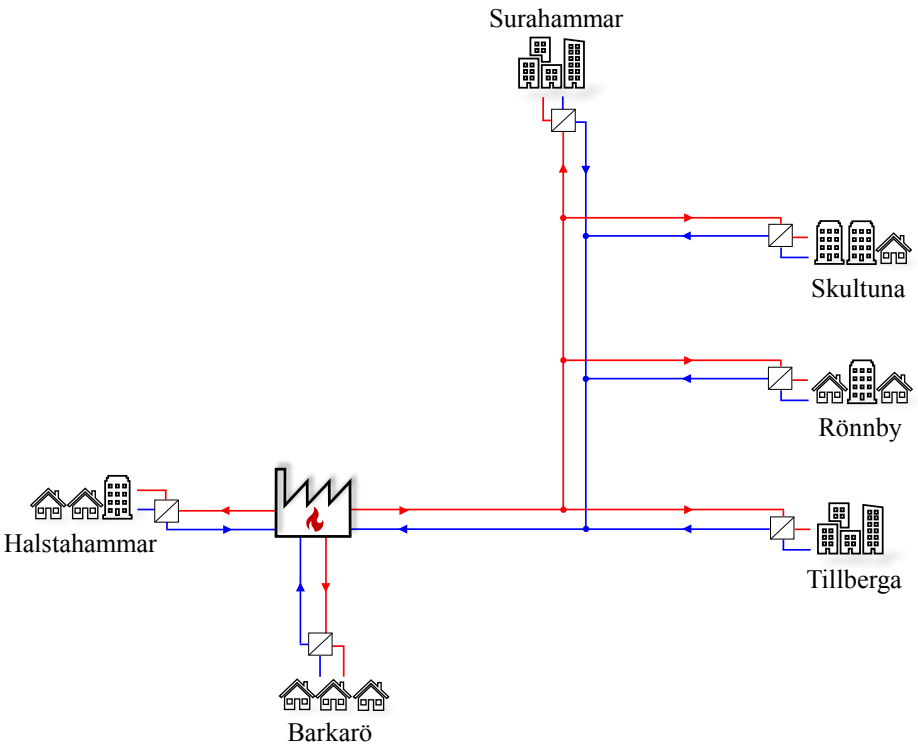

Fig. 5.15. Schematic representation of the Västerås district heating network.

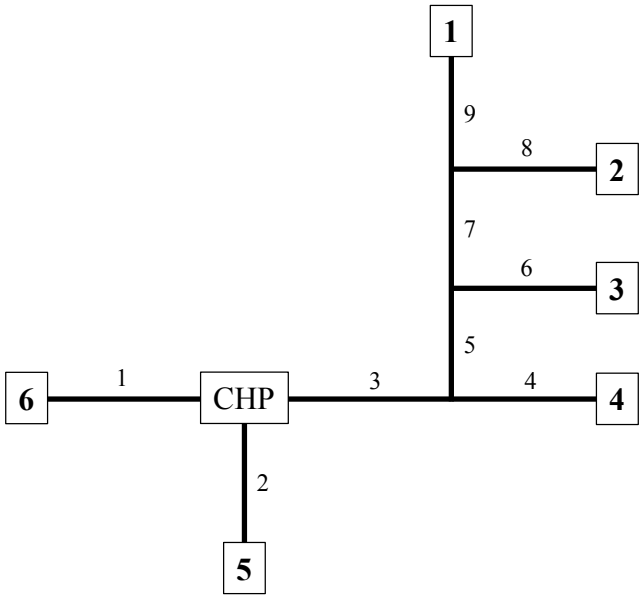

Fig. 5.16. Schematic representation of network with regions as nodes and pipeline segments as arcs.

where the rows refer to the nodes 1–6 while the columns refers to the arcs 1–9. The main properties of the arcs are summarized in Table 5.10.

Table 5.10. Properties of the main pipeline segments of the Västerås district heating network.

Arc	Internal diameter [mm]	External diameter [mm]	Insulation diameter [mm]	Length [km]
1	312.7	323.9	500	9
2	160.3	168.3	280	5.5
3	393.8	406.4	630	10
4	312.7	323.9	500	4.5
5	393.8	406.4	630	1
6	312.7	323.9	500	0.5
7	312.7	323.9	500	7
8	312.7	323.9	500	0.5
9	263	273	400	13

The MiL model is a network simulator setup in [23]. It is a detailed dynamic model of the global DHN originally developed in Dymola [181], which exploits the programming language Modelica and is widely used in simulating dynamic systems [182]. The individual components of a network, such as pipes, valves and pumps, are modeled by considering the governing physical phenomena. These components are connected according to the Västerås network configuration to form the global model. Its validation with historical network data provided by the system operator shows that the model is reliable and effectively represents network temperature dynamics, heat propagation and losses over pipeline lengths of several kilometers, as is for the present case. Indeed, the simulated supply and return temperatures are in good agreement with the actual trends [23].

The simulator is connected with MATLAB®/Simulink® by means of a Functional Mock-up Unit, which allows for model exchange and co-simulations in different environments.

5.3.2 Control architecture

The two-stage LP-NLP optimization algorithm detailed in Section 4.4 is embedded in the MPC. It establishes the optimal set-points for (i) mass flow rates to the peripheral regions and (ii) supply temperature from the CHP. The MiL model

simulates the heat propagation of the real network and, at every calculation step, returns the estimation of the actual system states (i.e. SoC of the regions). These are used as new initial conditions for updating and solving the next optimization problem.

Since the current system configuration does not allow the end-user indoor temperatures to be monitored, the procedure explained below is necessary to estimate the actual SoCs of the regions. The notation is clarified in Fig. 5.17.

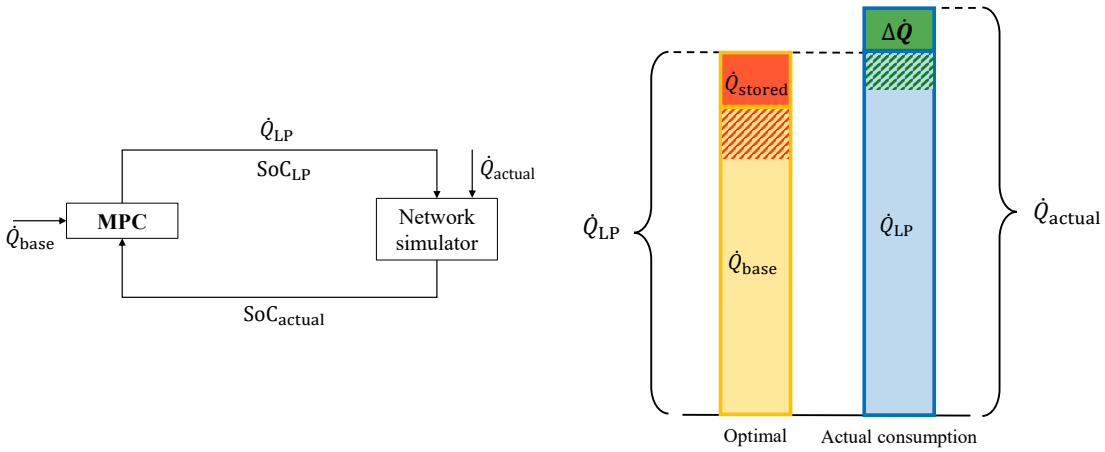

Fig. 5.17. Qualitative representation of the contributions to the optimal and actually consumed thermal power. The quantities $\dot{Q}_{\text{stored}}$ and $\Delta\dot{Q}$ can be positive (full area) or negative (dashed area). The total heat stored in the SoC is represented by the sum of $\dot{Q}_{\text{stored}}$ and $\Delta\dot{Q}$ in the current time-step.

It is firstly worth remembering that the optimization algorithm of the MPC receives the historical or predicted heat load as a disturbance ($\dot{Q}_{\text{base,i,k}}$) and calculates the network operating parameters that deliver the optimal thermal power ($\dot{Q}_{\text{LP,i,k}}$) which in turn includes the optimal storage in the SoCs. However, there is typically a difference between the predicted load and that actually consumed, due to various factors:

- errors in the prediction of the external temperature and, consequently, the thermal demand;
- different behavior of part of the consumers (e.g. a building may not be occupied and, hence, may not require heating).

Additionally, part of the consumers may decide not to actuate the storage, for instance by exploiting the space heaters differently or slightly varying the indoor comfort.

The following assumptions are therefore made:

- These random contributions are included in the current analysis by estimating the difference $\Delta\dot{Q}_{\mathrm{i,k}}$ between the predicted thermal power and the thermal power actually consumed as a fraction of $\dot{Q}_{\mathrm{base,i,k}}$ according to a uniform distribution in the range $\pm 5\,\%$.
- The actual thermal power consumed $\dot{Q}_{\mathrm{actual,i,k}}$ is fed to the MiL model.
- The actual return temperature from the i-th region at the k-th time-step $T_{\mathrm{R,i,k}}$, which is different from the set-point considered by the algorithm, is returned by the MiL model.
- In the current real system configuration, it is not possible to quantify and separate the random contributions listed above. Thus, it is assumed that the sum (with its corresponding sign) of the random contribution $\Delta\dot{Q}_{\mathrm{i,k}}$ is entirely stored in the heat capacity of the aggregated consumer and modifies the SoC foreseen by the optimization module, i.e. $\mathrm{SoC}_{\mathrm{LP,i,k}}$.

Eq. (5.10) expresses the relation between the thermal power actually consumed and the actual return temperature:

$$\dot{m}_{\mathrm{i,k}}\, c\, (T_{\mathrm{S,i,k}} - T_{\mathrm{R,i,k}}) - \dot{Q}_{\mathrm{loss,i,k}} = \dot{Q}_{\mathrm{actual,i,k}} \tag{5.10}$$

This balance equation is analogous to Eq. (4.37). The subtraction of the latter from the former leads to an expression of $\Delta\dot{Q}_{\mathrm{i,k}}$ in terms of the difference between actual return temperature and set-point return temperature as follows:

$$\Delta\dot{Q}_{\mathrm{i,k}} = \dot{Q}_{\mathrm{actual,i,k}} - \dot{Q}_{\mathrm{LP,i,k}} = \dot{m}_{\mathrm{i,k}}\, c\, (T_{\mathrm{R,SP}} - T_{\mathrm{R,i,k}}) \tag{5.11}$$

According to Eq. (5.11), the difference in the return temperature gives a measurement of the additional stored heat which, in turn, effectively modifies the predicted SoCs as follows:

$$\mathrm{SoC}_{\mathrm{actual,i,k}} = \mathrm{SoC}_{\mathrm{LP,i,k}} + \frac{\dot{m}_{\mathrm{i,k}}\, c\, (T_{\mathrm{R,SP}} - T_{\mathrm{R,i,k}})\, \Delta t}{2\, C\, \Delta T_{\mathrm{stored,max}}} \tag{5.12}$$

The new SoCs are used to update the system state and, hence, represent the new initial condition for the optimization problem at time-step $k+1$, according to the receding time horizon strategy. This procedure is repeated for the entire simulation.

5.3.3 Results

The MiL application comprising the DHN detailed model and the MPC controller is illustrated in Fig. 5.18.

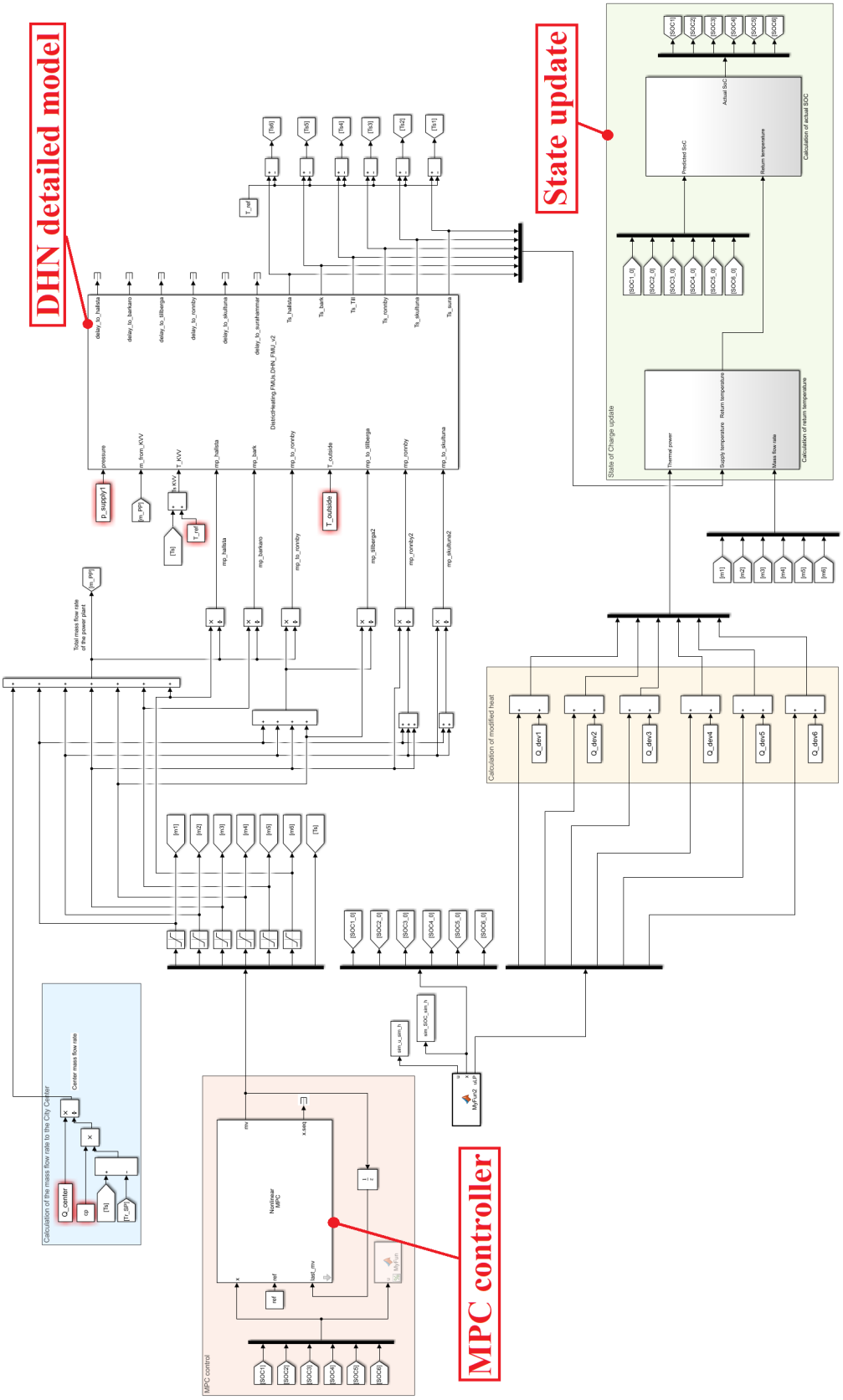

Fig. 5.18. Model-in-the-Loop application of the Västerås district heating network in the MATLAB®/Simulink® environment

The results of the real-time control with the developed MPC strategy are shown for the first week of February 2017. The prediction horizon and time-step are one day and one hour, respectively. The outdoor temperature, which greatly affects the baseline heat demand, is depicted in Fig. 5.19.

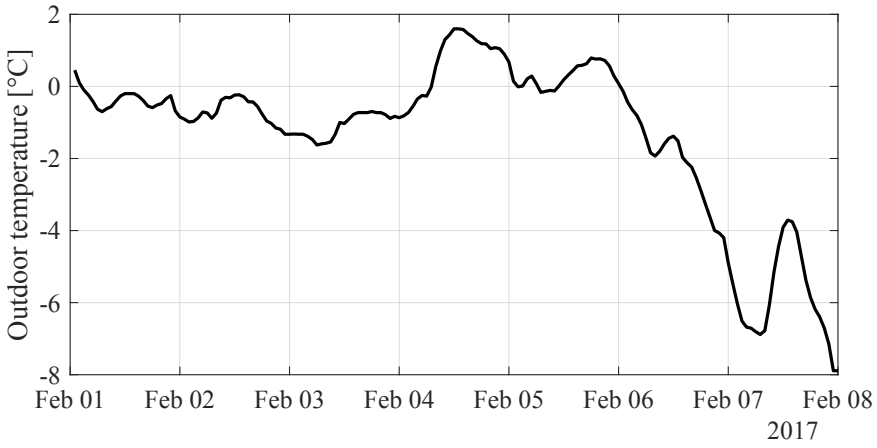

Fig. 5.19. Historical outdoor temperature over the simulation period.

A prediction horizon of one day is adopted in order to speed-up the simulation. Since the time delays to reach the different regions of the network are in the range of 2 h to 10 h, such a prediction horizon includes the propagation of the thermal power produced in the power plant and captures the main system dynamics, while reducing the simulation time.

The historical and new thermal power actually delivered to the end-users are illustrated in Fig. 5.20 and the performance indexes for evaluating these results are reported in Table 5.11. It is demonstrated that the primary objective of the analysis, which is to perform peak shaving by exploiting the region heat capacity and without endangering the indoor comfort, is achieved. This accomplishment comes together with a slight decrease or, in the worst case, a negligible increase (i.e. maximum 0.2 %) in energy consumption, depending on the region.

The heat supplied is subject to greater fluctuations over the entire simulation horizon compared to the analysis reported in Section 4.4.3. This is because the real-time MPC control acts in real conditions, in which the heat actually consumed is different from that predicted. Nevertheless, the receding time horizon strategy, according to which the variables and disturbance prediction are updated at each time-step, copes with this uncertainty. It is also worth noting, however, that significant maximum RVRs are obtained by taking each simulated day individually. Hence, the new management solution provides short-term benefits for

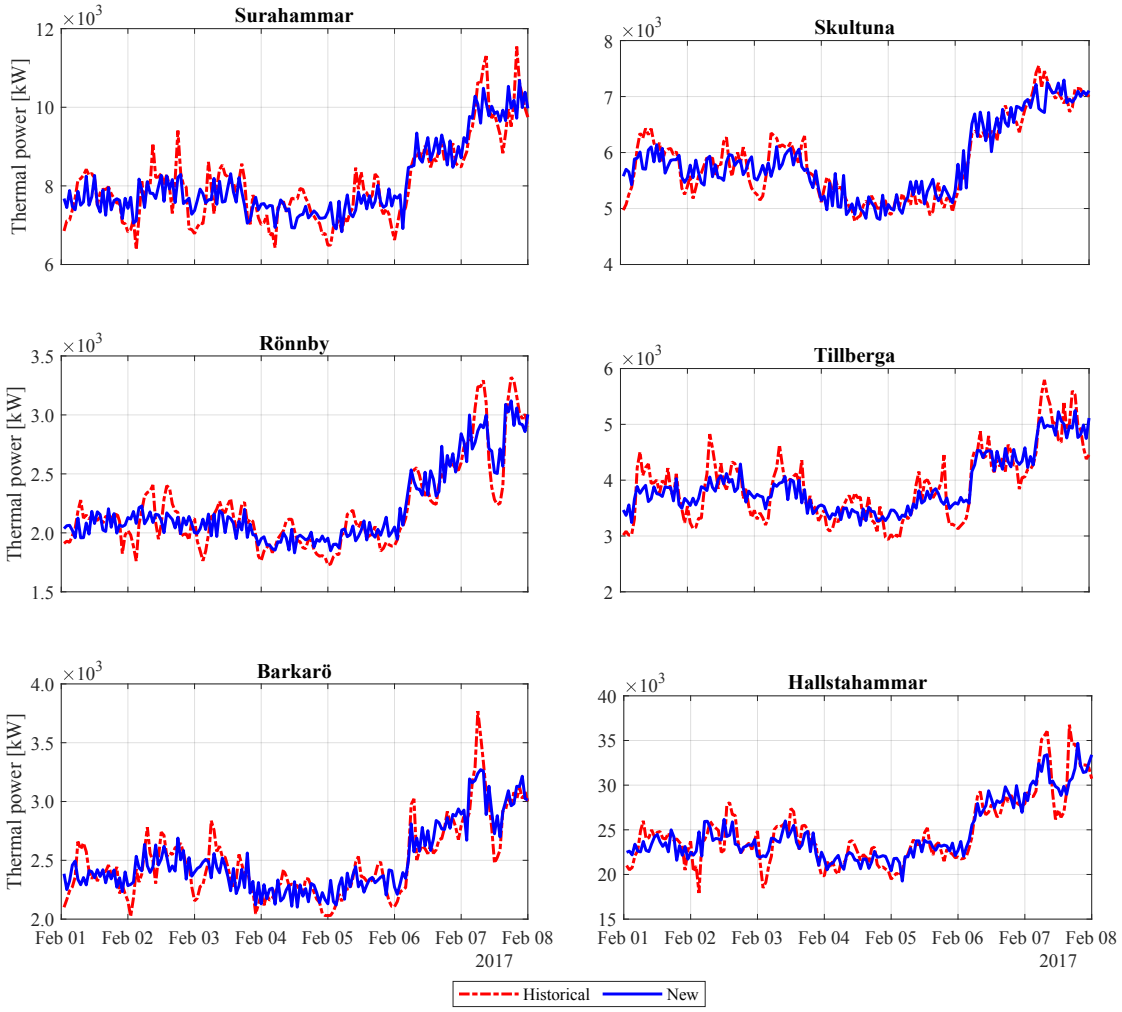

Fig. 5.20. Results of the MPC control of the Västerås network: historical and new thermal power to the regions.

the global network. This is further confirmed by the load duration curves of the simulated week shown in Fig. 5.21: the curves produced by the new management are significantly flatter than those obtained by historical data.

Fig. 5.22 depicts the operating parameters of the region of Skultuna, taken as a representative example, in terms of mass flow rates and temperatures supplied directly to the main substation heat exchanger. The actual return temperature is also shown and compared to the baseline case and to the set-point considered by the optimization module. The new variables decrease compared to the historical ones: this leads to lower consumption for the pump and lower heat losses from the pipelines. For instance, the optimal mass flow rate is decreased by 23 % and, moreover, is subject to smaller variations over the simulation period. The supply

Table 5.11. Results the MPC control of the Västerås network: peak shaving (PS), reduction in variation range (RVR) for the entire simulation, maximum daily RVR and total energy reduction (ER).

Region	PS [%]	Total RVR [%]	Max daily RVR [%]	ER [%]
Surahammar	11.9	25.5	59.2	-0.17
Skultuna	4.9	10.4	51.0	0.20
Rönnby	7.4	19.0	63.5	-0.10
Tillberga	13.5	28.1	62.7	0.16
Barkarö	13.2	33.1	53.6	-0.20
Hallstahammar	6.7	18.1	59.3	-0.002

temperature is also more constant while the return temperature fluctuates around the set-point, proving the acceptability of the assumption made. In addition, it is always maintained above the threshold of 30 °C, which is preferable for the global system operation. Similar considerations can be drawn for the other regions of the DHN.

The first part of the simulation in Figs. 5.22b and 5.22c shows a higher temperature that derives from the fact that the optimal supply temperature reaches the substation heat exchanger some hours after it outflows from the power plant, due to the network time delays. This diminishing evolution in the first simulation time-steps is different for the various regions, depending on the distance and water velocity. Indeed, it is underlined that, even though they are supplied by the same power plant, the actual temperatures that reach the substation heat exchanger are different due to the different rates of heat transfer from the pipelines to the soil, which depend on the network topology, length and demand.

In regard to the effects that the outdoor temperature imposes upon the controller, Fig. 5.23 illustrates the power plant supply temperature, which is valid for all regions, as a function of external environment temperature. The trend obtained with the MPC, highlighted by the regression fit lines, is significantly decreased compared to baseline. Furthermore, the new supply temperature is maintained more uniform, especially when the outdoor temperature is relatively low. Indeed, the absolute value of the slope decreases from 1.42 to 0.12. As far as this simulation period is concerned, the water is supplied at an optimal temperature lower than 80 °C, while in the original management strategies it varies between 80 °C and 95 °C. The relative reduction in the difference between supply temperature and

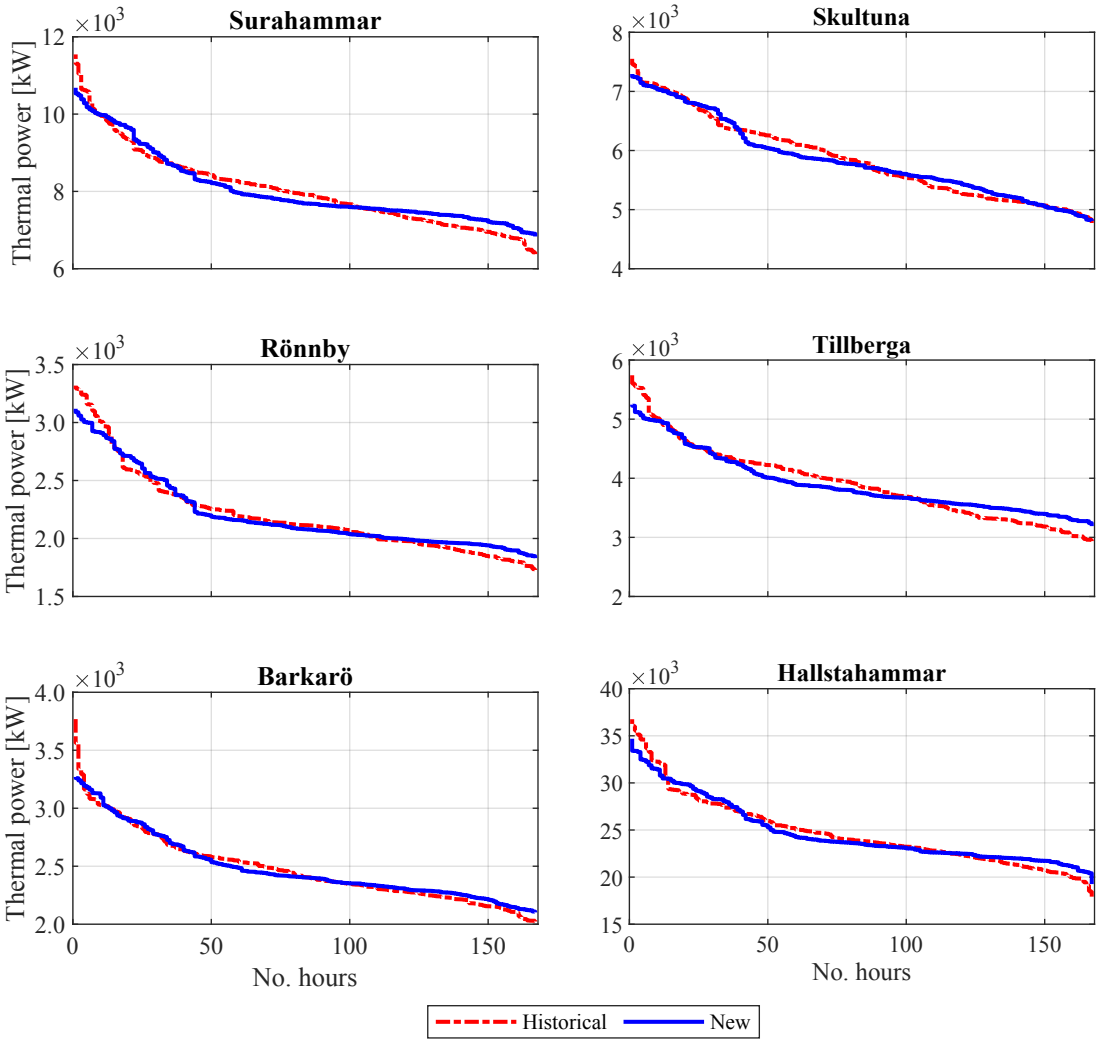

Fig. 5.21. Results of the MPC control of the Västerås network: historical and new load duration curves.

soil temperature (which is assumed as 10 °C in the simulations), which gives the perception of a reduction in heat losses from the pipelines, ranges from a minimum of 3.1 % for higher outdoor temperatures to a maximum of 20 % for lower outdoor temperatures, with an average reduction of 8.8 % over the considered time period. Other simulation periods can lead to further improvements, since the historical supply temperature, according to the network data, can reach values up to 110 °C. Hence, the secondary goal of the optimization, which consists of reducing the heat losses, is successfully implemented as well.

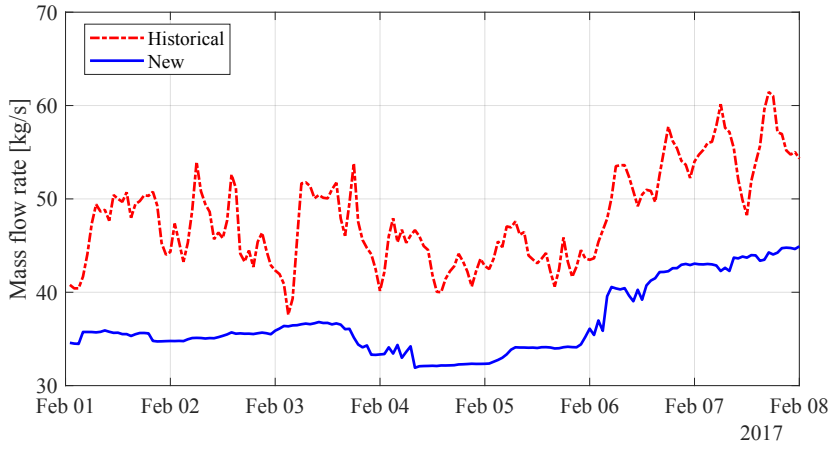

(a)

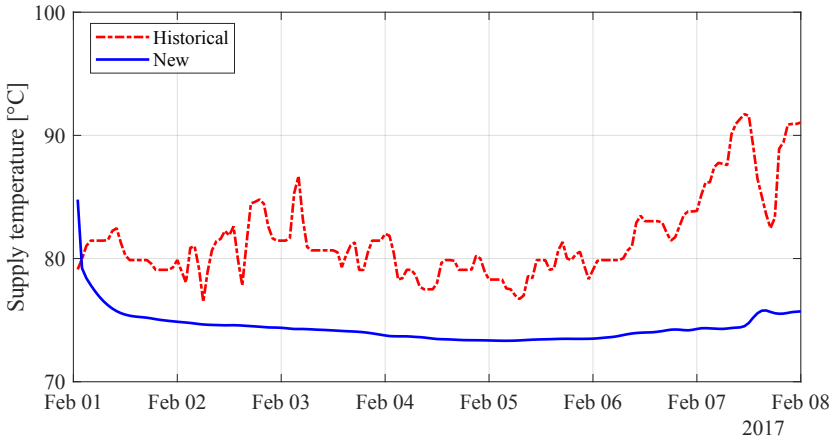

(b)

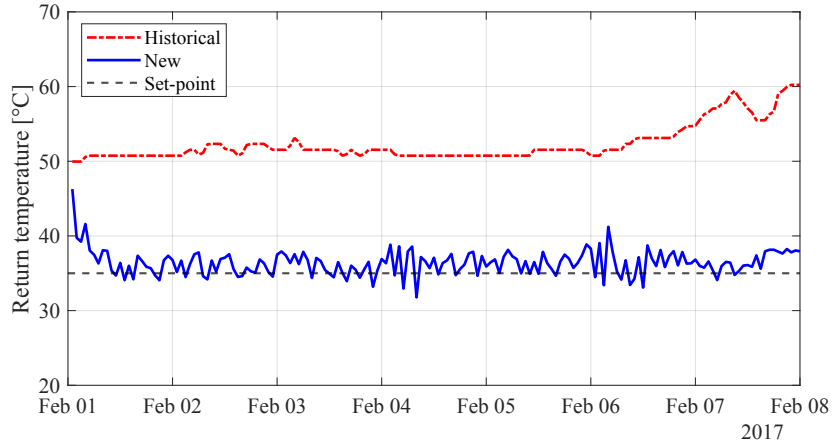

(c)

Fig. 5.22. Results of the MPC control of the Västerås network: historical and new (a) mass flow rates and (b) supply temperatures and (c) return temperatures of Skultuna.

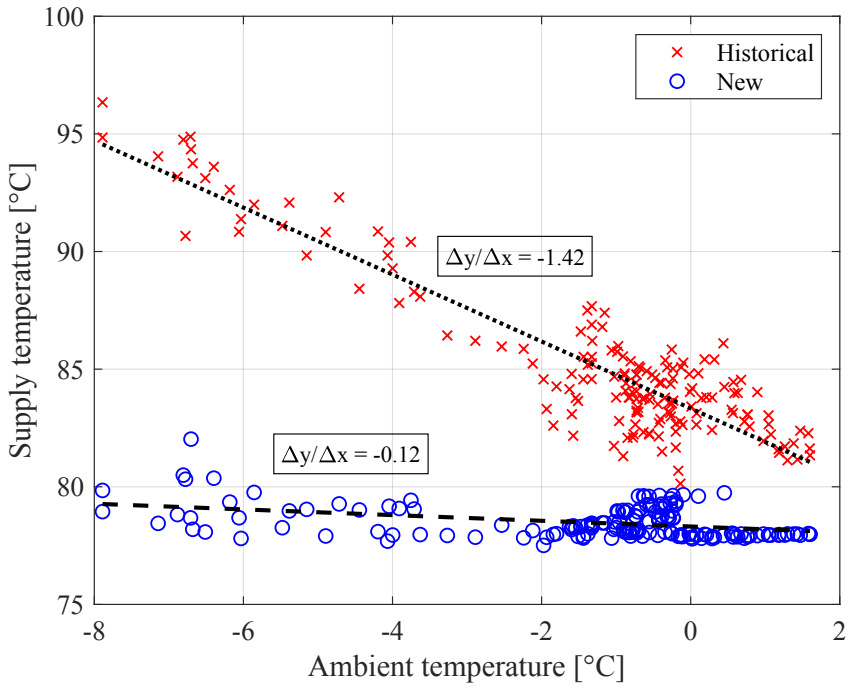

Fig. 5.23. Historical and new data of the supply temperature from the power plant with the related regression fit lines. The minimum, average and maximum reductions in the difference between supply and soil temperature are 3.1 %, 8.8 % and 20 %, respectively.

5.3.4 Discussion

As disclosed for the small-scale DHN applications, an integrated approach comprising (i) the development of simplified aggregated region models and optimization algorithms suitable for MPC and (ii) its MiL demonstration on a network simulator is an essential step leading to digitalization and smart control of large-scale DHNs.

There are also noteworthy perspectives for further improvements:

- The results of this control applications are achieved by adopting a conservative estimation of the heat capacity of the regions and a safe maximum deviation of their equivalent indoor temperature, i.e. 0.5 °C. A more significant peak shaving could be obtained by increasing this parameter or by testing more intense demand side management measures.

- A sensitivity analysis with the length of the prediction horizon would also be interesting to evaluate if the increase in computational time is justified

by an improved performance.

- Additional benefits might derive from the installation of dedicated thermal storage devices in the regions or areas that show a low storage potential and achieve a lower level of peak shaving (e.g. Skultuna). An in-depth investigation might provide suggestion on profitable design updates.

- This MPC is deterministic and, hence, does not include the uncertainty on disturbances such as the actual thermal demand. A robust approach should be adopted to improve its performance in real case studies.

However, there are also some limitations that should be addressed in future research:

- The SoC of each region is updated by assuming that the uncertainty about the thermal demand affects the SoC itself and not indoor comfort. This assertion can be verified with further modeling and experimental studies. An improved monitoring of the SoC, for instance by installing measurement devices in a network portion and conducting validation experiments, will conduct to a more reliable knowledge of the state of the network.

- The analysis is performed at main distribution network level, which means that only the main branches of the network supplying the peripheral regions are considered. The heat allocation to each individual building in the region has to be regulated by another level of control.

The proposed solution offers a direction to address the latter issue. Indeed, the MPC has been designed as scale-free and, therefore, can be extended to the different network levels (transmission, distribution, individual building substations in Fig. 5.24) without requiring significant changes or extensive tuning procedures [183]. This constitutes a fractal architecture, in which a cascade of similar elements is spread at different levels of detail [184]. Each level can communicate with the others and lead to a connected and globally optimal network.

Table 5.12 concludes the discussion on this method and its application by briefly summarizing its main advantages and limitations.

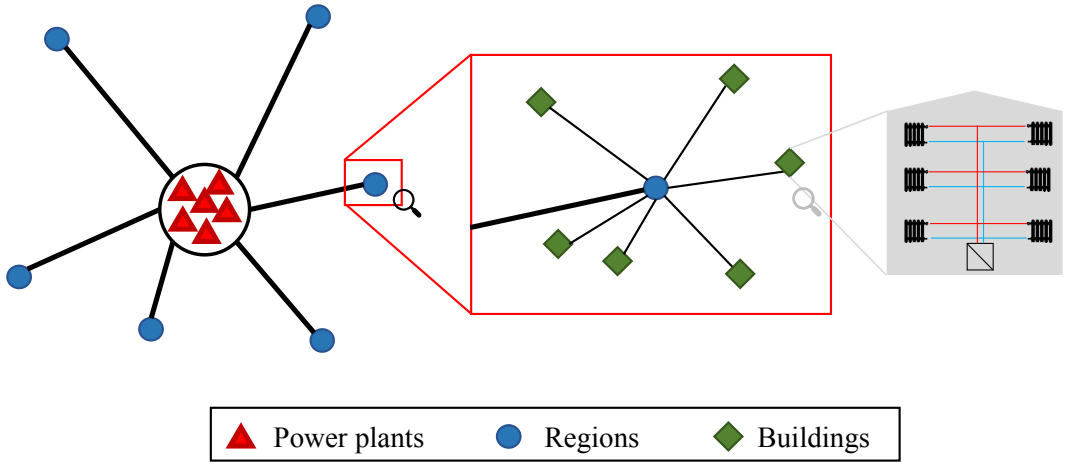

Fig. 5.24. Fractal architecture of district heating.

Table 5.12. Summary of advantages and limitations of the proposed smart controller for large-scale district heating.

Advantages	Limitations
• Fast tuning with small dataset • Applicable without extensive system knowledge • Coefficients can be adapted on new data • Peak shaving achieved • Lower temperature achieved	• Uncertainty on actual SoC • Control at distribution network level • Low-level controllers required to allocate load to end-users

6 Conclusions

The heating and cooling sector has the chance to become more efficient and to reduce carbon emissions in populated areas if innovative management and control approaches are adopted.

In this context, this thesis aimed to provide and demonstrate a complete set of new tools to develop and implement smart control in district heating systems. Indeed, a smart controller based on Model Predictive Control (MPC) requires two fundamental elements: a control-oriented dynamic model of the system and an optimization algorithm with a feasible trade-off between accuracy of the solution and computational burden.

This work has presented models and algorithms suitable to both small-scale and large-scale district heating networks which, due to the different system sizes and levels of complexity, have to be tackled independently.

Then, the verification of the obtained MPC controllers has been carried out by means of different applications in Model-in-the-Loop simulation platforms, in which a detailed model that emulates the real system's behavior is controlled by the controller code. In this way, various control strategies can be compared with the same boundary conditions and without affecting the real network.

Small-scale district heating: a gray-box dynamic model of a district heating branch and an optimization algorithm based on Dynamic Programming have been developed and embedded in an MPC, which has been demonstrated in a multi-agent hierarchical architecture. Each branch of the network is controlled by a dedicated MPC that minimizes the energy required for thermal comfort, while the heat production site is controlled by a supervisory MPC agent that minimizes the total cost and guarantees that heat is correctly supplied to the users downstream. Compared to a traditional control strategy, the MPC shows a 7 % cost reduction. The property of robustness of this solution has been further demonstrated by controlling the production site in presence of uncertainty, in particular regarding the potential request of flexibility service by the power grid operator. The approach is modular and can be extended to small-scale heating networks with other layouts.

Large-scale district heating: a gray-box dynamic model of aggregated network regions, including the aggregated heat capacity of the connected buildings, has been developed starting from coarse data available from the network main substations. This heat capacity has been exploited as thermal energy storage to achieve demand side management and reduction in supply temperature by means of a two-stage optimization algorithm: a Linear Programming stage with the objective

of shifting the peaks of the energy supplied to each region, and a subsequent Non-linear Programming stage with the objective of optimizing the network operating parameters. The proposed tools have been embedded in an MPC, which has been tested on the district heating system of the city of Västerås, Sweden. With reference to the network historical dataset, the results show a peak shaving up to 16 % and a reduction in heat losses from the distribution pipelines up to 20 %.

Overall, these innovative methods for smart control have in common some defining aspects:

- they are versatile and can be successfully applied to different space scales and objective functions;
- they are not case-specific, thus their extension to other systems with similar characteristics is straightforward;
- they maintain a physics-based approach. Their model identification and algorithm setup require small datasets which, differently from the large datasets needed for data-driven approaches, can be easily acquired in most systems.

Nevertheless, several aspects can be further investigated to improve the applicability of MPC and its results in terms of energy and cost saving:

- smart control of district heating will be studied in the framework of multi-source energy systems, which see the integration of multiple energy vectors and sector coupling devices;
- different methods and sources of uncertainty will be investigated in order to achieve fully robust or stochastic control;
- the proposed solutions will be demonstrated in existing case studies to increase their Technology Readiness Level.

In addition, one of the most promising future outcomes is the development of a technical synthesis of the proposed methods, in order to demonstrate a unified fractal methodology that can be potentially applied to any kind of heating network, from the micro-scale (i.e. building level) to the macro-scale (i.e. city level). This activity will be carried out in the framework of the DISTRHEAT project and will foster real-life implementation of smart control, in order to make heating and cooling systems optimal, cheaper and efficient.

A Appendix: Model-in-the-Loop platform

The Model-in-the-Loop simulation platform setup to test control strategies for small-scale DHNs comprises an in-house library of models of energy systems main components, developed in MATLAB®/Simulink®. This is a block diagram environment suitable for system-level design and dynamic simulation, and is equipped with a graphical editor for specific block customization and development [185]. The components blocks, depicted in Fig. A.1, can be easily assembled in a modular way to represent systems of different layouts and configurations. Moreover, it is possible to directly incorporate algorithms and functions developed in MATLAB® without the need of additional interfaces. Hence, coupling control algorithms developed with this language (Section 4.2) with dynamic simulation for MiL implementation is straightforward.

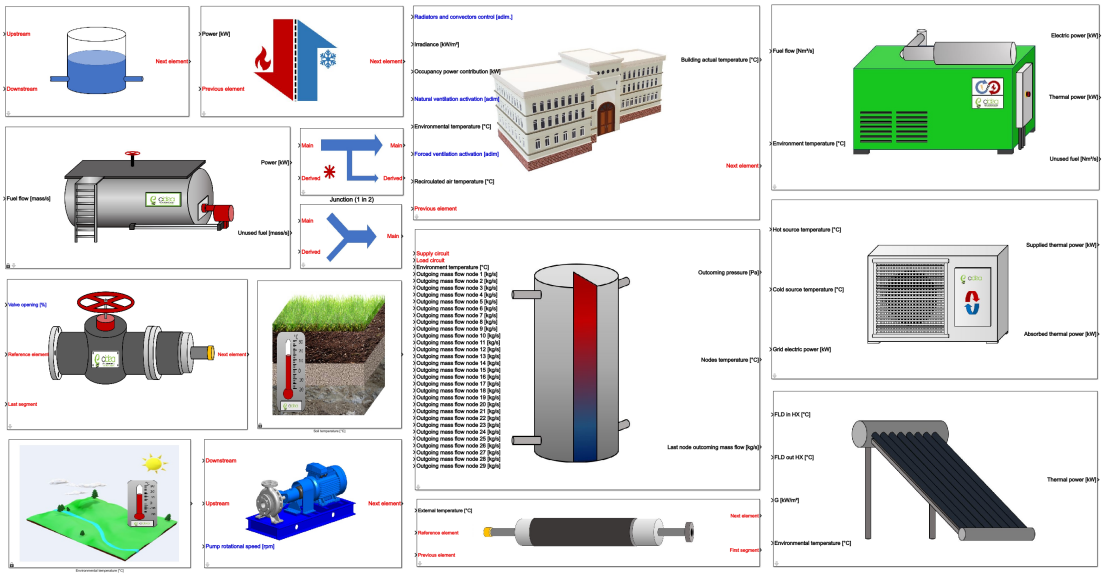

Fig. A.1. Main components of the library of energy systems developed in MATLAB®/Simulink®.

The models of energy system components adopt a direct causality by considering the physical flows of matter and energy that enter, exit or are stored within each component, in order to provide a proper physical representation [160]. It differs from the inverse causality used typically in optimization or planning models, in which the flux is calculated based on consumption. Moreover, the models consider the hydraulic and thermal domains and, consequently, the involved variables are mass flow rate, temperature and pressure. Each physical element is described by the governing conservation equations in differential or algebraic form, depend-

ing on whether the element provides or not accumulation of mass, momentum or energy.

For these reason, the library has proved in various studies [160, 161] to be a reliable tool for accurate simulations of different DHNs.

A brief overview of the main components is given in the following paragraphs, while their relevant features are summarized in Table A.1 [161]. They regard the following aspects:

- Algebraic/Dynamic: the component is algebraic (Al) if it does not involve a storage term and can be described by algebraic relations, while it is dynamic (Dy) if the storage term or memory (i.e. system state) is present and the evolution in time of the variables is described by means of differential equations;
- Lumped/Discretized: the component is represented by a lumped parameter model (L) or is discretized along one dimension (1D);
- Inputs, Outputs and States of the model, according to the chosen causality (if the model is algebraic, it does not have any state).

Boiler The boiler is represented by an algebraic, physics-based model that evaluates the effective thermal power produced by the combustion of a given amount of fuel. The governing equation is Eq. (A.1).

$$\dot{Q}_{\mathrm{b}} = \eta_{\mathrm{b}} \ (\dot{m}_{\mathrm{f}} LHV) \tag{A.1}$$

where $\dot{Q}_{\mathrm{b}}$ is the produced thermal power, $\dot{m}_{\mathrm{f}}$ and LHV are the fuel mass flow rate and lower heating value, respectively, and η_{b} is the boiler efficiency. The latter is corrected through a linear interpolation between the nominal and minimum load conditions, which are usually defined in the boiler manufacturer data-sheets, in order to consider the critical influence of load on the boiler performance. The correction (Eq. (A.2)) is in agreement with the most common technical standards, and is based on the dimensionless parameters Λ and Λ_{min}, which are the ratio of actual to nominal heat and the ratio of minimum to nominal heat generated by the boiler, respectively.

$$\eta_{\mathrm{b}} = \frac{\Lambda - \Lambda_{\mathrm{min}}}{1 - \Lambda_{\mathrm{min}}} \ (\eta_{\mathrm{nom}} - \eta_{\mathrm{min}}) + \eta_{\mathrm{min}} \tag{A.2}$$

where η_{nom} and η_{min} are the efficiency values at nominal and minimum load conditions, respectively.

Combined Heat and Power plant A Combined Heat and Power plant produces both electrical and thermal power, the latter of which can be recovered and supplied to a DHN. The CHP model is algebraic and evaluates the electric power production P_{el} and heat recovery $\dot{Q}_{\mathrm{rec}}$ (Eq. (A.3)) depending on the energy flow from the source P_{in} and the system efficiency chain.

$$P_{\mathrm{el}} = P_{\mathrm{in}}\,\eta_{\mathrm{th}}\,\eta_{\mathrm{m}}\eta_{\mathrm{el}} \tag{A.3a}$$

$$\dot{Q}_{\mathrm{rec}} = (1-\eta_{\mathrm{th}})\;P_{\mathrm{in}}\,\eta_{\mathrm{rec}} \tag{A.3b}$$

The thermodynamic efficiency η_{th} is corrected on the basis of the plant operation, with a linear interpolation between the nominal and minimum load efficiency values, similarly to the boiler efficiency correction. The heat provided to the district heating network is influenced by the recovery efficiency η_{rec}. Different types of CHPs can be represented in this way. For instance, in case of an internal combustion engine in CHP configuration, the inlet energy flow P_{in} is given by the combustion of the fuel mass flow rate $\dot{m}_{\mathrm{f}}$. Another plant type is constituted by Organic Rankine Cycle technologies, one of the most common applications of which is the exploitation of waste heat sources [163]. Indeed, thanks to the relatively low boiling point of the working fluid, it allows electrical and thermal power to be produced by low-temperature sources that would otherwise be wasted. The heat from the ORC condenser, in turn, can supply the district heating network. In this case, P_{in} is given by the low-temperature heat source.

Pump The pump is an algebraic model based on a heuristic modeling approach. Considering the Buckingham π theorem [186], a dimensionless curve, drawn from a set of measured operating points for a specific rotational speed, can be used to describe the performance of a series of geometrically similar pumps at various operating speeds, by means of the head and flow coefficients π_1 and π_2, given by Eq. (A.4).

$$\pi_1 = \frac{gH}{n^2D^2} \tag{A.4a}$$

$$\pi_2 = \frac{\dot{V}}{nD^3} \tag{A.4b}$$

The model parameters are the pump diameter D and the dimensionless map for the given pump type. The model then calculates the volumetric flow rate $\dot{V}$ processed by the pump with rotational speed n and pressure head H as inputs.

Expansion vessel Expansions vessels are fundamental elements of any closed water heating systems since they handle pressure fluctuations related to thermal

expansions and mass flow rate transients. Basically, an expansion vessel is a tank partially filled with air, whose function is to act like a pressure buffer: the higher the water level, the higher the air pressure and, consequently, the water pressure. Similarly, a water discharge leads to a vessel pressure reduction. The proposed dynamic model represents the air damping effect by means of the differential equation Eq. (A.5) derived from the continuity equation:

$$p_{\mathrm{w}} = p_{\mathrm{a}} = p_{\mathrm{a},0} \left(\frac{V_{\mathrm{a},0}}{V_{\mathrm{a},0} - \frac{dV_{\mathrm{w}}}{dt}} \right)^{k} \tag{A.5}$$

where the water volume V_{w} (i.e.model state variable) evolves over time depending on the initial condition and on the difference between incoming and outgoing mass flow rates. Air is assumed as an ideal gas expanding or compressing in adiabatic conditions, while $p_{\mathrm{a},0}$ and $V_{\mathrm{a},0}$ are the initial air pressure and volume in the vessel, respectively, and k is the specific heat capacity ratio. From a computational point of view, this state-determined model is required for decoupling algebraic models, which might otherwise give rise to undesirable algebraic loops.

Pipeline The developed pipeline model considers both the thermal dynamics and the hydraulics of the heat transfer fluid. Several pipeline models can be interconnected, so that a generic complex distribution topology can be split into a sequence of pipeline segments with their own characteristics. The circulating mass flow rate $\dot{m}$ is calculated once for the entire pipeline sequence, by means of a differential equation derived from the momentum continuity equation Eq. (A.6) and depending on the differential pressure between upstream ($p_{\max}$) and downstream ($p_{\min}$) of the pipeline:

$$\frac{1}{\rho\, A_{\mathrm{in}(1)}} \frac{d\dot{m}}{dt} = \frac{(p_{\max} - p_{\min} - \sum_{\mathrm{i}} (\Delta p)_{\mathrm{i}})\; A_{\mathrm{in}(1)}}{\sum_{\mathrm{i}} \Delta M_{\mathrm{i}}} \tag{A.6}$$

where $A_{\mathrm{in}(1)}$ is the cross-sectional area of the first pipeline segment and M_{i} is the fluid mass contained in the i-th segment. The total pressure drop is calculated as the sum of all the pipeline segment contributions and considers geodetic, distributed and concentrated losses, given by Eq. (A.7).

$$\Delta p = p_{\mathrm{geo}} + p_{\mathrm{dist}} + p_{\mathrm{conc}} = \rho\, g\; (z_{\mathrm{in}} - z_{\mathrm{out}}) + \lambda \frac{L}{D_{\mathrm{in}}} \frac{\rho\, w^2}{2} + k_{\mathrm{r}} \frac{\rho\, w^2}{2} \tag{A.7}$$

where z_{in} and z_{out} are the inlet and outlet section heights, w is the fluid velocity, and L and D_{in} are the segment length and internal diameter, respectively. The flow coefficient λ is calculated through the Haaland empirical correlation while the

resistance coefficient k_r is found in the data-sheets. The outlet temperature T_w is determined by means of the energy conservation equation Eq. (A.8) for each pipeline segment, the thermal model of which is lumped:

$$M\, c_\mathrm{w}\, \frac{dT_\mathrm{w}}{dt} = \dot{m}\, c_\mathrm{w}\, (T_\mathrm{w,in} - T_\mathrm{w}) - A\, U\, (T_\mathrm{w} - T_\mathrm{soil}) \tag{A.8}$$

It includes the net enthalpy flow and heat transfer with the soil, which is influenced by the pipeline geometry and thermal properties.

Junction The junction allows flows to be mixed of split in the network intersections. The junction model is dynamic and relies on the energy balance and continuity equations for the pressure and temperature calculation of the water outflow. The mass flow rate is calculated as the sum of the incoming mass flow rates from the converging branches. The pressure is calculated in the same way as that of the expansion vessel mentioned above. As regards the thermal dynamics, heat accumulation and thermal losses are neglected and, therefore, the outlet temperature T_out is determined by means of an algebraic form of the energy balance equation, as in Eq. (A.9).

$$T_\mathrm{out} = \frac{\sum_i^n \left(\dot{m}_\mathrm{in} c_\mathrm{w} T_\mathrm{in}\right)_i}{\sum_i^n \left(\dot{m}_\mathrm{in} c_\mathrm{w}\right)_i} \tag{A.9}$$

In the case of flow splitting, the temperature of the outflow equals that of the inflow since there is no mixing.

Control valve In a distribution system, valves are used to control energy flows toward the users. For this specific purpose, valves can be seen as controllable fittings that regulate the water pressure drop by completely or partially obstructing the pipeline cross-section. The valve model is algebraic and relies on a derived form of the Darcy-Weisbach equation Eq. (A.10).

$$\Delta p_\mathrm{valve} = \frac{\dot{m}^2}{\rho_\mathrm{w}\, \left(\phi K_\mathrm{v}\right)^2} \tag{A.10}$$

where K_v is the nominal flow coefficient and ϕ is a factor representing the effects of valve opening. This relationship is derived from the valve characteristic curve, which is usually provided by the manufacturer and can be easily entered by the user. Similarly to the junction, thermal losses across the valve are neglected.

Heat exchanger The heat exhanger is modeled as a dynamic element relying on the differential form of the energy conservation equation Eq. (A.11):

$$M\, c_\mathrm{w}\, \frac{dT_\mathrm{w}}{dt} = \dot{m}\, c_\mathrm{w}\, (T_\mathrm{w,in} - T_\mathrm{w}) + \dot{Q} \tag{A.11}$$

where $\dot{Q}$ is the heat transferred to the primary fluid and can derive from different sources, such as a production unit (e.g. boiler) or a secondary fluid. The pressure drops are evaluated with the equivalent length method in order to simplify the model setting. Regardless of the heat exchanger type, once the rated values of pressure drop and fluid velocity are known, the model evaluates the overall resistance coefficient k_r, and then the pressure drops are calculated according to Eq. (A.12):

$$\Delta p_\mathrm{HEX} = k_\mathrm{r} \frac{\rho\, w^2}{2} \tag{A.12}$$

Thermal energy storage The Thermal Energy Storage is fundamental for decoupling heat generation and consumption in district heating systems, providing an additional degree of freedom in heating management. Indeed, the operation scheduling of the heat generation systems can be varied regardless of the thermal demand profile, in order to match the most favorable conditions. The proposed model has been developed and validated by Cadau et al. [187], and it is suitable for the simulation of a sensible heat water TES, with a focus on thermal stratification. It is a multi-node, one-dimensional, plug-flow model [188] designed to be part of a district heating network. The storage tank is divided into a customizable number of layers, namely nodes, in which the temperature is uniform. Only the vertical temperature gradient inside the tank is considered. The nodes are sorted in decreasing order of temperature starting from the top to the bottom of the tank. The continuity and energy balance equations are implemented for each node. The tank water inflow rate is automatically allocated to the node with the closest temperature. The outflow rates are defined as model inputs, except for that of the lowest node, which is calculated by the model through the conservation equation applied to the whole tank. The dynamic energy balance determines the node temperature by considering the net enthalpy flow, heat transfer between adjacent nodes (i.e. convection and conduction) and thermal losses through the tank envelope. The details on the full mathematical models are reported in [187].

Building Buildings are the final users of every heat distribution network. The proposed model provides a simplified but reliable representation of their thermal behavior, suitable for district heating systems. For this purpose, the building is considered as a system with a given mass, exchanging heat with the environment, the network and the air flow due to natural and mechanical ventilation. These contributions are considered by means of a parametric form of the energy conservation

equation Eq. (A.13)

$$\frac{dT_{\mathrm{bld}}}{dt} = \alpha\ (T_{\mathrm{ext}} - T_{\mathrm{bld}}) + \beta\ \left(\dot{Q}_{\mathrm{hs}} + \dot{Q}_{\mathrm{rad}} + \dot{Q}_{\mathrm{occ}}\right) + \gamma\ (T_{\mathrm{ext}} - T_{\mathrm{bld}}) + \delta\ (T_{\mathrm{air}} - T_{\mathrm{bld}}) \tag{A.13}$$

The variation of the indoor temperature T_{bld} depends on four different terms as follows:

- heat dissipation through the building envelope;
- the thermal power transferred to the building by the heating system $\dot{Q}_{\mathrm{hs}}$, by solar radiation $\dot{Q}_{\mathrm{rad}}$ and the heat gain from occupants $\dot{Q}_{\mathrm{occ}}$;
- natural ventilation or infiltrations;
- mechanical ventilation influenced by the presence of a heat recovery ventilation system, which brings the inlet air at T_{air}.

These terms are characterized by the performance coefficients α, β, γ and δ, which can be determined from experimental measurements or proper simulations with a detailed building model. The proposed model also determines the amount of heat transferred by the heating network, which is affected by the space heater operation (e.g. radiators and fan coil units) through the regulation of the overall heat transfer coefficient. The water return temperature is consequently determined by the energy balance equation applied to the substation, which represents the interconnection between the primary side of the DHN and the local heating system.

Table A.1. Overview of the relevant features of the component models of the District Heating Network library.

Component	Algebraic Dynamic	Lumped Discretized	Inputs	Outputs	States
Boiler	Al	L	Fuel mass flow rate	Thermal power	-
ORC plant	A	L	Thermal power to ORC evaporator	Electrical and recovered thermal power	-
Pump	Al	L	Pump rotational speed, pressure head	Water mass flow rate	-
Expansion vessel	Dy	L	Inlet and outlet water mass flow rate	Water pressure	Water volume
Pipeline	Dy	1D	Inlet water mass flow rate, pressure and temperature, outlet pressure	Outlet water mass flow rate and temperature	Pipe water temperature
Junction	Dy	L	Inlet water mass flow rates and temperatures	Water outlet temperature and pressure	Water volume
Control valve	A	L	Valve opening, inlet water mass flow rate, temperature and pressure	Water outlet pressure	-
Heat exchanger	Dy	L	Inlet water mass flow rate, pressure and temperature, thermal power	Outlet water pressure and temperature	Water temperature
Thermal energy storage	Dy	1D	Inlet and outlet water mass flow rates, inlet pressure and temperature	Outlet water pressure and temperature	Node temperature
Building	Dy	L	Supply water mass flow rate and temperature, heat gains, control input of space heaters	Return water temperature	Building temperature

References

[1] IPCC. *Climate Change 2013: The Physical Science Basis. Contribution of Working Group I to the Fifth Assessment Report of the Intergovernmental Panel on Climate Change*. Tech. rep. 2013.

[2] IPCC. *Climate Change 2007: Impacts, Adaptation and Vulnerability. Contribution of Working Group II to the Fourth Assessment Report of the Intergovernmental Panel on Climate Change*. Tech. rep. 2007.

[3] United Nations Treaty Collection. *Paris Agreement, Chapter XXVII - Environment*. 2015.

[4] International Energy Agency. *Energy Technology Perspectives 2020*. Tech. rep. 2020.

[5] European Commission. *Communication from the Commission to the Council, the European Parliament, the European Economic and Social Committee and the Committee of the Regions - A European strategic energy technology plan (Set-plan) - 'Towards a low carbon future'*. 2007.

[6] European Commission Directorate-General for Energy. *Clean energy for all Europeans*. Luxembourg, 2019. DOI: 10.2833/21366.

[7] European Commission. *Communication from the Commission to the European Parliament, the European Council, the Council, the European Economic and Social Committee and the Committee of the Regions - The European Green Deal*. 2019.

[8] International Energy Agency. *World Energy Outlook 2020*. Tech. rep. Paris, 2020.

[9] European Commission. *Communication from the Commission to the European Parliament, the Council, the European Economic and Social Committee and the Committee of the Regions - Stepping up Europe's 2030 climate ambition*. 2020.

[10] S. Paardekooper, R. S. Lund, B. V. Mathiesen, M. Chang, U. R. Petersen, L. Grundahl, A. David, J. Dahlbæk, I. A. Kapetanakis, H. Lund, N. Bertelsen, K. Hansen, D. W. Drysdale, and U. Persson. *Heat Roadmap Europe Quantifying the Impact of Low-carbon Heating and Cooling Roadmaps*. Tech. rep. Aalborg Universitetsforlag, 2018.

[11] European Commission. *Communication from the Commission to the European Parliament, the Council, the European Economic and Social Committee and the Committee of the Regions - A Renovation Wave for Europe - greening our buildings, creating jobs, improving lives*. 2020.

[12] H. Lund, S. Werner, R. Wiltshire, S. Svendsen, J. E. Thorsen, F. Hvelplund, and B. V. Mathiesen. "4th Generation District Heating (4GDH). Integrating smart thermal grids into future sustainable energy systems." In: *Energy* 68 (2014), pp. 1–11. DOI: 10.1016/j.energy.2014.02.089.

[13] H. Lund, P. A. Østergaard, M. Chang, S. Werner, S. Svendsen, P. Sorknæs, J. E. Thorsen, F. Hvelplund, B. O. G. Mortensen, B. V. Mathiesen, C. Bojesen, N. Duic, X. Zhang, and B. Möller. "The status of 4th generation district heating: Research and results". In: *Energy* 164 (2018), pp. 147–159. DOI: 10.1016/j.energy.2018.08.206.

[14] S. Buffa, M. Cozzini, M. D'Antoni, M. Baratieri, and R. Fedrizzi. "5th generation district heating and cooling systems: A review of existing cases in Europe". In: *Renewable and Sustainable Energy Reviews* 104 (2019), pp. 504–522. DOI: 10.1016/j.rser.2018.12.059.

[15] S. Frederiksen and S. Werner. *District Heating and Cooling*. Lund: Studentlitteratur AB, 2013. ISBN: 978914408530.

[16] H. Lund, P. A. Østergaard, D. Connolly, and B. V. Mathiesen. "Smart energy and smart energy systems". In: *Energy* 137 (2017), pp. 556–565. DOI: 10.1016/j.energy.2017.05.123.

[17] P. Leoni, R. Geyer, and R.-R. Schmidt. "Developing innovative business models for reducing return temperatures in district heating systems: Approach and first results". In: *Energy* 195 (2020), p. 116963. DOI: 10.1016/j.energy.2020.116963.

[18] L. Laakkonen, T. Korpela, J. Kaivosoja, M. Vilkko, Y. Majanne, and M. Nurmoranta. "Predictive Supply Temperature Optimization of District Heating Networks Using Delay Distributions". In: *Energy Procedia* 116 (2017), pp. 297–309. DOI: 10.1016/j.egypro.2017.05.076.

[19] A. R. Mazhar, S. Liu, and A. Shukla. "A state of art review on the district heating systems". In: *Renewable and Sustainable Energy Reviews* 96 (2018), pp. 420–439. DOI: 10.1016/j.rser.2018.08.005.

[20] T. Van Oevelen, D. Vanhoudt, C. Johansson, and E. Smulders. "Testing and performance evaluation of the STORM controller in two demonstration sites". In: *Energy* 197 (2020), p. 117177. DOI: 10.1016/j.energy.2020.117177.

[21] DHC+ Technology Platform - Euroheat & Power. *Digital Roadmap for District Heating and Cooling*. 2019.

[22] Gestore dei Servizi Energetici S.p.A. (GSE). *Teleriscaldamento e Teleraffrescamento 2018 - Diffusione delle reti ed energia fornita in Italia - Nota di approfondimento Maggio 2020*.

[23] N. Zimmerman, K. Kyprianidis, and C.-F. Lindberg. "Achieving Lower District Heating Network Temperatures Using Feed-Forward MPC". In: *Materials* 12.15 (2019), p. 2465. DOI: 10.3390/ma12152465.

[24] D. Olsthoorn, F. Haghighat, and P. A. Mirzaei. "Integration of storage and renewable energy into district heating systems: A review of modelling and optimization". In: *Solar Energy* 136 (2016), pp. 49–64. DOI: 10.1016/j.solener.2016.06.054.

[25] J. DeCarolis, H. Daly, P. Dodds, I. Keppo, F. Li, W. McDowall, S. Pye, N. Strachan, E. Trutnevyte, W. Usher, M. Winning, S. Yeh, and M. Zeyringer. "Formalizing best practice for energy system optimization modelling". In: *Applied Energy* 194 (2017), pp. 184–198. DOI: 10.1016/j.apenergy.2017.03.001.

[26] I. del Hoyo Arce, S. Herrero López, S. López Perez, M. Rämä, K. Klobut, and J. A. Febres. "Models for fast modelling of district heating and cooling networks". In: *Renewable and Sustainable Energy Reviews* 82 (2018), pp. 1863–1873. DOI: 10.1016/j.rser.2017.06.109.

[27] J. Allegrini, K. Orehounig, G. Mavromatidis, F. Ruesch, V. Dorer, and R. Evins. "A review of modelling approaches and tools for the simulation of district-scale energy systems". In: *Renewable and Sustainable Energy Reviews* 52 (2015), pp. 1391–1404. DOI: 10.1016/j.rser.2015.07.123.

[28] M. Chertkov and N. N. Novitsky. "Thermal Transients in District Heating Systems". In: *Energy* 184 (2019), pp. 22–33. DOI: 10.1016/j.energy.2018.01.049.

[29] B. van der Heijde, M. Fuchs, C. Ribas Tugores, G. Schweiger, K. Sartor, D. Basciotti, D. Müller, C. Nytsch-Geusen, M. Wetter, and L. Helsen. "Dynamic equation-based thermo-hydraulic pipe model for district heating and cooling systems". In: *Energy Conversion and Management* 151 (2017), pp. 158–169. DOI: 10.1016/j.enconman.2017.08.072.

[30] A. Dénarié, M. Aprile, and M. Motta. "Heat transmission over long pipes: New model for fast and accurate district heating simulations". In: *Energy* 166 (2019), pp. 267–276. DOI: 10.1016/j.energy.2018.09.186.

[31] E. Guelpa and V. Verda. "Compact physical model for simulation of thermal networks". In: *Energy* 175 (2019), pp. 998–1008. DOI: 10.1016/j.energy.2019.03.064.

[32] A. Menapace, W. Boscheri, M. Baratieri, and M. Righetti. "An efficient numerical scheme for the thermo-hydraulic simulations of thermal grids". In: *International Journal of Heat and Mass Transfer* 161 (2020), p. 120304. DOI: 10.1016/j.ijheatmasstransfer.2020.120304.

[33] M. A. Ancona, M. Bianchi, L. Branchini, and F. Melino. "District heating network design and analysis". In: *Energy Procedia* 45 (2014), pp. 1225–1234. DOI: 10.1016/j.egypro.2014.01.128.

[34] H. V. Larsen, B. Bøhm, and M. Wigbels. "A comparison of aggregated models for simulation and operational optimisation of district heating networks". In: *Energy Conversion and Management* 45 (2004), pp. 1119–1139. DOI: 10.1016/j.enconman.2003.08.006.

[35] T. Sommer, M. Sulzer, M. Wetter, A. Sotnikov, S. Mennel, and C. Stettler. "The reservoir network: A new network topology for district heating and cooling". In: *Energy* 199 (2020), p. 117418. DOI: 10.1016/j.energy.2020.117418.

[36] A. Zajacs and A. Borodinecs. "Assessment of development scenarios of district heating systems". In: *Sustainable Cities and Society* 48 (2019), p. 101540. DOI: 10.1016/j.scs.2019.101540.

[37] L. Giraud, R. Baviere, M. Vallée, and C. Paulus. "Presentation, Validation and Application of the DistrictHeating Modelica Library". In: *Proceedings of the 11th International Modelica Conference, Versailles, France, September 21-23, 2015* 118 (2015), pp. 79–88. DOI: 10.3384/ecp1511879.

[38] H. Kauko, K. H. Kvalsvik, D. Rohde, A. Hafner, and N. Nord. "Dynamic modelling of local low-temperature heating grids: A case study for Norway". In: *Energy* 139 (2017), pp. 289–297. DOI: 10.1016/j.energy.2017.07.086.

[39] G. Schweiger, P. O. Larsson, F. Magnusson, P. Lauenburg, and S. Velut. "District heating and cooling systems – Framework for Modelica-based simulation and dynamic optimization". In: *Energy* 137 (2017), pp. 566–578. DOI: 10.1016/j.energy.2017.05.115.

[40] G. Barone, A. Buonomano, C. Forzano, and A. Palombo. "A novel dynamic simulation model for the thermo-economic analysis and optimisation of district heating systems". In: *Energy Conversion and Management* 220 (2020), p. 113052. DOI: 10.1016/j.enconman.2020.113052.

[41] A. Benonysson, B. Bøhm, and H. F. Ravn. "Operational optimization in a district heating system". In: *Energy Conversion and Management* 36.5 (1995), pp. 297–314. DOI: 10.1016/0196-8904(95)98895-T.

[42] W. Ma, S. Fang, G. Liu, and R. Zhou. "Modeling of district load forecasting for distributed energy system". In: *Applied Energy* 204 (2017), pp. 181–205. DOI: 10.1016/j.apenergy.2017.07.009.

[43] G. Mustafaraj, D. Marini, A. Costa, and M. Keane. "Model calibration for building energy efficiency simulation". In: *Applied Energy* 130 (2014), pp. 72–85. DOI: 10.1016/j.apenergy.2014.05.019.

[44] A. Buonomano and A. Palombo. "Building energy performance analysis by an in-house developed dynamic simulation code: An investigation for different case studies". In: *Applied Energy* 113 (2014), pp. 788–807. DOI: 10.1016/j.apenergy.2013.08.004.

[45] K. Foteinaki, R. Li, T. Péan, C. Rode, and J. Salom. "Evaluation of energy flexibility of low-energy residential buildings connected to district heating". In: *Energy and Buildings* 213 (2020), p. 109804. DOI: 10.1016/j.enbuild.2020.109804.

[46] E. J. Kim, G. Plessis, J. L. Hubert, and J. J. Roux. "Urban energy simulation: Simplification and reduction of building envelope models". In: *Energy and Buildings* 84 (2014), pp. 193–202. DOI: 10.1016/j.enbuild.2014.07.066.

[47] L. Lundström, J. Akander, and J. Zambrano. "Development of a space heating model suitable for the automated model generation of existing multi-family buildings - a case study in Nordic climate". In: *Energies* 12.3 (2019), p. 485. DOI: 10.3390/en12030485.

[48] D. Coakley, P. Raftery, and M. Keane. "A review of methods to match building energy simulation models to measured data". In: *Renewable and Sustainable Energy Reviews* 37 (2014), pp. 123–141. DOI: 10.1016/j.rser.2014.05.007.

[49] A. A. Famuyibo, A. Duffy, and P. Strachan. "Developing archetypes for domestic dwellings - An Irish case study". In: *Energy and Buildings* 50 (2012), pp. 150–157. DOI: 10.1016/j.enbuild.2012.03.033.

[50] J. A. Fonseca and A. Schlueter. "Integrated model for characterization of spatiotemporal building energy consumption patterns in neighborhoods and city districts". In: *Applied Energy* 142 (2015), pp. 247–265. DOI: 10.1016/j.apenergy.2014.12.068.

[51] J. F. Marquant, L. A. Bollinger, R. Evins, and J. Carmeliet. "A new combined clustering method to Analyse the potential of district heating networks at large-scale". In: *Energy* 156 (2018), pp. 73–83. DOI: 10.1016/j.energy.2018.05.027.

[52] R. Yin, E. C. Kara, Y. Li, N. DeForest, K. Wang, T. Yong, and M. Stadler. "Quantifying flexibility of commercial and residential loads for demand response using setpoint changes". In: *Applied Energy* 177 (2016), pp. 149–164. DOI: 10.1016/j.apenergy.2016.05.090.

[53] E. Calikus, S. Nowaczyk, A. Sant'Anna, H. Gadd, and S. Werner. "A data-driven approach for discovering heat load patterns in district heating". In: *Applied Energy* 252 (2019), p. 113409. DOI: 10.1016/j.apenergy.2019.113409.

[54] M. Leśko, W. Bujalski, and K. Futyma. "Operational optimization in district heating systems with the use of thermal energy storage". In: *Energy* 165 (2018), pp. 902–915. DOI: 10.1016/j.energy.2018.09.141.

[55] G. Suryanarayana, J. Lago, D. Geysen, P. Aleksiejuk, and C. Johansson. "Thermal load forecasting in district heating networks using deep learning and advanced feature selection methods". In: *Energy* 157 (2018), pp. 141–149. DOI: 10.1016/j.energy.2018.05.111.

[56] D. Koschwitz, J. Frisch, and C. van Treeck. "Data-driven heating and cooling load predictions for non-residential buildings based on support vector machine regression and NARX Recurrent Neural Network: A comparative study on district scale". In: *Energy* 165 (2018), pp. 134–142. DOI: 10.1016/j.energy.2018.09.068.

[57] M. Benzaama, L. Rajaoarisoa, B. Ajib, and S. Lecoeuche. "A data-driven methodology to predict thermal behavior of residential buildings using piecewise linear models". In: *Journal of Building Engineering* 32 (2020), p. 101523. DOI: 10.1016/j.jobe.2020.101523.

[58] A. Vandermeulen, B. van der Heijde, and L. Helsen. "Controlling district heating and cooling networks to unlock flexibility: A review". In: *Energy* 151 (2018), pp. 103–115. DOI: 10.1016/j.energy.2018.03.034.

[59] E. Guelpa and V. Verda. "Thermal energy storage in district heating and cooling systems: A review". In: *Applied Energy* 252.May (2019), p. 113474. DOI: 10.1016/j.apenergy.2019.113474.

[60] A. Vandermeulen. "Quantification and optimal control of district heating network flexibility". PhD thesis. KU Leuven, 2020.

[61] A. Vandermeulen, T. Van Oevelen, B. van der Heijde, and L. Helsen. "A simulation-based evaluation of substation models for network flexibility characterisation in district heating networks". In: *Energy* 201 (2020), p. 117650. DOI: 10.1016/j.energy.2020.117650.

[62] M. Kouhia, T. Laukkanen, H. Holmberg, and P. Ahtila. "District heat network as a short-term energy storage". In: *Energy* 177 (2019), pp. 293–303. DOI: 10.1016/j.energy.2019.04.082.

[63] K. Sartor and P. Dewallef. "Integration of heat storage system into district heating networks fed by a biomass CHP plant". In: *Journal of Energy Storage* 15 (2018), pp. 350–358. DOI: 10.1016/j.est.2017.12.010.

[64] J. Le Dréau and P. Heiselberg. "Energy flexibility of residential buildings using short term heat storage in the thermal mass". In: *Energy* 111 (2016), pp. 991–1002. DOI: 10.1016/j.energy.2016.05.076.

[65] B. J. Claessens, D. Vanhoudt, J. Desmedt, and F. Ruelens. "Model-free control of thermostatically controlled loads connected to a district heating network". In: *Energy and Buildings* 159 (2018), pp. 1–10. DOI: 10.1016/j.enbuild.2017.08.052.

[66] M. Arnaudo, M. Topel, P. Puerto, E. Widl, and B. Laumert. "Heat demand peak shaving in urban integrated energy systems by demand side management - A techno-economic and environmental approach". In: *Energy* 186 (2019). DOI: 10.1016/j.energy.2019.115887.

[67] Z. Ma, A. Knotzer, J. D. Billanes, and B. N. Jørgensen. "A literature review of energy flexibility in district heating with a survey of the stakeholders' participation". In: *Renewable and Sustainable Energy Reviews* 123 (2020), p. 109750. DOI: 10.1016/j.rser.2020.109750.

[68] J. Kensby, A. Trüschel, and J. O. Dalenbäck. "Potential of residential buildings as thermal energy storage in district heating systems - Results from a pilot test". In: *Applied Energy* 137 (2015), pp. 773–781. DOI: 10.1016/j.apenergy.2014.07.026.

[69] D. Romanchenko, J. Kensby, M. Odenberger, and F. Johnsson. "Thermal energy storage in district heating: Centralised storage vs. storage in thermal inertia of buildings". In: *Energy Conversion and Management* 162 (2018), pp. 26–38. DOI: 10.1016/j.enconman.2018.01.068.

[70] D. F. Dominković, P. Gianniou, M. Münster, A. Heller, and C. Rode. "Utilizing thermal building mass for storage in district heating systems: Combined building level simulations and system level optimization". In: *Energy* 153 (2018), pp. 949–966. DOI: 10.1016/j.energy.2018.04.093.

[71] M. Turski and R. Sekret. "Buildings and a district heating network as thermal energy storages in the district heating system". In: *Energy and Buildings* 179 (2018), pp. 49–56. DOI: 10.1016/j.enbuild.2018.09.015.

[72] G. Reynders, J. Diriken, and D. Saelens. "Bottom-up modeling of the Belgian residential building stock: influence of model complexity". In: *9th International Conference on System Simulation in Buildings, Liege, December 10-12, 2014* (2014).

[73] M. Killian and M. Kozek. "Ten questions concerning model predictive control for energy efficient buildings". In: *Building and Environment* 105 (2016), pp. 403–412. DOI: 10.1016/j.buildenv.2016.05.034.

[74] C. Saletti, A. Gambarotta, and M. Morini. "Development, analysis and application of a predictive controller to a small-scale district heating system". In: *Applied Thermal Engineering* 165 (2020), p. 114558. DOI: 10.1016/j.applthermaleng.2019.114558.

[75] S. Salakij, N. Yu, S. Paolucci, and P. Antsaklis. "Model-Based Predictive Control for building energy management. I: Energy modeling and optimal control". In: *Energy and Buildings* 133 (2016), pp. 345–358. DOI: 10.1016/j.enbuild.2016.09.044.

[76] J. Kensby. "Smart Eenergy Grids -Utilization of Space Heating Flexibility". PhD thesis. Chalmers University of Technology, 2017.

[77] W. Gu, J. Wang, S. Lu, Z. Luo, and C. Wu. "Optimal operation for integrated energy system considering thermal inertia of district heating network and buildings". In: *Applied Energy* 199 (2017), pp. 234–246. DOI: 10.1016/j.apenergy.2017.05.004.

[78] T. Korpela, J. Kaivosoja, Y. Majanne, L. Laakkonen, M. Nurmoranta, and M. Vilkko. "Utilization of District Heating Networks to Provide Flexibility in CHP Production". In: *Energy Procedia* 116 (2017), pp. 310–319. DOI: 10.1016/j.egypro.2017.05.077.

[79] D. Schmidt, A. Kallert, M. Blesl, S. Svendsen, H. Li, N. Nord, and K. Sipilä. "Low Temperature District Heating for Future Energy Systems". In: *Energy Procedia* 116 (2017), pp. 26–38. DOI: 10.1016/j.egypro.2017.05.052.

[80] E. Guelpa, S. Deputato, and V. Verda. "Thermal request optimization in district heating networks using a clustering approach". In: *Applied Energy* 228 (2018), pp. 608–617. DOI: 10.1016/j.apenergy.2018.06.041.

[81] A. Kazagic, A. Merzic, E. Redzic, and D. Tresnjo. "Optimization of modular district heating solution based on CHP and RES - Demonstration case of the Municipality of Visoko". In: *Energy* 181 (2019), pp. 56–65. DOI: 10.1016/j.energy.2019.05.132.

[82] X. Li, W. Li, R. Zhang, T. Jiang, H. Chen, and G. Li. "Collaborative scheduling and flexibility assessment of integrated electricity and district heating systems utilizing thermal inertia of district heating network and aggregated buildings". In: *Applied Energy* 258.November 2019 (2020), p. 114021. DOI: 10.1016/j.apenergy.2019.114021.

[83] G. Sandou, S. Font, S. Tebbani, A. Hiret, and C. Mondon. "Predictive control of a complex district heating network". In: *Proceedings of the 44th IEEE Conference on Decision and Control, and the European Control Conference, CDC-ECC '05* (2005), pp. 7372–7377. DOI: 10.1109/CDC.2005.1583351.

[84] A. I. Dounis and C. Caraiscos. "Advanced control systems engineering for energy and comfort management in a building environment-A review". In: *Renewable and Sustainable Energy Reviews* 13 (2009), pp. 1246–1261. DOI: 10.1016/j.rser.2008.09.015.

[85] S. Prívara, J. Široký, L. Ferkl, and J. Cigler. "Model predictive control of a building heating system: The first experience". In: *Energy and Buildings* 43 (2011), pp. 564–572. DOI: 10.1016/j.enbuild.2010.10.022.

[86] P. May-Ostendorp, G. P. Henze, C. D. Corbin, B. Rajagopalan, and C. Felsmann. "Model-predictive control of mixed-mode buildings with rule extraction". In: *Building and Environment* 46.2 (2011), pp. 428–437. DOI: 10.1016/j.buildenv.2010.08.004.

[87] P. H. Shaikh, N. B. M. Nor, P. Nallagownden, I. Elamvazuthi, and T. Ibrahim. "A review on optimized control systems for building energy and comfort management of smart sustainable buildings". In: *Renewable and Sustainable Energy Reviews* 34 (2014), pp. 409–429. DOI: 10.1016/j.rser.2014.03.027.

[88] G. Serale, M. Fiorentini, A. Capozzoli, D. Bernardini, and A. Bemporad. "Model Predictive Control (MPC) for enhancing building and HVAC system energy efficiency: Problem formulation, applications and opportunities". In: *Energies* 11.3 (2018), p. 631. DOI: 10.3390/en11030631.

[89] A. Kathirgamanathan, M. De Rosa, E. Mangina, and D. P. Finn. "Data-driven predictive control for unlocking building energy flexibility: A review". In: *Renewable and Sustainable Energy Reviews* 135 (2021), p. 110120. DOI: 10.1016/j.rser.2020.110120.

[90] D. Lindelöf, H. Afshari, M. Alisafaee, J. Biswas, M. Caban, X. Mocellin, and J. Viaene. "Field tests of an adaptive, model-predictive heating controller for residential buildings". In: *Energy and Buildings* 99 (2015), pp. 292–302. DOI: 10.1016/j.enbuild.2015.04.029.

[91] S. R. West, J. K. Ward, and J. Wall. "Trial results from a model predictive control and optimisation system for commercial building HVAC". In: *Energy and Buildings* 72 (2014), pp. 271–279. DOI: 10.1016/j.enbuild.2013.12.037.

[92] G. Bianchini, M. Casini, D. Pepe, A. Vicino, and G. G. Zanvettor. "An integrated model predictive control approach for optimal HVAC and energy storage operation in large-scale buildings". In: *Applied Energy* 240.February (2019), pp. 327–340. DOI: 10.1016/j.apenergy.2019.01.187.

[93] A. Mugnini, G. Coccia, F. Polonara, and A. Arteconi. "Performance assessment of data-driven and physical-based models to predict building energy demand in model predictive controls". In: *Energies* 13.12 (2020), p. 3125. DOI: 10.3390/en13123125.

[94] S. Fazlollahi, G. Becker, A. Ashouri, and F. Maréchal. "Multi-objective, multi-period optimization of district energy systems: IV - A case study". In: *Energy* 84 (2015), pp. 365–381. DOI: 10.1016/j.energy.2015.03.003.

[95] H. Dorotić, T. Pukšec, and N. Duić. "Multi-objective optimization of district heating and cooling systems for a one-year time horizon". In: *Energy* 169 (2019), pp. 319–328. DOI: 10.1016/j.energy.2018.11.149.

[96] B. Lyons, E. O'Dwyer, and N. Shah. "Model reduction for Model Predictive Control of district and communal heating systems within cooperative energy systems". In: *Energy* 197 (2020), p. 117178. DOI: 10.1016/j.energy.2020.117178.

[97] E. O'Dwyer, I. Pan, S. Acha, and N. Shah. "Smart energy systems for sustainable smart cities: Current developments, trends and future directions". In: *Applied Energy* 237.October 2018 (2019), pp. 581–597. DOI: 10.1016/j.apenergy.2019.01.024.

[98] S. Long, O. Marjanovic, and A. Parisio. "Generalised control-oriented modelling framework for multi-energy systems". In: *Applied Energy* 235 (2019), pp. 320–331. DOI: 10.1016/j.apenergy.2018.10.074.

[99] W. Birk, K. T. Atta, and F. Uden. "Improving district heating system operation through control configuration selection and adaptive control". In: *18th European Control Conference, ECC 2019* (2019), pp. 2944–2949. DOI: 10.23919/ECC.2019.8795742.

[100] J. Hou, H. Li, and N. Nord. "Optimal control of secondary side supply water temperature for substation in district heating systems". In: *E3S Web of Conferences 111* 111 (2019), p. 06015. DOI: 10.1051/e3sconf/201911106015.

[101] N. Aoun, R. Bavière, M. Vallée, A. Aurousseau, and G. Sandou. "Modelling and flexible predictive control of buildings space-heating demand in district heating systems". In: *Energy* 188 (2019). DOI: 10.1016/j.energy.2019.116042.

[102] F. Verrilli, S. Srinivasan, G. Gambino, M. Canelli, M. Himanka, C. Del Vecchio, M. Sasso, and L. Glielmo. "Model Predictive Control-Based Optimal Operations of District Heating System with Thermal Energy Storage and Flexible Loads". In: *IEEE Transactions on Automation Science and Engineering* 14.2 (2017), pp. 547–557. DOI: 10.1109/TASE.2016.2618948.

[103] G. Lennermo, P. Lauenburg, and S. Werner. "Control of decentralised solar district heating". In: *Solar Energy* 179.December 2018 (2019), pp. 307–315. DOI: 10.1016/j.solener.2018.12.080.

[104] D. Vanhoudt, B. J. Claessens, R. Salenbien, and J. Desmedt. "An active control strategy for district heating networks and the effect of different thermal energy storage configurations". In: *Energy and Buildings* 158 (2018), pp. 1317–1327. DOI: 10.1016/j.enbuild.2017.11.018.

[105] T. Yigitcanlar, K. C. Desouza, L. Butler, and F. Roozkhosh. "Contributions and risks of artificial intelligence (AI) in building smarter cities: Insights from a systematic review of the literature". In: *Energies* 13.6 (2020), p. 1473. DOI: 10.3390/en13061473.

[106] J. Jellema and H. A. Mulder. "Public engagement in energy research". In: *Energies* 9.3 (2016), p. 125. DOI: 10.3390/en9030125.

[107] C. Saletti, M. Morini, and A. Gambarotta. "The Status of Research and Innovation on Heating and Cooling Networks as Smart Energy Systems within Horizon 2020". In: *Energies* 13 (2020), p. 2835. DOI: 10.3390/en13112835.

[108] P. Moseley. "EU support for innovation and market uptake in smart buildings under the Horizon 2020 framework programme". In: *Buildings* 7.4 (2017), p. 105. DOI: 10.3390/buildings7040105.

[109] P. Clerici Maestosi, P. Civiero, and G. Massa. "European Union funding Research Development and Innovation projects on Smart Cities: the state of the art in 2019". In: *International Journal of Sustainable Energy Planning and Management* 24 (2019), pp. 7–20. DOI: 10.5278/ijsepm.3493.

[110] D. Longo, G. Olivieri, R. Roversi, G. Turci, and B. Turillazzi. "Energy Poverty and Protection of Vulnerable Consumers. Overview of the EU Funding Programs FP7 and H2020 and Future Trends in Horizon Europe Danila". In: *Energies* 13 (2020), p. 1030. DOI: 10.3390/en13051030.

[111] European Commission. *CORDIS, EU research results (www.cordis.europa.eu/en).*

[112] International Energy Agency. *Global Energy Review 2020. The impacts of the COVID-19 crisis on global energy demand and CO2 emissions*. Tech. rep. 2020.

[113] European Commission. *Horizon Europe. The next research and innovation framework programme.*

[114] T. Witelski and M. Bowen. *Methods of Mathematical Modelling: Continuous Systems and Differential Equations*. Springer International Publishing, 2015. ISBN: 9783319230429. DOI: 10.1007/978-3-319-23042-9.

[115] V. Kecman. *State-Space Models of Lumped and Distributed Systems. Lecture Notes in Control and Information Sciences, vol 112*. Springer, Berlin, Heidelberg, 1988. ISBN: 978-3-540-50082-7. DOI: 10.1007/BFb0040973.

[116] B. A. Stickler and E. Schachinger. *Basic Concepts in Computational Physics*. Springer International Publishing, 2016. ISBN: 978-3-319-27263-4. DOI: 10.1007/978-3-319-27265-8.

[117] E. Walter and L. Pronzato. *Identification of Parametric Models from Experimental Data*. Springer-Verlag London, 1997. ISBN: 978-3-540-76119-8.

[118] H. A. Nielsen and H. Madsen. "Modelling the heat consumption in district heating systems using a grey-box approach". In: *Energy and Buildings* 38 (2006), pp. 63–71. DOI: 10.1016/j.enbuild.2005.05.002.

[119] J. Nocedal and S. J. Wrigth. *Numerical Optimization*. Springer, New York, NY, 2006. ISBN: 978-0-387-30303-1. DOI: 10.1007/978-0-387-40065-5.

[120] E. A. Humo. "On a direct method of optimization". In: *Mathematics and Computers in Simulation* 12.3 (1970), pp. 122–129. DOI: 10.1016/S0378-4754(70)80010-6.

[121] N. Pompini. "Development and application of methodologies for the optimization of energy systems". PhD thesis. University of Parma, 2015.

[122] R. Fletcher. *Practical Methods of Optimization*. 2nd Editio. John Wiley & Sons, Inc, 2000. ISBN: 978-0-471-49463-8.

[123] A. Ganjehkaviri, M. N. Mohd Jaafar, S. E. Hosseini, and H. Barzegaravval. "Genetic algorithm for optimization of energy systems: Solution uniqueness, accuracy, Pareto convergence and dimension reduction". In: *Energy* 119 (2017), pp. 167–177. DOI: 10.1016/j.energy.2016.12.034.

[124] A. Stoppato, G. Cavazzini, G. Ardizzon, and A. Rossetti. "A PSO (particle swarm optimization)-based model for the optimal management of a small PV(Photovoltaic)-pump hydro energy storage in a rural dry area". In: *Energy* 76 (2014), pp. 168–174. DOI: 10.1016/j.energy.2014.06.004.

[125] K. Bamdad, M. E. Cholette, L. Guan, and J. Bell. "Ant colony algorithm for building energy optimisation problems and comparison with benchmark algorithms". In: *Energy and Buildings* 154 (2017), pp. 404–414. DOI: 10.1016/j.enbuild.2017.08.071.

[126] E.-G. Talbi. *Metaheuristics: From Design to Implementation*. New Jersey, US: John Wiley & Sons, Inc, 2009. ISBN: 978-0-470-27858-1.

[127] D. E. Kirk. *Optimal Control Theory: An Introduction*. Courier Corporation, 2012. ISBN: 9780486135076.

[128] R. E. Bellman. *Dynamic Programming*. Princeton N.J.: Princeton University Press, 1957.

[129] O. Sundström and L. Guzzella. "A generic dynamic programming Matlab function". In: *Proceedings of the IEEE International Conference on Control Applications* 7 (2009), pp. 1625–1630. DOI: 10.1109/CCA.2009.5281131.

[130] P. Casoli, A. Gambarotta, N. Pompini, and L. Riccò. "Hybridization methodology based on DP algorithm for hydraulic mobile machinery - Application to a middle size excavator". In: *Automation in Construction* 61 (2016), pp. 42–57. DOI: 10.1016/j.autcon.2015.09.012.

[131] C. Dainese, M. Faè, A. Gambarotta, M. Morini, M. Premoli, G. Randazzo, M. Rossi, M. Rovati, and C. Saletti. "Development and application of a Predictive Controller to a mini district heating network fed by a biomass boiler". In: *Energy Procedia* 159 (2019), pp. 48–53. DOI: 10.1016/j.egypro.2018.12.016.

[132] H. Bahlawan, M. Morini, M. Pinelli, and P. R. Spina. "Dynamic programming based methodology for the optimization of the sizing and operation of hybrid energy plants". In: *Applied Thermal Engineering* 160 (2019), p. 113967. DOI: 10.1016/j.applthermaleng.2019.113967.

[133] The MathWorks. *Optimization Toolbox User's Guide R2014b*. Tech. rep. 2014.

[134] A. Bischi, L. Taccari, E. Martelli, E. Amaldi, G. Manzolini, P. Silva, S. Campanari, and E. Macchi. "A detailed MILP optimization model for combined cooling, heat and power system operation planning". In: *Energy* 74 (2014), pp. 12–26. DOI: 10.1016/j.energy.2014.02.042.

[135] J. A. Andersson, J. Gillis, G. Horn, J. B. Rawlings, and M. Diehl. "CasADi: a software framework for nonlinear optimization and optimal control". In: *Mathematical Programming Computation* 11.1 (2019). DOI: 10.1007/s12532-018-0139-4.

[136] Y. Li, K. H. Ang, and G. C. Chong. "PID Control System Analysis and Design: Problems, Remedies, and Future Directions". In: *IEEE Control Systems Magazine* 26.1 (2006), pp. 32–41. DOI: 10.1109/MCS.2006.1580152.

[137] R. D'Andrea and G. E. Dullerud. "Distributed Control Design for Spatially Interconnected systems". In: *IEEE Transactions on Automatic Control* 48.9 (2003), pp. 1478–1495. DOI: 10.1109/tac.2003.816954.

[138] F. Bünning, R. Sangi, and D. Müller. "A Modelica library for the agent-based control of building energy systems". In: *Applied Energy* 193 (2017), pp. 52–59. DOI: 10.1016/j.apenergy.2017.01.053.

[139] F. Bünning, M. Wetter, M. Fuchs, and D. Müller. "Bidirectional low temperature district energy systems with agent-based control: Performance comparison and operation optimization". In: *Applied Energy* 209 (2018), pp. 502–515. DOI: 10.1016/j.apenergy.2017.10.072.

[140] L. Uusitalo, A. Lehikoinen, I. Helle, and K. Myrberg. "An overview of methods to evaluate uncertainty of deterministic models in decision support". In: *Environmental Modelling and Software* 63 (2015), pp. 24–31. DOI: 10.1016/j.envsoft.2014.09.017.

[141] E. F. Camacho and C. Bordons. *Model Predictive Control*. Springer-Verlag London, 1999.

[142] L. Grüne and J. Pannek. *Nonlinear Model Predictive Control. Theory and Algorithms*. Springer-Verlag London, 2011. ISBN: 9780857295002.

[143] M. Morari and J. H. Lee. "Model predictive control: Past, present and future". In: *Computers and Chemical Engineering* 23 (1999), pp. 667–682. DOI: 10.1016/S0098-1354(98)00301-9.

[144] D. Q. Mayne. "Model predictive control: Recent developments and future promise". In: *Automatica* 50.12 (2014), pp. 2967–2986. DOI: 10.1016/j.automatica.2014.10.128.

[145] A. Bemporad and M. Morari. "Robust Model Predictive Control: A Survey". In: *Lecture Notes in Control and Information Sciences* 245 (2007), pp. 207–226. DOI: 10.1007/BFb0109870.

[146] M. Ellis, H. Durand, and P. D. Christofides. "A tutorial review of economic model predictive control methods". In: *Journal of Process Control* 24.8 (2014), pp. 1156–1178. DOI: 10.1016/j.jprocont.2014.03.010.

[147] J. Ma, S. J. Qin, and T. Salsbury. "Application of economic MPC to the energy and demand minimization of a commercial building". In: *Journal of Process Control* 24.8 (2014), pp. 1282–1291. DOI: 10.1016/j.jprocont.2014.06.011.

[148] C. Saletti, N. Zimmerman, M. Morini, K. Kyprianidis, and A. Gambarotta. "A Scale-Free Dynamic Model for District Heating Aggregated Regions". In: *Preprints* (2020), pp. 1–19. DOI: 10.20944/preprints202006.0320.v1.

[149] A. Gambarotta, M. Morini, M. Rossi, and M. Stonfer. "A Library for the Simulation of Smart Energy Systems: The Case of the Campus of the University of Parma". In: *Energy Procedia* 105 (2017), pp. 1776–1781. DOI: 10.1016/j.egypro.2017.03.514.

[150] C. Cesaraccio, D. Spano, P. Duce, and R. L. Snyder. "An improved model for determining degree-day values from daily temperature data". In: *International Journal of Biometeorology* 45.4 (2001), pp. 161–169. DOI: 10.1007/s004840100104.

[151] X. Yuan, X. Yali, and W. Qiongyao. "Dynamic temperature model of district heating system based on operation data". In: *Energy Procedia* 158 (2019), pp. 6570–6575. DOI: 10.1016/j.egypro.2019.01.073.

[152] P. Nageler, R. Heimrath, T. Mach, and C. Hochenauer. "Prototype of a simulation framework for georeferenced large-scale dynamic simulations of district energy systems". In: *Applied Energy* 252 (2019), p. 113469. DOI: 10.1016/j.apenergy.2019.113469.

[153] Energimyndigheten (Swedish Energy Agency). *Energistatistik för flerbostadshus 2016 (Energy statistics for multi-dwelling buildings in 2016)*. 2017.

[154] *Guidebook. UK homes losing heat up to three times faster than European neighbours. URL: https://www.tado.com/t/en/uk-homes-losing-heat-up-to-three-times-faster-than-european-neighbours/.* 2020.

[155] S. Idowu, S. Saguna, C. Åhlund, and O. Schelén. "Forecasting heat load for smart district heating systems: A machine learning approach". In: *2014 IEEE International Conference on Smart Grid Communications, SmartGridComm 2014* (2015), pp. 554–559. DOI: 10.1109/SmartGridComm.2014.7007705.

[156] S. Sajjadi, S. Shamshirband, M. Alizamir, P. L. Yee, Z. Mansor, A. A. Manaf, T. A. Altameem, and A. Mostafaeipour. "Extreme learning machine for prediction of heat load in district heating systems". In: *Energy and Buildings* 122 (2016), pp. 222–227. DOI: 10.1016/j.enbuild.2016.04.021.

[157] A. Propoi and F. Willekens. "A Dynamic Linear Programming Approach to National Settlement System". In: *Environment and Planning A: Economy and Space* 10 (1978), pp. 561–576. DOI: 10.1068/a100561.

[158] A. R. Plummer. "Model-in-the-loop testing". In: *Proceedings of the Institution of Mechanical Engineers. Part I: Journal of Systems and Control Engineering* 220.3 (2006), pp. 183–199. DOI: 10.1243/09596518JSCE207.

[159] A. Gambarotta, M. Morini, and C. Saletti. "Development of a model-based Predictive Controller for a heat distribution network". In: *Energy Procedia* 158 (2019), pp. 2896–2901. DOI: 10.1016/j.egypro.2019.01.944.

[160] N. Cadau, A. De Lorenzi, A. Gambarotta, M. Morini, and C. Saletti. "A Model-in-the-Loop application of a Predictive Controller to a District Heating system". In: *Energy Procedia* 148 (2018), pp. 352–359. DOI: 10.1016/j.egypro.2018.08.088.

[161] A. De Lorenzi, A. Gambarotta, M. Morini, M. Rossi, and C. Saletti. "Setup and testing of smart controllers for small-scale district heating networks: An integrated framework". In: *Energy* 205 (2020), p. 118054. DOI: 10.1016/j.energy.2020.118054.

[162] J. S. Pereira, J. B. Ribeiro, R. Mendes, G. C. Vaz, and J. C. André. "ORC based micro-cogeneration systems for residential application - A state of the art review and current challenges". In: *Renewable and Sustainable Energy Reviews* 92 (2018), pp. 728–743. DOI: 10.1016/j.rser.2018.04.039.

[163] S. Quoilin, M. V. D. Broek, S. Declaye, P. Dewallef, and V. Lemort. "Techno-economic survey of organic rankine cycle (ORC) systems". In: *Renewable and Sustainable Energy Reviews* 22 (2013), pp. 168–186. DOI: 10.1016/j.rser.2013.01.028.

[164] I. González-Pino, E. Pérez-Iribarren, A. Campos-Celador, and J. Terés-Zubiaga. "Analysis of the integration of micro-cogeneration units in space heating and domestic hot water plants". In: *Energy* 200 (2020), p. 117584. DOI: 10.1016/j.energy.2020.117584.

[165] E. S. Barbieri, F. Melino, and M. Morini. "Influence of the thermal energy storage on the profitability of micro-CHP systems for residential building applications". In: *Applied Energy* 97 (2012), pp. 714–722. DOI: 10.1016/j.apenergy.2012.01.001.

[166] Turboden S.p.A. *Brochure: Steam & Power. ORC cogeneration system for your manufacturing process.* 2019.

[167] A. Campos Celador, M. Odriozola, and J. M. Sala. "Implications of the modelling of stratified hot water storage tanks in the simulation of CHP plants". In: *Energy Conversion and Management* 52 (2011), pp. 3018–3026. DOI: 10.1016/j.enconman.2011.04.015.

[168] ISPRA Istituto Superiore per la Protezione e la Ricerca Ambientale. *Comunicato stampa: Nel 2017, tra i paesi che producono più elettricità, l'Italia seconda solo alla Svezia per uso di fonti rinnovabili.* 2019.

[169] P. Mancarella. "MES (multi-energy systems): An overview of concepts and evaluation models". In: *Energy* 65 (2014), pp. 1–17. DOI: 10.1016/j.energy.2013.10.041.

[170] A. Moser, D. Muschick, M. Gölles, P. Nageler, H. Schranzhofer, T. Mach, C. Ribas Tugores, I. Leusbrock, S. Stark, F. Lackner, and A. Hofer. "A MILP-based modular energy management system for urban multi-energy systems: Performance and sensitivity analysis". In: *Applied Energy* 261 (2020), p. 114342. DOI: 10.1016/j.apenergy.2019.114342.

[171] E. Widl, B. Leitner, D. Basciotti, S. Henein, T. Ferhatbegovic, and R. Hofmann. "Combined optimal design and control of hybrid thermal-electrical distribution grids using co-simulation". In: *Energies* 13.8 (2020), p. 1945. DOI: 10.3390/en13081945.

[172] A. V. Olympios, N. Le Brun, S. Acha, N. Shah, and C. N. Markides. "Stochastic real-time operation control of a combined heat and power (CHP) system under uncertainty". In: *Energy Conversion and Management* 216 (2020), p. 112916. DOI: 10.1016/j.enconman.2020.112916.

[173] T. A. N. Heirung, J. A. Paulson, J. O'Leary, and A. Mesbah. "Stochastic model predictive control - how does it work?" In: *Computers and Chemical Engineering* 114 (2018), pp. 158–170. DOI: 10.1016/j.compchemeng.2017.10.026.

[174] M. B. Saltik, L. Özkan, J. H. Ludlage, S. Weiland, and P. M. Van den Hof. "An outlook on robust model predictive control algorithms: Reflections on performance and computational aspects". In: *Journal of Process Control* 61 (2018), pp. 77–102. DOI: 10.1016/j.jprocont.2017.10.006.

[175] M. I. Alizadeh, M. Parsa Moghaddam, N. Amjady, P. Siano, and M. K. Sheikh-El-Eslami. "Flexibility in future power systems with high renewable penetration: A review". In: *Renewable and Sustainable Energy Reviews* 57 (2016), pp. 1186–1193. DOI: 10.1016/j.rser.2015.12.200.

[176] Terna. *Regolamento recante le modalità per la creazione, qualificazione e gestione di unità virtuali abilitate miste (UVAM) al mercato dei servizi di dispacciamento*. Tech. rep.

[177] A. Zakaria, F. B. Ismail, M. S. Lipu, and M. A. Hannan. "Uncertainty models for stochastic optimization in renewable energy applications". In: *Renewable Energy* 145 (2020), pp. 1543–1571. DOI: 10.1016/j.renene.2019.07.081.

[178] W. Gang, G. Augenbroe, S. Wang, C. Fan, and F. Xiao. "An uncertainty-based design optimization method for district cooling systems". In: *Energy* 102 (2016), pp. 516–527. DOI: 10.1016/j.energy.2016.02.107.

[179] D. Z. Fu, Z. Y. Zheng, J. Gui, R. Xiao, G. H. Huang, and Y. P. Li. "Development of a fuel management model for a multi-source district heating system under multi-uncertainty and multi-dimensional constraints". In: *Energy Conversion and Management* 153 (2017), pp. 243–256. DOI: 10.1016/j.enconman.2017.10.002.

[180] L. Moretti, E. Martelli, and G. Manzolini. "An efficient robust optimization model for the unit commitment and dispatch of multi-energy systems and microgrids". In: *Applied Energy* 261 (2020), p. 113859. DOI: 10.1016/j.apenergy.2019.113859.

[181] *DYMOLA Systems Engineering website. URL: https://www.3ds.com/products-services/catia/products/dymola/.*

[182] K. Hermansson, C. Kos, F. Starfelt, K. Kyprianidis, C. F. Lindberg, and N. Zimmerman. "An Automated Approach to Building and Simulating Dynamic District Heating Networks". In: *IFAC-PapersOnLine* 51.2 (2018), pp. 855–860. DOI: 10.1016/j.ifacol.2018.04.021.

[183] *DISTRHEAT Project website. URL: https://www.distrheat.eu/.*

[184] C. Czerkauer-yamu and P. Frankhauser. "A Multi-Scale (Multi-Fractal) Approach for a Systemic Planning Strategy from a Regional to an Architectural Scale". In: *Real Corp 2010 (Competence Center of Urban and Regional Planning, Association for Promotion and Research of Urban Planning and Regional Development in the Information Society)* May (2010).

[185] The MathWorks. *Simulink Getting Started Guide R2020a.* Tech. rep. 2020.

[186] E. Buckingham. "On Physically Similar Systems: Illustrations of the Use of Dimensional Equations". In: *Physical Review* 4.4 (1914), pp. 345–376.

[187] N. Cadau, A. De Lorenzi, A. Gambarotta, and M. Morini. "Development and Analysis of a Multi-Node Dynamic". In: *Energies* 12.22 (2019), p. 4275. DOI: 10.3390/en12224275.

[188] R. De Césaro Oliveski, A. Krenzinger, and H. A. Vielmo. "Comparison between models for the simulation of hot water storage tanks". In: *Solar Energy* 75.2 (2003), pp. 121–134. DOI: 10.1016/j.solener.2003.07.009.